POOL BOILING HEAT TRANSFER ENHANCEMENT

WITH SINK ELECTRICAL DISCHARGE MACHINED SURFACES

POOL BOILING HEAT TRANSFER ENHANCEMENT

WITH SINK ELECTRICAL DISCHARGE MACHINED SURFACES

By

Gurpyar Dhadda, B. Eng.

A Thesis

Submitted to School of Graduate Studies in partial fulfillment

Of the requirements for the degree of

Master of Applied Science

McMaster University

Hamilton, Canada

MASTER OF APPLIED SCIENCE (2019)   McMaster University

(Mechanical Engineering)   Hamilton, Ontario, Canada

TITLE: Pool boiling heat transfer enhancement with

                          sink electrical discharge machined surfaces

AUTHOR: Gurpyar Dhadda, B. Eng.

SUPERVISORS: Dr. Philip Koshy

                          Dr. Mohamed Hamed

Number of pages: XIII, 112

Abstract

Heat transfer technologies based on boiling refer to applications like heat pumps, waste heat recovery systems, power plants and electronic components cooling. The widespread use of boiling as the heat transfer mode is due to high heat transfer coefficients associated with the phase change from liquid to vapor. Boiling heat transfer coefficients can be further enhanced by modifying the texture or chemical composition of the interface at which boiling occurs. The objective of this research is to fabricate textured surfaces with electrical discharge machining (EDM) and investigate the enhancement in pool boiling heat transfer, concerning machining and surface characterization parameters. It is complemented by a qualitative analysis of bubble dynamics with high-speed imaging, to provide insights into the differences in boiling performance associated with the changes in surface topography. Sink electrical discharge machined surfaces demonstrated ten times higher heat transfer coefficient compared to a polished surface with the highest value of 237 kW/m^{2}K at $\Delta T_{sat} = 3.4$ K during these studies.

Acknowledgments

Table of Contents

Nomenclature

SYMBOL	DESCRIPTION	UNITS
h_{fg}	Latent heat of vaporization	kJ/kg
C_p	Specific heat	kJ/kgK
q''	Wall heat flux	kW/m^2
ΔT_{sat}	Wall superheat	K
ΔT_{nuc}	Nucleation superheat	K
σ	Surface tension	N/m
r_{nuc}	Nucleation radius	mm
p	Pressure	Pa
ρ	Density	kg/m^3
$f_{b,n}$	Bubble frequency	s^{-1}
$D_{b,n}$	Bubble diameter	mm
k	Thermal conductivity	W/mK
A	Area	m^2
α	Thermal diffusivity	m^2/s
$t_{w,n}$	Waiting time	s
h_{turb}	Turbulent heat transfer coefficient	kW/m^{2}K
g	Gravitational acceleration	m/s^2
T_{wall}	Wall temperature	K
T_a	Ambient temperature	K
P_r	Reduced pressure	-
ν	Kinematic viscosity	m^2/s
μ	Dynamic viscosity	Ns/m^2
Pr	Prandtl Number	-
h, HTC	Heat transfer coefficient	kW/m^{2}K

t_e	Discharge duration	µs
i_e	Pulse current	A
MAE	Mean absolute error	-
ONB	Onset of Nucleate boiling	K

Subscripts

f	Fluid
v	Vapor
s	Surface
sat	Saturation

List of figures

List of Tables

1 Introduction

Given recent advances in various engineering fields such as in modern devices in the fields of power generation, material processing, and electronic cooling, research on heat transfer rate enhancement techniques by surface engineering has garnered a lot of interest. These techniques are becoming essential for devising compact heat exchangers with predictable heat transfer coefficients for thermal management of high heat loads.

A comparison of heat transfer coefficients for various mechanisms of heat transfer [1] shows that boiling is the most efficient mechanism of heat transfer:

- Free Convection: 2 - 1000 W/m^{2}K

- Forced Convection: 25 - 20,000 W/m^{2}K

- Boiling: 2500 - 100,000 W/m^{2}K

This efficiency owes to the high latent heat of vaporisation (for water, h_{fg} = 2264.4 kJ/kg at 100 °C, 1 atm pressure) associated with phase change, compared to its sensible heat (for water, Cp ΔT = 4.2 kJ/kg for 1 °C temperature change at 100 °C, 1 atm pressure).

Heat transfer coefficient associated with the boiling mechanism is sensitive to working fluid thermophysical properties, operating conditions (fluid flow, saturation pressure, and subcooling) and heating surface conditions. Various promising techniques have shown the ability to further enhance the boiling performance. These techniques can be divided into 2

1

categories: (a) active technique like fluid or surface vibration, mechanical and/or electrohydrodynamic forces to induce fluid currents, and (b) passive techniques like modification of fluid properties (refrigerants, nanofluids etc.) and surface engineering (surface material, texture, wettability). Passive enhancement techniques require no external power, are cost-effective, and are easy to implement in compact cooling enclosures [2].

Surface engineering encompasses techniques related to the modification of the geometry of heating surface at the macroscale, microscale or nanoscale level, or surface physicochemical properties by coatings. The goal here is to optimize the shape, size and physiochemistry of surface features to achieve the highest boiling heat transfer coefficient for a given fluid, under specified thermophysical operating conditions. Surface characterization of these enhanced surfaces has been challenging, and efforts have been put forward for determining the features on surfaces that play a decisive role in pool boiling heat transfer mechanism. Various engineered surfaces have been proposed in the past to modify the surface properties that include the geometrical shape and surface wettability (physical and chemical) and exploit them for application in boiling heat transfer enhancement. These include: (a) micro/nanostructured finned surfaces, tunnel or re-entrant cavities fabricated using polishing, mechanical deformation, rolling, knurling, milling, electrical discharge machining and sandblasting, (b) surface coating techniques using Al_2O_3, TiO_2, CuO_2, Fe_2O_3 nanoparticles or Polytetrafluoroethylene (PTFE), (c) MEMS/NEMS techniques by etching, and (d) porous mesh and foam attachments. A

review of heat transfer enhancement techniques using surface engineering has been given in [2,3].

In this chapter, a brief introduction of pool boiling and a review of electrical discharge machining to create surfaces for boiling heat transfer enhancement are presented.

1.1 Pool boiling

Pool boiling of a fluid refers to a phase change process in which vapor bubbles are formed at the solid-liquid interface on a heated surface and in the superheated liquid layer adjacent to the heated surface, under natural convection conditions. Pool boiling can be represented by a boiling curve that was first reported in 1934 by Nukiyama [4]. The curve Fig. 1.1 is a representation of the variation of wall heat flux (q") with wall superheat (ΔT_{sat}) for a surface submerged in a pool of saturated fluid. The wall superheat (ΔT_{sat}) is defined as the difference between the wall temperature and the saturation temperature of the fluid at the system pressure. Boiling is a complex phenomenon characterized by the combined effect of various physical forces like surface tension, inertial forces, buoyancy, and internal pressure influencing the liquid and vapor phase at different magnitudes and direction at various thermophysical conditions of boiling. The boiling curve can be obtained either by controlled temperature or controlled heat flux boundary conditions. Fig. 1.1 shows the different regimes encountered when a fluid is subjected to boiling.
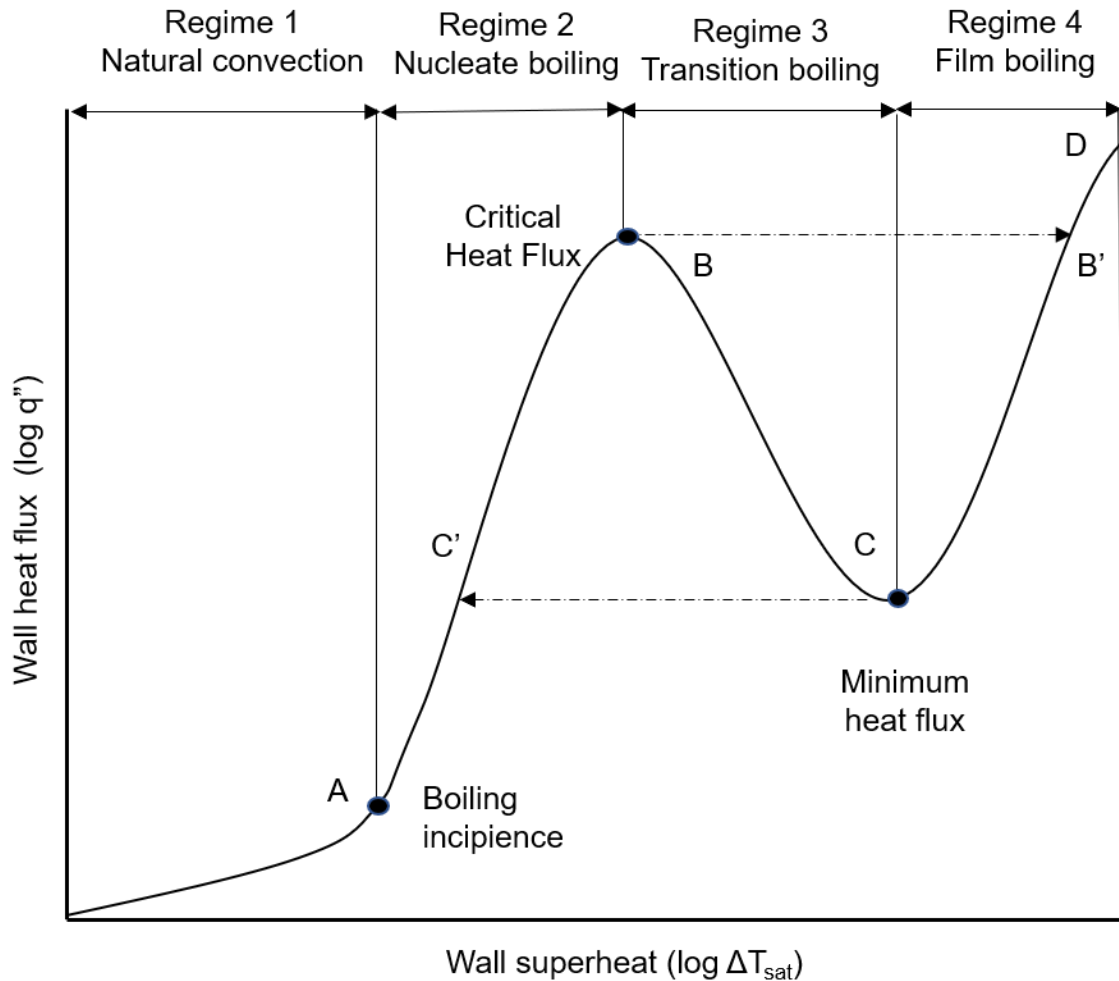
Figure 1.1: The pool boiling curve.

The first regime is the natural convection regime that operates under the influence of buoyancy. As the heat flux is increased, at a certain superheat, vapor bubbles are observed on the heated surface. This point is called the onset of nucleate boiling (ONB) point or boiling incipience point (A). Initially, bubbles appear at scattered sites on the surface, and they start growing and departing from their point of contact. These bubbles originate from scratches, cavities, and pits on the surface where embryo nuclei get trapped

4

during initial wetting. Beyond this point on the boiling curve, a dramatic increase in the slope of the boiling curve is observed because of an increasing number of bubbles departing from a large number of nucleation sites over the surface. This phase is followed by a fully developed nucleate boiling regime where bubbles start to merge in the vertical and horizontal directions and rise in the form of mushroom-like columns and slugs. At point B called the point of critical heat flux (CHF), a layer of vapor blankets the entire heated surface and restricts the heat transfer from the heated surface to the liquid. As a result, the temperature of the heated surface rises abruptly, which is followed by the film boiling regime. If the system is surface temperature controlled, the boiling phenomenon moves to transition region where heat flux from surface decreases with increase in temperature via point C. If the system is heat flux controlled, it moves directly to point B'. In the film boiling regime, radiation becomes an important mode of heat transfer.

The critical heat flux sets the maximum heat flux that boiling can operate in, after which the abrupt increase in surface temperature can be damaging to the heated surface. Most heat transfer enhancement techniques are useful in regimes 1 and 2, i.e., natural convection and nucleate boiling regimes. Heat transfer enhancement is achieved via: (a) early onset of nucleate boiling (b), and higher heat flux for given superheat in regimes 1 and 2.

1.2   Surface engineering for pool boiling enhancement

Pool boiling is a surface phenomenon. Therefore, surface condition (e.g., texture) plays a key role in influencing the boiling performance. Engineered surfaces created by various machining techniques have been found to provide enhancement in boiling performance compared to surfaces with no features. Researchers in the past have been able to achieve enhancement up to 600% for some highly wetting fluids like n-pentane [5] and heat transfer coefficients up to 995 kW/m^{2}K [6]. Most engineered surfaces are characterized by a single parameter of average roughness Ra, and widely used correlations are based on this parameter. However, surfaces with the same Ra can have different topography [7]. Moreover, Ra is an amplitude parameter that does not consider the spacing between surface features. Therefore, using Ra as the sole defining parameter to indicate the effects of surface texture on the phenomenon of boiling can lead to correlations that cannot be generalized for all operating conditions. Therefore, it becomes crucial to characterize the surface using hybrid parameters that consider amplitude and spacing of the surface features and incorporate the role of all these parameters on pool boiling heat transfer enhancement.

1.3   Electrical discharge machining

Electrical discharge machining (EDM) is a non-conventional machining process in which material is removed from a workpiece by electrical discharges. These rapidly recurring electrical discharges remove material in the form of debris from the workpiece when the oppositely charged tool electrode is brought close to it in the presence of a dielectric fluid

to a gap of 10 - 100 µm. The EDM process is stabilized by an accompanied flushing mechanism that aids in the removal of debris from the gap and regeneration of dielectric strength of fluid after each discharge. The operator sets the discharge duration (t_e), pulse current (i_e) and open circuit voltage (U) for controlling the EDM process. Modern generators provide additional parameters to optimize material removal rate, tool wear ratio, and surface finish. Fig. 1.2 shows the process diagram of EDM.
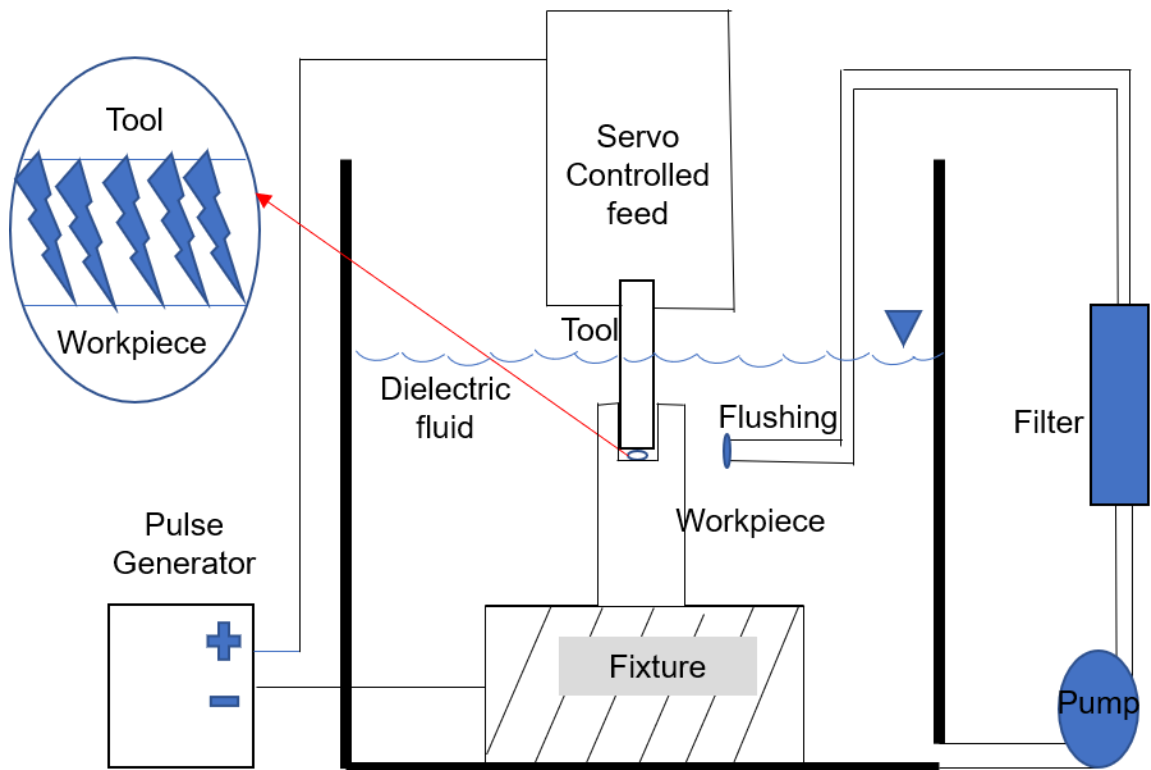
Figure 1.2: Electrical discharge machining process.

The pulse off-time (t_{off}), which is defined as the time interval between successive pulses, plays a critical role in stabilizing the discharge process. Electrical discharge machining process is only suitable for conductive materials, and the process depends only on the

thermal and electrical properties of the material. Mechanical properties like hardness and tensile strength are not a constraint for this machining process. The surface structure formed by EDM process is in the form of overlapping craters. The shape and size of these craters are dependent on the pulse energy q, which is given by:

$$q = U_e * i_e * t_e,$$ 2.6

where U_e is the discharge voltage, which is around 20 V, i_e is the pulse current and t_e is the pulse discharge duration. The discharge duration t_e is considered from the point after ignition delay when the discharge starts happening. The details of the process at the gap during a pulse discharge with instantaneous values of voltage (U) and current (I) during the machining is shown in Fig. 1.3. These sequences of pulses are provided by transistor-based direct current (DC) generator. The tool electrode is controlled by a servo feed controller which moves it near the workpiece in the form of pecking motion for erosion time in a cycle. When the gap is small enough to overcome the dielectric electric field strength between the gap, the dielectric ionizes and forms a plasma channel, a discharge happens, and current (i_e) flows from the tool electrode to work electrode. Because of this plasma, the temperature in the gap reaches 6000 °C, and workpiece material starts melting with the heat of the plasma. This plasma expands for the discharge duration (t_e), and a vapor bubble is formed as a result. The material is removed from the workpiece due to vaporisation and fusion after heat input reduction because of drop in current. The vapor bubble starts

collapsing and the gap returns to initial condition [8]. The carbon from dielectric gets deposited on positive electrode and protect the tool from wear in the next erosion cycle.
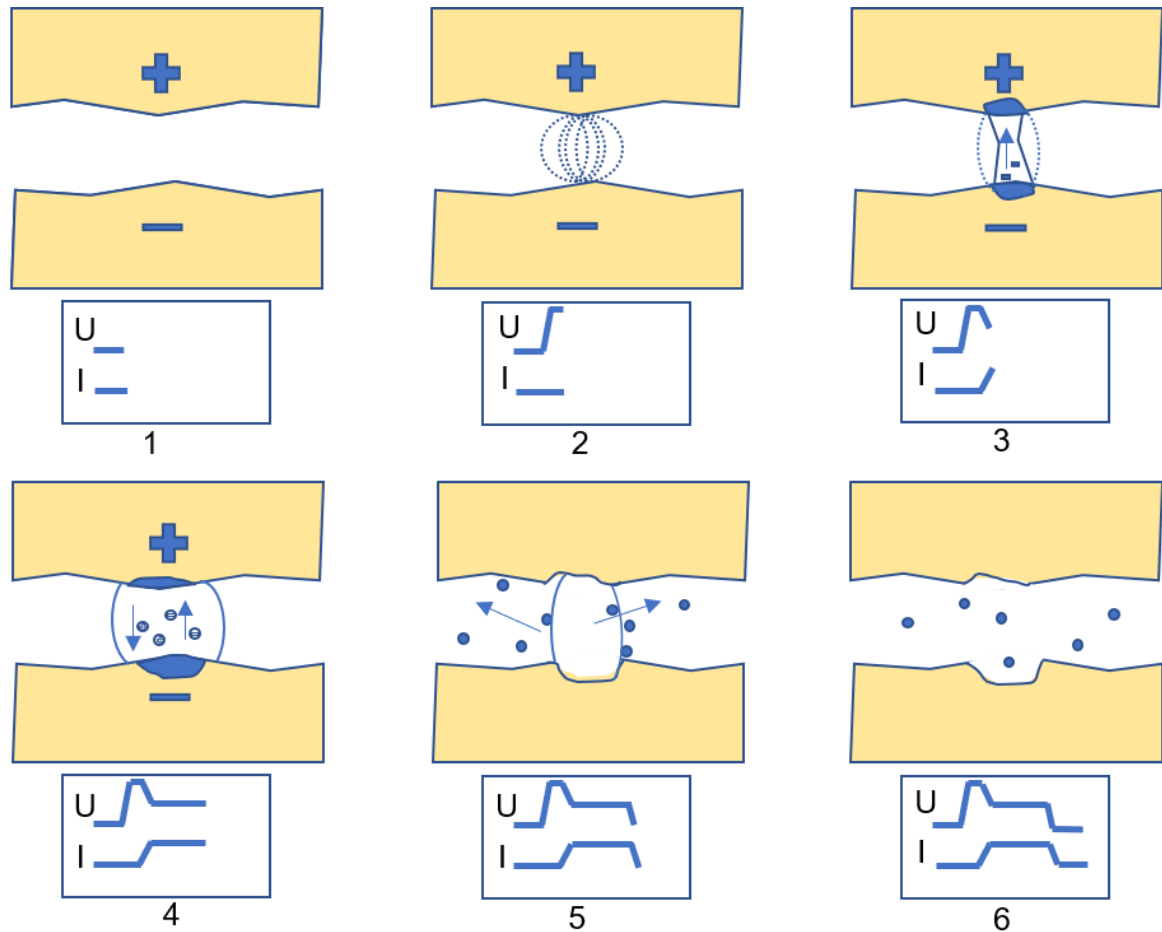
Figure 1.3: Gap phenomenon (1) Initial condition (2) Electrical field generation (3) Plasma formation (4) Plasma expansion and melting of material (5) Material removal during bubble collapse (6) Crater formation and return to initial condition

The EDM process is advantageous in machining isotropic surfaces with a wide range of controllable roughness parameters including variable aspect ratio of surface features by choice of only a few process variables. The EDM surface is composed of

9

different layers [9]. The microstructure reveals the formation of 3 types of layer, i.e., the white layer, the base material, and the layer with small microcracks during re-hardening of the surface. Surfaces generated by electrical discharge machining are generally positively skewed. The typical time to texture a 10 x 10 mm^2 surface is less than a minute. A good practice is to use a current density of 10 A/cm^2, which keeps the EDM process stable (by preventing arcing for optimum material removal rate) as shown by Bratnik [10].

1.4   Scope and organization of the thesis

This thesis is focussed on developing engineered surfaces by electrical discharge machining and studying the boiling heat transfer performance of these enhanced surfaces. The motivation for using the EDM textured surface for boiling heat transfer was due to the potential of EDM craters to serve as effective nucleation sites for boiling. EDM seems a suitable manufacturing process due to the isotropic, positively-skewed nature of generated surfaces, the flexibility of controlling roughness parameters, rapid texturing, and the ability to use a secondary process on textured surfaces to create re-entrant cavities, which are considered more stable for boiling.

In chapter 2, a comprehensive literature review is presented on engineered surfaces for enhancing boiling heat transfer, the theory of nucleation, and surface characterization in boiling studies. Chapter 3 summarizes the experimental setup and procedure. In chapter 4, the experimental results and discussions from this study are presented. Conclusions and recommendation of future work are provided in chapter 5.

2 Literature review

2.1 Engineered surfaces for high boiling heat transfer coefficients

Various heat transfer enhancement methods have been developed in past decades, using which, heat transfer coefficients have been increased significantly. In this section, we will look at some of the surfaces that produced the highest boiling performance. Berenson [5] noticed a 600% change in heat transfer coefficient because of a change in preparation method from polishing to lapping. This change was attributed to the difference in number of active nucleation sites on the surface, owing to the different preparation method. Working on the similar lines, various researchers developed artificial nucleation sites that are stable and transfer high heat at low superheat, which have subsequently been developed into commercial enhanced heat transfer geometries such as, Trane bent fin developed by Webb et al. [11], Hitachi Thermoexcel-E by Nakayama et al. [12] and several others. These enhanced surfaces have been implemented in heat exchangers and found to be very effective for designing compact thermal devices. Coating the surface with a porous layer can significantly improve the heat transfer coefficient due to capillary wicking action. Nakayama et al. [12] created tunnel and pore structure (Fig. 2.1) by gouging microchannels and covering tunnels with a copper plate, and was able to obtain a heat transfer coefficient of 350 kW/m^{2}K at ΔT = 3.5 K. They attributed this enhancement to the increase in latent heat flux inside the tunnels during 'dried-up mode', 'suction-evaporation mode' and 'flooded mode', depending upon the state of liquid and vapor in the tunnels.

11
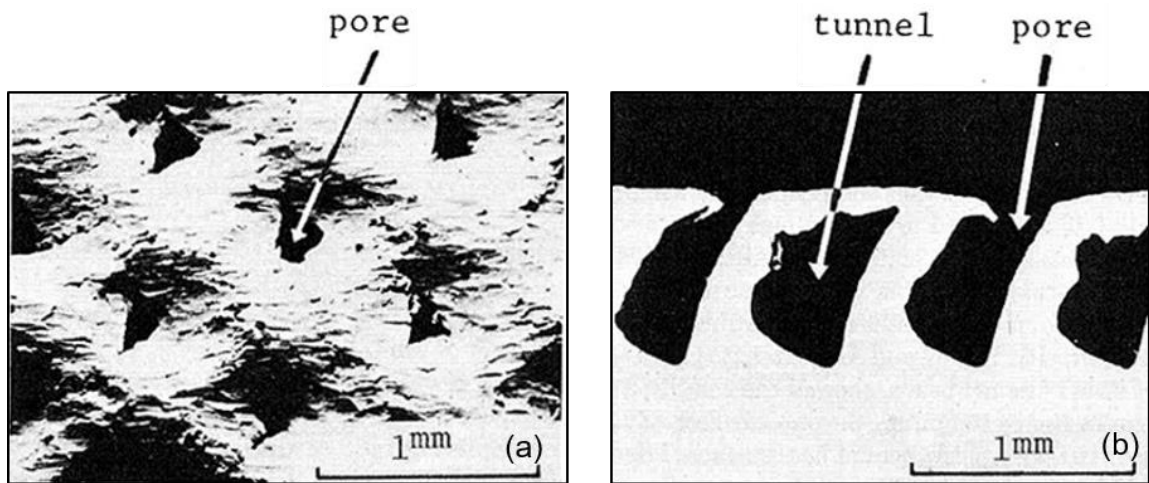
Figure 2.1: (a) Top view and (b) Section view of tunnel and pore structure [12]

Kandlikar [13] used an embossing process to create features on a surface that separated the flow of water and vapor flow, and was able to get a very high boiling heat transfer coefficient of 600 kW/m²K at $\Delta T = 5$ K. The evaporation momentum forces acting on bubbles originating from nucleation sites of sharp corners of microchannels significantly improved the boiling heat transfer. Later, Patil and Kandlikar [6] used electrodeposition of super-hydrophilic microporous coating on microchannels made by CNC milling and were able to achieve a whopping heat transfer coefficient of 995 kW/m²K at $\Delta T = 3$ K. The microchannels served as water-supply conduits, and the porous layer acted as nucleation sites. The enhancement was explained on the basis of separate paths for liquid and vapor which helps in removing heat at lower wall superheat via enhanced micro-convection. The microchannel geometry with characteristic lengths from 200 - 1000 µm and coating thickness of 57 - 81 µm were used in their studies as shown in Fig. 2.2.
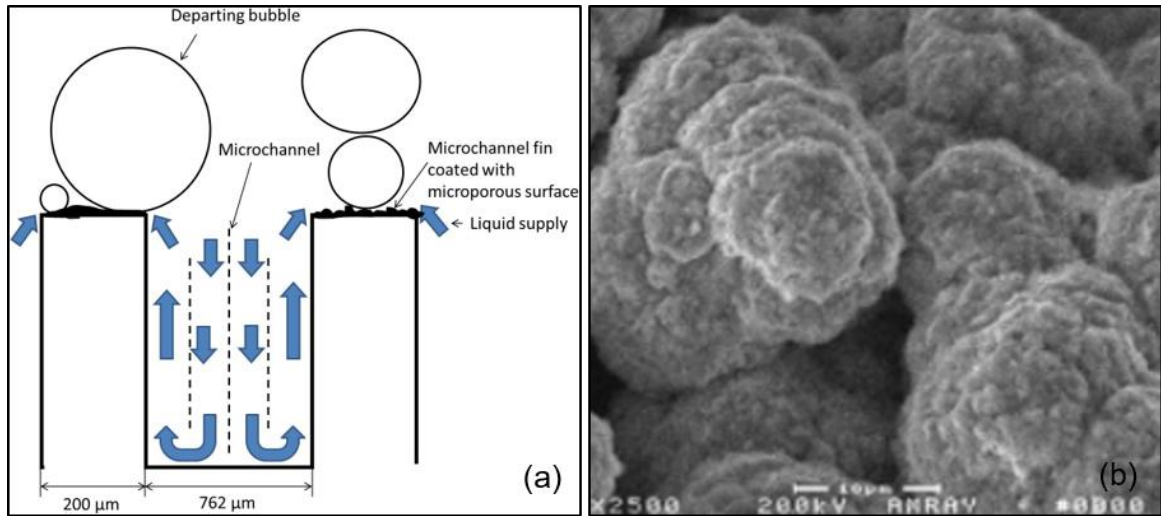
Figure 2.2: (a) Microchannels (b) Porous layer on microchannels [6]

Recently, Jun et al. [14] used sintered copper particles and got a heat transfer coefficient of 400 kW/m^{2}K at $\Delta T = 5$ K. The increased heat transfer coefficient was optimized for coating thickness of 78 µm, 94 µm and 290 µm for 10 µm, 25 µm and 67 µm average particle sized (APS) copper particles (Figure 2.3). The enhancement was explained on the basis of an increased number of re-entrant cavities.
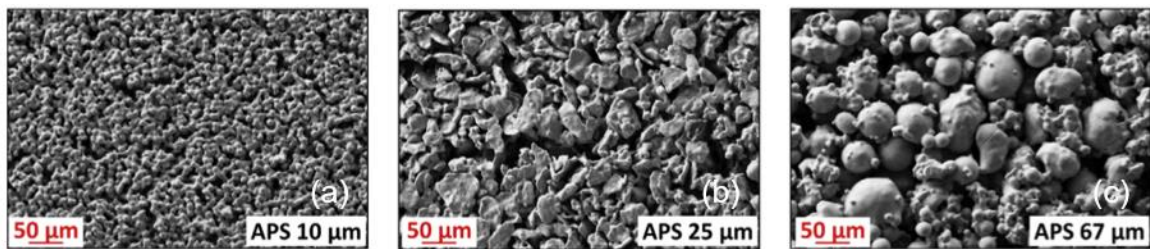
Figure 2.3: Sintered copper particles of thickness (a) 10µm (b) 25 µm (c) 67µm [14]

Rahman and McCarthy [15] used microchannels of length 300 µm to 3 mm made by wire electrical discharge machining with various copper oxide nano-structured coatings

13

(characteristic length 50 nm to 50 µm) as shown in Figure 2.4. They found that the critical heat flux for surface increased due to capillary wicking, but bubble nucleation got suppressed. However, an increase in the number of microchannels helped enhance heat transfer tremendously up to 461 kW/m^2 K at $\Delta T = 5$ K. The spatial ordering of liquid and vapor flow paths was found responsible for enhancement in HTC.
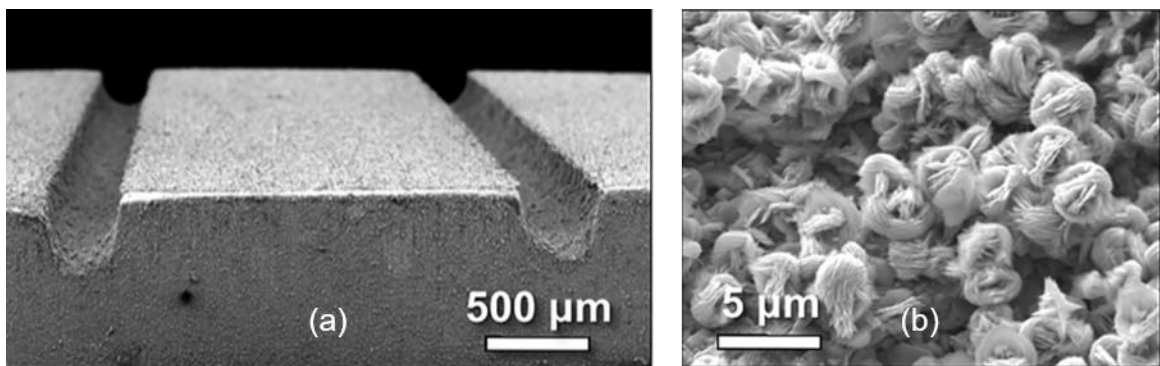
Figure 2.4: (a) Microchannels with wire EDM (b) CuO coating [15]

Various other manufacturing techniques are available in the literature to fabricate surfaces with high heat transfer coefficients. These techniques have been summarised in Table 2-1; categorized by the technique, material type, characteristic lengths of surface features, working fluid and the highest heat transfer coefficient (HTC) obtained during these studies. Heat transfer coefficients in the range 22.6 - 995 kW/m^{2}K have been observed with these engineered structures.

Table 2-1: Engineered surfaces with high boiling heat transfer

Research	Technique (Material)	Characteristic lengths	Fluid	Highest HTC (kW/m²K)
Webb 1972 [11]	Bent fin tube by machining and bending (Cu)	Gap between cavities (0.0015"-0.0035") Pitch of cavities (33-66 fins per inch) Fin height (0.015"-0.03") Thickness (0.005"-0.01")	R-11	22.6 at ΔT_{sat} = 10 °C
Nakayama 1980 [12]	Tunnel and Pore structure by gouging (Cu)	Tunnel pitch (0.6-0.72 mm) Cross-section height (0.4-0.62 mm) Width (0.15-0.25 mm) Pore pitch (0.6-0.72 mm)	H_2O, R-11, Liquid N_2	350 at ΔT_{sat} = 3.3 °C
Li, Paterson 2007 [16]	Microporous coated surface by sintering of isotropic copper wire screens (Cu)	Coating thickness (0.21-1.38 mm) Porosity (0.4-0.737) Wire diameter (56-191 µm) Pore size (120 -232 µm) Diameter (0.3-0.2 mm)	H_2O	180 at ΔT_{sat} = 5 °C
Chen 2008 [17]	Copper and Silicone nanowires bonded to Silicon wafers (Si, Cu)	Si nanowires height (40-50 µm) Diameter (20-300 nm) Cu nanowires height (40-50 µm) Diameter (200 nm) 60 µm thick porous alumina membrane with 200 nm pore size and 50% porosity	H_2O	80 at ΔT_{sat} = 30 °C
Mori 2009 [18]	Honeycomb porous plate (Cu)	Wall thickness (0.4 mm) Vapor channel width (1.3 mm) Height (1.2-10 mm) Average pore radius (0.04 µm) Median pore radius (0.13 µm) Porosity = 24.8%	H_2O	60 at ΔT_{sat} = 30 °C
Weibel 2010 [19]	Sintered copper powder wick surfaces (Cu)	Thickness of wick (600-1200 µm) Particle size (45-355 µm)	H_2O	200 at ΔT_{sat} = 6.5 °C

Yang 2010 [20]	Copper foam covers welded over plane copper (Cu)	Copper foam thickness (1-5 mm) Number of pores per inch length of metal foam (30-90) Porosity = 0.88-0.95	H_2O	150 at $\Delta T_{sat} = 9 \, °C$
Yao 2011 [21]	Electrochemical deposition of copper nanowires (Cu, Ag, Si)	Surface roughness of substrate 5.2-400nm Nanowire height (5-25 µm)	H_2O	145 at $\Delta T_{sat} = 11°C$
Cooke 2012 [22]	Microchannel by CNC milling (Cu)	Channel width (197-400 µm) Fin width (200-300 µm) Channel depth (100-445 µm) Number of channels (16-25) *Ra* of milled surface (0.38 µm)	H_2O	260 at $\Delta T_{sat} = 10 \, °C$
Kandlikar 2013 [13]	Fins by Embossing (Cu)	Depth of groove (200 µm) Corner angle (60°) No. of channels (7,8)	H_2O	600 at $\Delta T = 5 \, °C$
Patil, Kandlikar 2014 [6]	Electrodeposition of microporous coating on microchannels made by CNC milling (Cu)	Microchannel (Fin width 200-1000 µm) Channel width (300-762 µm) Channel depth (200-400 µm) Number of channels (5-20) Coating thickness (57-81 µm)	H_2O	995 at $\Delta T_{sat} = 3 \, °C$
Jun et al. 2016 [14]	Microporous coating (HTCMC) by sintering (Cu)	Copper powder size (10-67 µm)	H_2O	400 at $\Delta T_{sat} = 5 \, °C$
Rahman, McCarthy et al. 2017 [15]	Microchannel by wire electrical discharge machining followed by coating with Copper oxide nanostructured coatings (Cu)	Microchannel (0.3–3 mm) Coating (50 nm -50 µm)	H_2O	461 at $\Delta T_{sat} = 5 \, °C$

2.1.1 Application of electrical discharge machining

Jones [23] used Electrical Discharge Machining (EDM) to prepare surfaces with different *Ra* values (1.08 µm to 10 µm) (Fig. 2.5) and observed the roughness to have a different effect on boiling heat transfer for different fluids as shown in Fig. 2.6. For water, the intermittent roughness displayed similar heat transfer coefficients, but the roughest surface showed the highest boiling performance. However, for the more wetting liquid FC-77 (at reduced pressure, $P_r = 0.0064$), the heat transfer coefficient increased continually with increasing roughness. A photographic investigation of boiling on EDM surfaces was done by McHale [24], and bubble diameter, frequency, nucleation density were plotted against Jakob number for the different surfaces. McHale concluded the departure diameter, waiting period, bubble frequency and nucleation site density to be an active function of surface roughness.
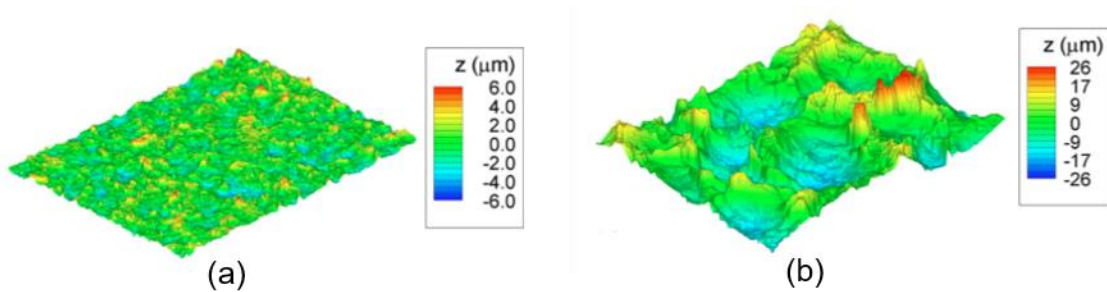
Figure 2.5: EDM surfaces with (a) Ra = 1.2 µm (b) Ra = 5.89 µm [23]

(a) Water (P$_r$ = 0.0046) (b) FC-77 (P$_r$ = 0.064)
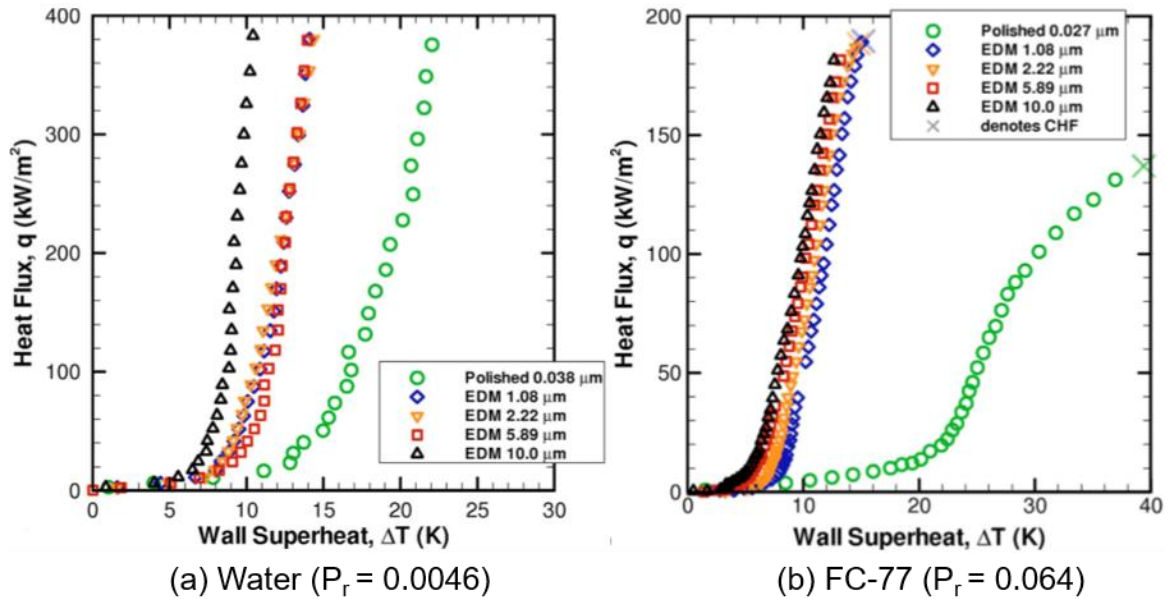
Figure 2.6: Boiling curves for (a) Water at P$_r$ = 0.0046 (b) FC-77 at P$_r$ = 0.0064 [23]

Geisler et al. [25] used electrical discharge machined surfaces in combination with microchannels and found enhancement as compared to other surfaces taking into account the effect of reduced pressure. They attributed low flux enhancement to Bond Number (ratio of gravitational to surface tension forces) and found that the enhancement is insensitive to channel aspect ratio. Vishal et al. [26] created square-pillar structures using wire EDM and found a 250% enhancement in boiling heat transfer for water and 100% enhancement for isopropyl alcohol as compared to a polished surface. They observed that the aspect ratio of pillars was important for enhancement in water, but it had no significant effect for isopropyl alcohol. A square network of interacting liquid vapor flow was responsible for heat transfer enhancement. The heat transfer coefficient increased with an increase in spacing between pillars because of prevention of obstruction of bubble growth,

18

and better convection. Similarly, the increasing depth led to more surface area and a greater number of active nucleation sites.

2.1.2 Other machining techniques based on spherical cavities

Messina et al. [27] found out that shallow pits are more effective than well-formed pits for boiling heat transfer enhancement of Freon 113. The pits of various aspect ratio (up to diameter/depth = 33) were prepared by using a photographic etching method. They also found that there is an upper limit to heat transfer enhancement with increasing nucleation site density.

Jabardo [28] observed the effect of boiling on sandblasted surfaces on R-134A and R-123 and found the heat transfer coefficient to decrease with an increase in the roughness sandblasted copper surfaces after $Ra > 3\mu$m. He asserted that lower active sites density due to an increased size of cavity and flooding of cavities are responsible for the deterioration of boiling heat transfer. He further pointed out that there is a certain roughness after which heat transfer does not increase, and determined that the effect of the surface microstructure is important in boiling studies.

2.2 Theoretical aspects

In this thesis, the primary emphasis will be on enhancing the boiling heat transfer coefficient in the following two regimes:

1. Convective regime

2. Nucleate boiling Regime

In the convective regime, heat transfer occurs via the thermal boundary layer developed over the heated surface, and fluid flows under the effect of only buoyancy due to the density difference developed owing to the temperature gradient in the bulk fluid. In the earliest studies, Fuji and Imura [29] suggested heat transfer coefficient for a plane horizontal plate (length = 30 cm, Rayleigh Number (Ra) < 5 X 10^8) in terms of Nusselt Number (Nu) of free convection regime for laminar buoyancy driven flow as a function of Rayleigh Number (Ra) in the form:

$$Nu = f(Ra) = 0.13(Gr.Pr)^{0.33} \hspace{3cm} 2.1$$

Where Gr is Grashof Number and Pr is Prandtl Number for the given fluid. The factors that intensify the free convection heat transfer coefficient are high-density gradient inside the liquid, a larger area of contact, low diffusivity and low viscosity of the liquid under laminar, transition or turbulent flow under natural buoyancy driving conditions. The surface roughness plays a decisive role in heat transfer via the augmented effect of all the factors mentioned above. The convective regime is followed by nucleate boiling regime on the boiling curve, which is identified by a sharp increase in the slope of the boiling curve.

This onset of nucleate boiling (ONB) point is influenced by the superheat required to activate and sustain bubble growth over nucleation sites on the surface. The exact point at which the boiling starts is not easy to identify because of incipience overshoot [2]; therefore, extrapolation techniques are employed to identify ONB. Once the system is in the nucleate boiling regime, a large heat amount of heat is transferred from the heated surface via nucleation sites. It should be noted that nucleation can happen inside the bulk fluid as well, and is called homogeneous nucleation. Heterogeneous nucleation happens at the nucleation sites on the surface. The homogeneous superheat (ΔT_{nuc}), i.e., the temperature difference across the liquid and vapor phase across the bubble boundary required to sustain such a bubble interface of radius of curvature r_{nuc} is given by

$$\Delta T_{\text{nuc}} = \frac{2\sigma}{r_{\text{nuc}} \left(\frac{dp}{dT}\right)_{\text{sat}}} \qquad\qquad 2.2$$

where σ represents the surface tension at the liquid-vapor interface and $(dp/dT)_{sat}$ represents the slope of the saturation curve of liquid. This equation is obtained by combining the Laplace equation of excess pressure in a bubble, and the Clausius Clapeyron equation for the state as suggested by Griffith and Wallis [30]. The equation provides insight into the existence and growth of the bubble as a function of wall superheat over the heated surface. The pre-existing bubble sites with larger r_{nuc} will be activated with a smaller superheat compared to pre-existing bubble sites with smaller r_{nuc}. This is the reason why boiling incipience for polished surfaces occurs at higher wall superheats than surfaces with larger cavities. This equation also tells that a bubble can exist in the subcooling phase of boiling

if this condition is satisfied. This is the basis for the stability of re-entrant cavities which can exist with negative r_{nuc}. Bangkoff [31] developed wettability criteria for entrapment of vapor nuclei during initial wetting of rough surface with conical cavities with cavity angle 2Φ based on geometric considerations, where θ_a is the advancing contact angle. Fig. 2.7 shows the amount of vapor trapped based on cavity angle and advancing contact angle of liquid.

(a) $\theta_a > 2\varphi$ (nuclei entrapped)

(c) $\theta_a > 2\varphi$ (narrow cavity, small nuclei)

(b) $\theta_a < 2\varphi$ (no nuclei)

(d) $\theta_a > 2\varphi$ (deep cavity, large nuclei)
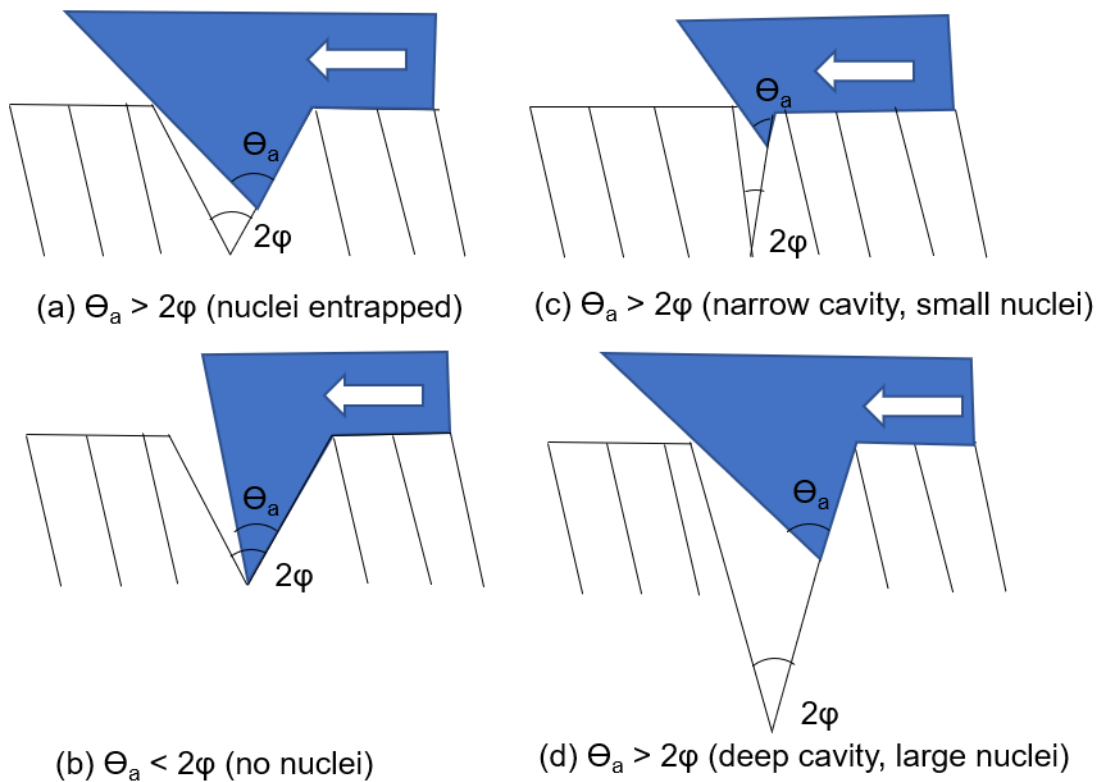
Figure 2.7: Conditions for vapor embryo entrapment for different sizes of cavities and advancing contact angle (a-d)

A highly wetting liquid like dielectric fluorochemical does not trap vapor nuclei as shown in Fig. 2.7 (b) if the advancing contact angle is higher than the cavity angle. Fig. 2.7

(c) and (d) shows the amount of vapor trapped for narrow and deep cavities. As these cavities trap different amount of vapor depending on wettability, different superheat will be required to nucleate a bubble from each of these cavities.

Similar wettability criteria was developed by Wang and Dhir [32], who suggested a criterion based on minimum Helmholtz free energy (a function of surface tension/surface energies of the new surface formed during wetting) assuming changing shape for constant volume of liquid and gas for different conical, spherical and sinusoidal cavities in a uniform temperature field. The incipience superheat was derived for these cavities by Wang and Dhir as well. The amount of liquid entrapped during advancing liquid condition can be considered equivalent to a liquid-vapor interface of the same volume as shown in Fig. 2.8 and subsequent growth analysis of bubble can be carried out on this radius of curvature of interface [33].

(a) Advancing liquid condition   (b) Liquid vapor interface
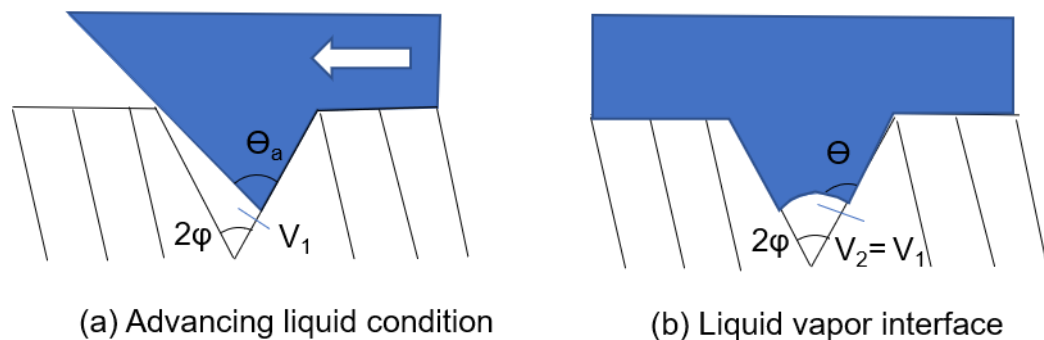
Figure 2.8: Simplification for analysis of liquid-vapor interface in a cavity [33]

During the growth period of a bubble, the bubble grows differently for different level of wettability as shown in Fig 2.9. Based on cavity angle (2Φ) and static contact angle

(θ), a bubble grows according to geometrical relations developed by Webb et al. [34] for interface radius of curvature (r), for given geometrical conditions. Boiling is more stable in a re-entrant cavity because a bubble can grow with negative superheat and, the cavity has more tendency to trap vapors during initial wetting.
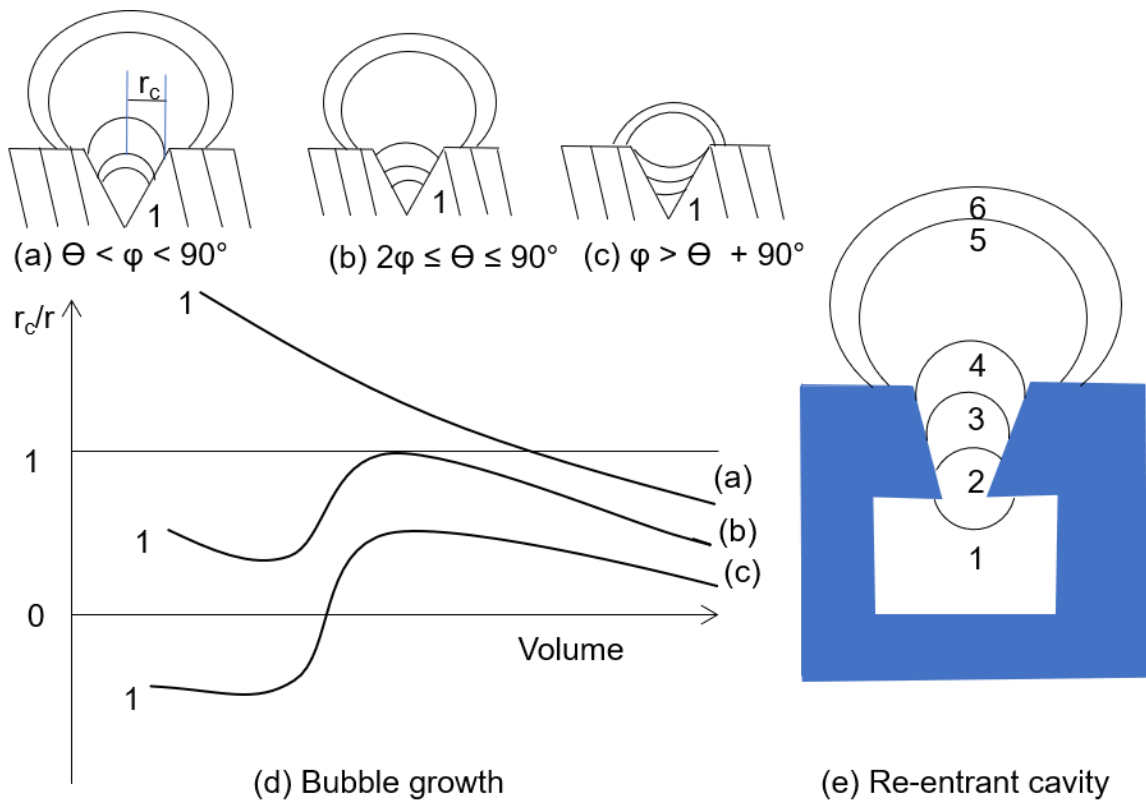
Figure 2.9: Bubble growth cycle for various conditions: (a-c) conical cavities (d) variation of bubble radius as a function of volume and (e) re-entrant cavity [33]

The nucleation superheat equation (Eq. 2.2) was derived assuming a constant temperature field, but during the bubble waiting period (at the start of boiling cycle), heat transfer by transient conduction near the surface takes place after bubble departure. Hsu

criterion [35] describes that only a set of nucleation sites will be active for a given wall superheat, and it sets the maximum and minimum radius of bubble radius that can grow in the temperature field. According to this criterion, the bubble radius originating from a cavity with mouth radius (r_c) larger than $r_{cric, max}$ will collapse due to subcooling, while cavity radius r_c smaller than $r_{cric, min}$ will require a larger superheat to grow. For example, it was shown that for water at atmospheric pressure with a thermal boundary layer thickness ($\delta_t = 0.2$ mm), no nucleation site from mouth radius (r_c) above 0.1 mm can be activated at any superheat. Once the nucleate boiling develops, the bubble growth can extend from one cavity into adjacent cavities, thereby activating those cavities as well. This can lead to incipience overshoot which is random in nature.

In the fully developed nucleate boiling regime, the boiling heat transfer can be mechanistically modeled as a sum of 3 significant heat transfers modes [36] which are convection, vaporization and transient conduction. These 3 modes can be related to various bubble dynamic parameters associated with bubble growth, such as bubble frequency (f_b), bubble departure diameter (D_b), number of nucleation sites (N_t) and waiting time (t_w).

$$q''_{total} = \frac{\pi}{6A} \rho_v h_{fg} \sum_{n=1}^{N_t} (f_{b,n} D_{b,n}^3) + \frac{2\pi k_l (T_w - T_{sat})}{A\sqrt{\pi \alpha_l}} \sum_{n=1}^{N_t} (D_{b,n}^2 (\sqrt{t_{w,n}} f_{b,n})) \qquad 2.3$$

$$+ [1 - \frac{\pi}{4A} \sum_{n=1}^{N_t} (D_{b,n})^2] h_{turb} (T_w - T_{sat})$$

where $q"_{total}$ is heat flux from the surface of area A with wall superheat ($T_w - T_{sat}$) submerged under liquid of thermal conductivity (k_l) and thermal diffusivity (α). Term 1 represents heat transferred via latent heat of evaporation (h_{fg}), term 2 represents quenching heat flux that corresponds to thermal boundary layer around the bubble and heated surface, and term 3 represents convective heat transfer coefficient. The proportion of heat tranfer due to microlayer evaporation decreases as the wall heat flux increases [37]. Gerardi et al. [36] observed that the temperature around a nucleation site varies substantially during nucleation during the entire bubble development cycle and most of the heat is spent as a quench flux opposed to latent heat for vaporization. Halton et al. [38] suggested that the relative magnitude of surface tension and inertial forces compared to buoyancy forces determines the bubble departure diameter. The larger bubble departure diameter implies smaller active cavities on the surface.

From a theoretical understanding of the influence of the surface features on the number, size, and shape of nucleation sites, bubble growth rate, departure diameter, waiting period, nucleation site density, bubble frequency, it is evident that surface features can greatly influence the heat transfer rate across the surface. The boiling phenomenon can only be described completely by considering the effect of cavity dimensions on these bubble dynamic parameters, following which a simplistic correlation of the form h = f (Crater size) can be developed. In the absence of a complete theory of boiling, the empirical correlations based on surface roughness parameters can provide insights, and help develop better mechanistic models.

2.2.1 Influence of initial wetting state on boiling heat transfer

Apart from Bangkoff's wettability criterion, which looks at wetting in terms of advancing contact angle and cavity angle, and does not consider capillary pressure, the liquid normal to a rough surface can exhibit 2 states of macroscopic static contact angle depending on the difference between its Laplace pressure and capillary pressure. A surface in Wenzel state exhibits higher boiling curve compared to that in the metastable Cassie Baxter state due to the 3 phase contact line pinning that prevents vapor blanketing state as shown by Fig. 2.10 by Allred [39]. Cassie Baxter state can be changed to Wenzel state by degassing the entrapped air with an external heater before boiling experiment. However, degassing is generally performed before pool boiling experiments to assure that all surfaces are in Wenzel state, and bubbles grow individually on the nucleation site. Wenzel state is preferred for aspect ratio higher than 5.5 for micropillars, as found in [40]. The homogeneous wetting is represented by Wenzel state, and the apparent contact angle is obtained by multiplying Young's static contact angle with roughness ratio r (r = true area of contact/apparent area of contact). For heterogenous wetting, the apparent contact angle is obtained by using Cassie Baxter equation, which takes into account roughness ratio (r) and the fraction of solid surface area wet by the liquid (f).
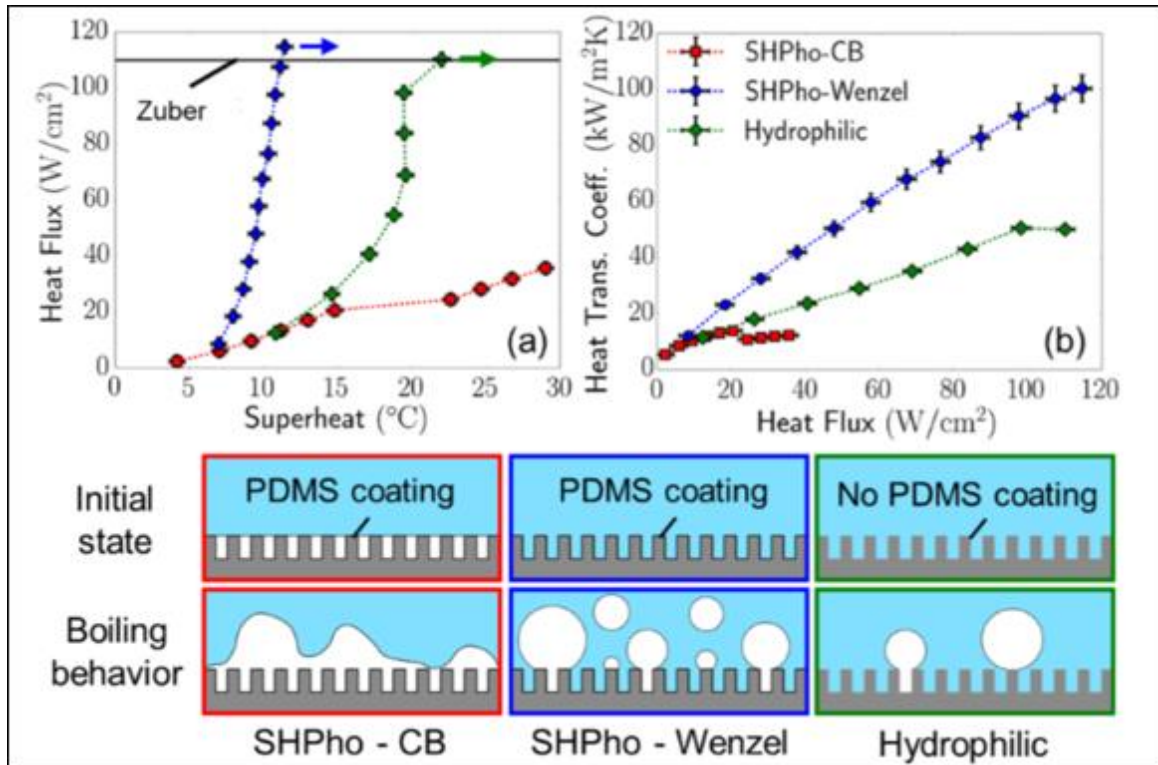
Figure 2.10: Influence of initial wetting condition on boiling [39]

2.3   Surface characterization parameters and boiling correlations

Much research has been carried out to correlate surface characteristics with boiling behavior. Earlier studies of natural convection on structured plates have determined heat transfer enhancement as a function of surface feature heights. For the macro-roughness features, most of the heat transfer analysis is based on fin (extended surface) efficiency analysis. Contradictory results have been found in the literature. Some authors advocate that heat transfer is unaffected by roughness as long as roughness features are larger than the thermal boundary layer, or at least unaffected at the base of the roughness feature [41].

Experimental and numerical studies by Pretot et al. [42] showed that, under laminar conditions for a sinusoidal profile (amplitude = 0.1 - 0.6 cm, period = 2 - 6 cm) at a heat flux density of 15-60 W/m^2 for two fluids (air or water), Nusselt Number is indeed higher above peaks as compared to above valleys, where heat conduction is the dominant mode of heat transport as shown in Figure 2.11.
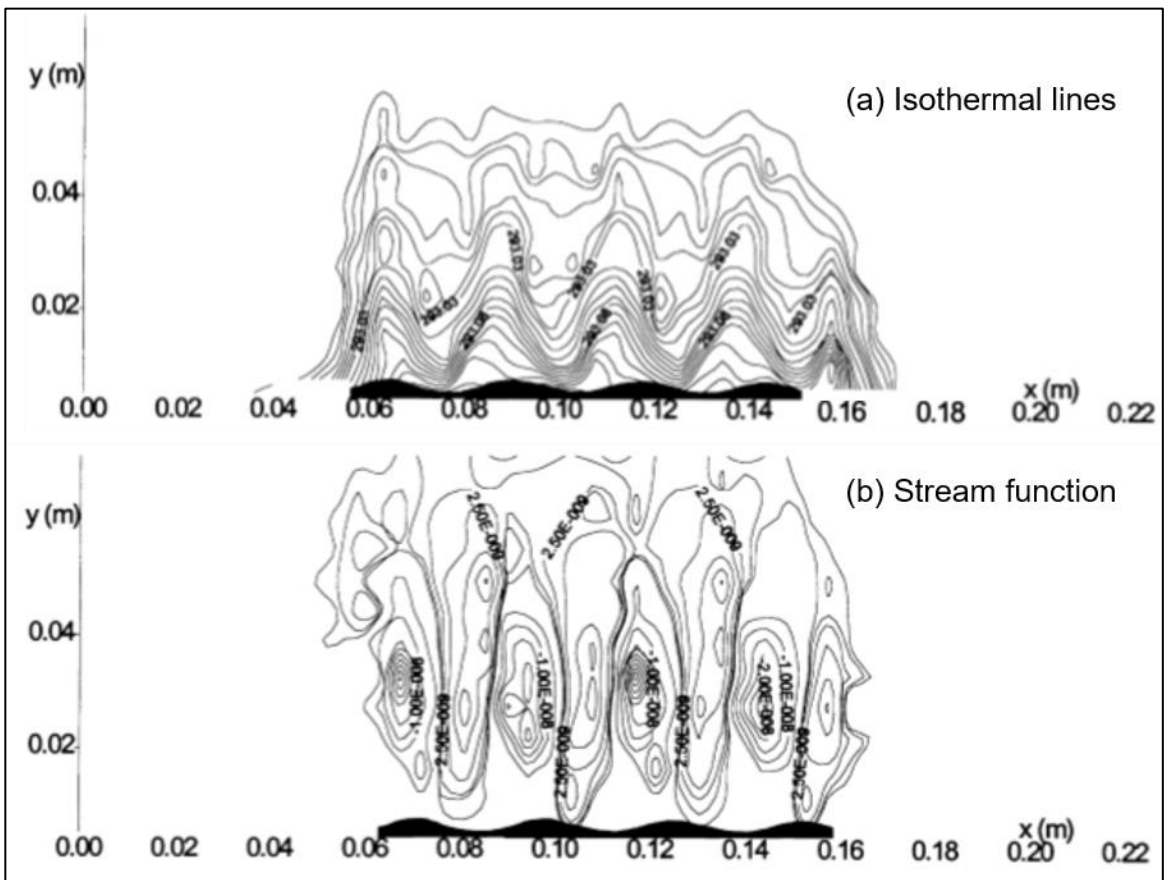
Figure 2.11: (a) Temperature field, (b) Velocity field for surface with sinusoidal profile field for water at q" = 25 W/m^2 [42]

They found that Nusselt Number decreases with an increase in amplitude and decrease in the period of protuberances. Figure 2.12 shows the isothermal lines and stream function for a flat surface for comparison [43].
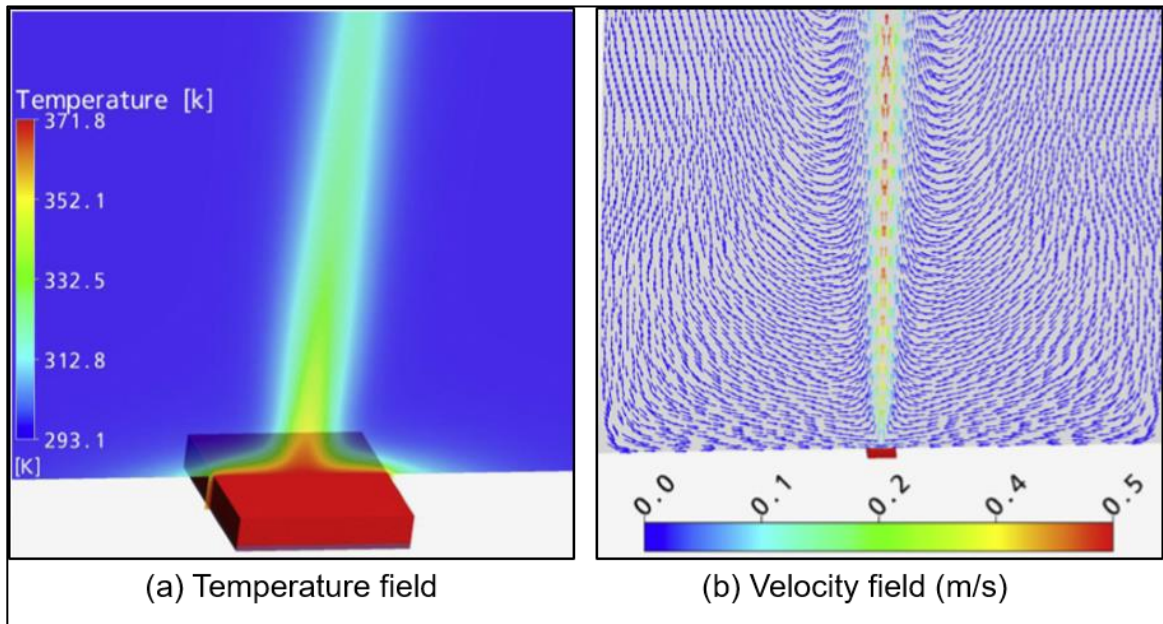
Figure 2.12: Temperature field, (b) Velocity field for plane surface (air) [43]

Other studies showed that surface roughness could change heat transfer because of the disturbance of thermal boundary layer in laminar to turbulent transition region [44], or roughness induces more turbulence in some cases [45]. The local Nusselt number is a strong function of Rayleigh Number, and different factors can accumulate to change the behavior of heat transfer, depending upon the thermodynamic phase of working medium (liquid/gas).

Recently, researchers have considered the effect of microroughness features on convection heat transfer. In a study by Kim et al. [46], micro fin arrays with fin heights of

100 and 200 µm were fabricated, having six different array spacings of 30, 60, 90, 160, 260, and 360 µm. They found the heat transfer coefficient with 100 µm fin to be higher than that of 200 µm, and the HTC to increase with an increase in spacing, and that plate orientation had little effect on heat transfer coefficient as heat diffusion was found to be dominant over buoyancy effects. Similar results were obtained by Mahmoud et al. [43]. The correlation suggested by Kim et al. [46] was developed for air in taking microroughness into account:

$$Nu_r = 1.18 \left[Ra_r \left(\frac{r}{H}\right)^4 \left(\frac{r}{L}\right)^4 \right]^{0.147} \qquad 2.4$$

where Nusselt Number is $Nu_r = (h_c r)/k$, Rayleigh Number is $Ra_r = (g\beta (T_w - T_a) r^3)/v\alpha$, $r = 2HS/(H+S)$, where H = fin height and S being fin spacing and β, v, k are the thermal expansion coefficient, kinematic viscosity and thermal conductivity of the liquid, respectively.

For the nucleate boiling regime, the surface texture indices as advocated by ISO standards have been found incapable of explaining heat transfer behavior. Various correlations have been proposed in the past to study the effect of average roughness *Ra* for a wide range of fluids. Branson [5] in 1962 found that a lapped surface had 600% higher boiling heat transfer coefficient than a surface made by polishing of comparable roughness. Chowdhury and Winterton [47] concluded that boiling heat transfer coefficient increases with roughness as along as a similar method of surface preparation is used. On the other

hand, Vachon [48] found out that heat transfer coefficient does not increase after a particular value of roughness. Jones et al. [23] experimentally studied the pool boiling on EDM textured surfaces with roughness range (Ra 1-10 µm). They observed similar boiling heat transfer coefficient for intermittent roughness (Ra 1-5 µm), but extraordinary high boiling heat transfer coefficients for the roughest surface $Ra = 10$ µm (Fig. 2.13). For similar roughness range, boiling heat transfer increased continually for FC-77. These observations point out the weakness in using Ra as a universal characterizing parameter for boiling heat transfer.
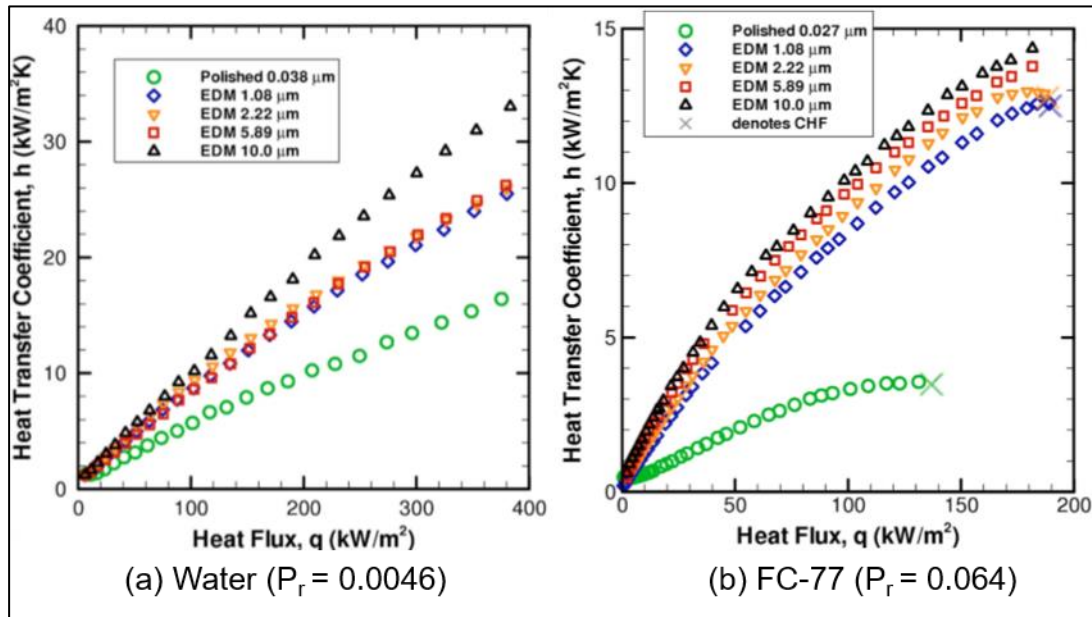
Figure 2.13: Heat transfer coeffieicnt curves for (a) Water at ($P_r = 0.0046$)
(b) FC-77 at ($P_r = 0.0064$) [23]

On the contrary, Jobardo [28] found the heat transfer coefficient to start decreasing after a certain value of Ra for surfaces made by sandblasting on both refrigerants R-134a

and R-123. He asserted the system pressure and surface wettability to be important factors which should be accounted for developing correlations for boiling heat transfer. The roughness values in their studies are comparable to the values assessed in [23].
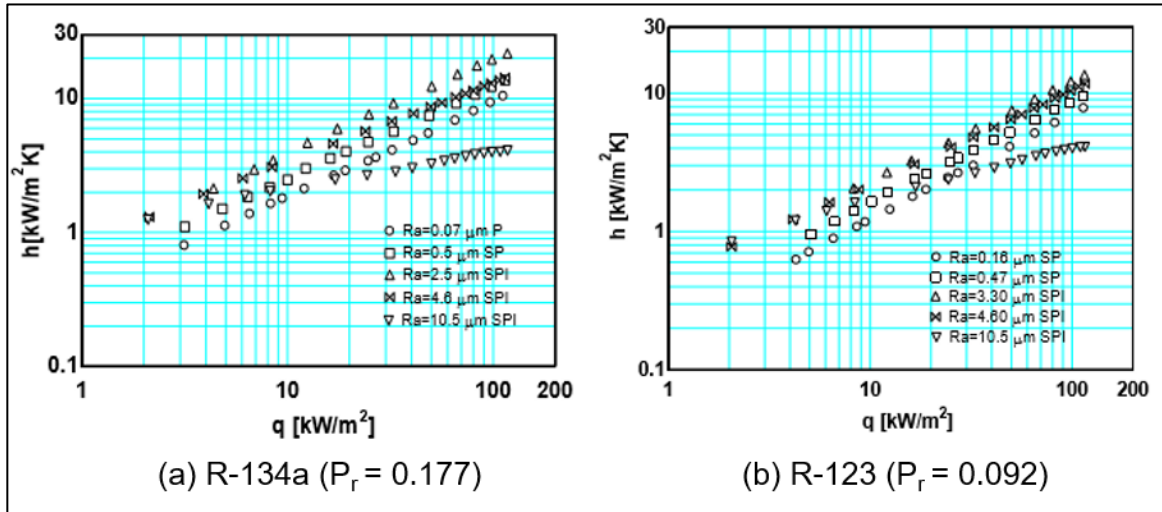
Figure 2.14: Heat transfer coefficient curves for (a) R-134a at P_r = 0.177 (b) R-123 at (P_r = 0.092) [28]

Kim et al. [49] found that the boiling heat transfer coefficient for etched surfaces increased with roughness as shown in Figure 2.15. All these studies point to the same conclusion that defining a surface with just one roughness parameter (average roughness *Ra*) can be misleading in characterizing a surface for boiling heat transfer.
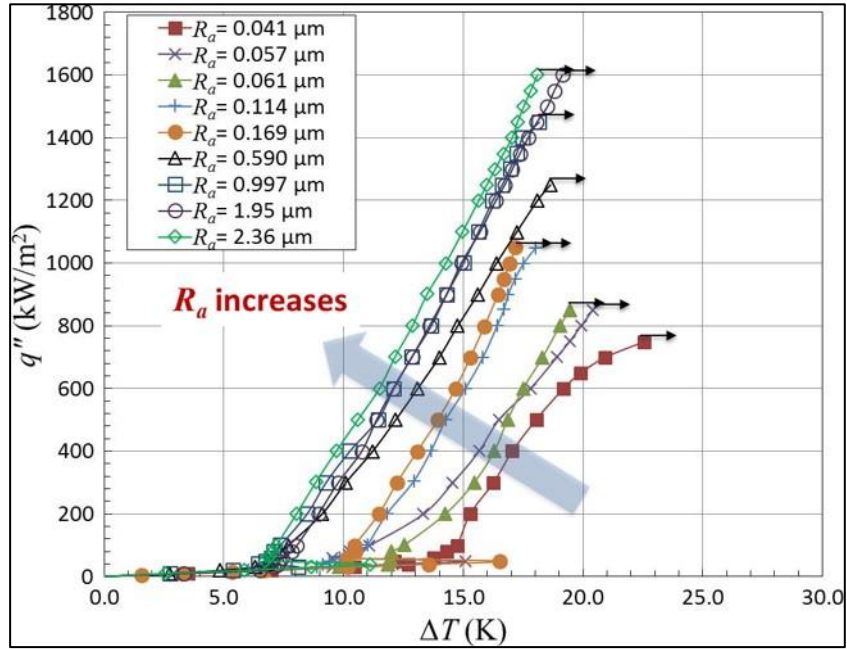
Figure 2.15: Boiling curves for micromachined surfaces by Kim et al. [49]

Rohsenow correlation (Equation 2.5) is the most commonly used correlation to account for the surface-liquid combination. Values of C_{sf} ($C_{sf} = 0.011$ for Aluminum ($Ra = 3.6\mu m$)) are available for various surface liquid combinations [50].

$$q'' = \mu_l h_{fg} \sqrt{\frac{g(\rho_l - \rho_v)}{\sigma}} \left[\frac{c_{p,l}\Delta T}{C_{sf} h_{fg}. \mathrm{P}\, \mathrm{r}_l^b} \right]^a \tag{2.5}$$

In the literature, h (heat transfer coefficient) for a fluid is correlated as $h = f(R^m)$, where m can be a function of reduced pressure and contact angle. For aluminum and water, Jones [23] proposed h to be proportional to $h\, \alpha\, Ra^{0.1}$ for $0.038 < Ra < 10\,\mu m$ and suggested that h depends on the type of fluid as well. Other correlations like Cooper [51], Liener [52], Gorenflo [53] are available for a wide range of liquids, but they are suitable for specified

34

roughness and operating conditions. Generally, m varies from 0.09 for water to 0.2 for higher wetting liquids like R-11, R-123, R-134a etc. for roughness values up to 10 µm [53, 23, 48].

Kim et al. [55] used roughness ratio to account for the influence of surface modification, which was within 30% of what is predicted by pin-fin analysis. McHale [56] in 2013 used some hybrid parameters to account for surface effects. He used parameters like Area ratio (Ar), Mean roughness (Ra), Mean surface normal angle (Φ_m) and maximum surface curvature (k_{max}) in filtered and unfiltered form (filtered by cut off wavelength equal to base of bubble departure diameter) and derived Mean Absolute Errors (MAE) in predicting heat transfer coefficients for his experiments as wells as from [23]. He found MAE of 17.7%, 13.8% and 9.9% for FC-72, FC-77 and water respectively by choosing Ra as the characterizing parameter. Also, he found filtered Ar to be best parameter to correlate boiling heat transfer for all fluids. For water, MAE with Ar, Ra, Φ_m, k_{max} was 8%, 9.9%, 8.2%, and 14.2% respectively, but he found no significant improvement in terms of MAE by filtering.

Mpholo [57] used the 2D profile data of Jones et al. [23] to determine the effect of the size of active nucleation sites on boiling incipience. However, he asserted that choosing a profile that depends on the resolution of the instrument cannot give the complete effect of surface profile on boiling and questioned the validity of macroscopic contact angle to analyse the microscopic cavities for boiling.

ISO-4287:1997 provides several other roughness parameters that can be categorised as amplitude parameters like *Ra*, *Rq*, *Rp*, *Rv*, *Rz*, spacing parameters such as *Rs*, *Rsm*, and other derived parameters like *Rsk*, *Rku*, *Rmr* [58]. Some of these parameters have been used by various authors to characterize boiling heat transfer as shown in Table 2-2.

Table 2-2: Boiling heat transfer correlation based on roughness parameters

Author	Dependence	Parameter $R(\mu m)$	Heat Flux (kW/m^2)	Surface / Preparation	Pressure (P_r)
Fedders [54]	$h \propto R_{p,old}^{0.133}$	$R_{p,old}$ 0.1 − 3.6	50	Stainless steel Sandpaper, Sandblasting	0.013 − 0.09
	$h \propto R_{p,old}^{0.12}$		1000		0.012
	$h \propto R_{p,old}^{0.10}$		1000		0.089
B Jones [23]	$h \propto R_a^{0.1}$	Ra 0.03 − 10	50-300	Aluminum Sandpaper, EDM	0.0046
Mchale [56]	$h \propto aR_a + b$	Ra 0.03 − 10	50-300	Aluminum Sandpaper, EDM	0.0046
	$h \propto aR_{a,fl} + b$				
	$h \propto aA_r + b$				
	$h \propto aA_{r,fl} + b$				
	$h \propto a\emptyset_m + b$				
	$h \propto a\emptyset_{m,fl} + b$				
	$h \propto ak_m + b$				
	$h \propto ak_{m,fl} + b$				
Kim [49]	$h \propto aR_a^{0.109}$	Ra 0.04 − 2.3	800	Copper Sandpaper	Unspecified

Luke et al. [59] suggested using a parameter P5* (Fig. 2.16) that is defined by statistical measurements of 3-point contact of roller of radius (2500 - 25000 µm) to determine the number of potential nucleation sites on surface profile. They found good agreement qualitatively in terms of number and distribution of nucleation sites. However, location of specific theoretical nucleation sites did not match the experimental nucleation sites
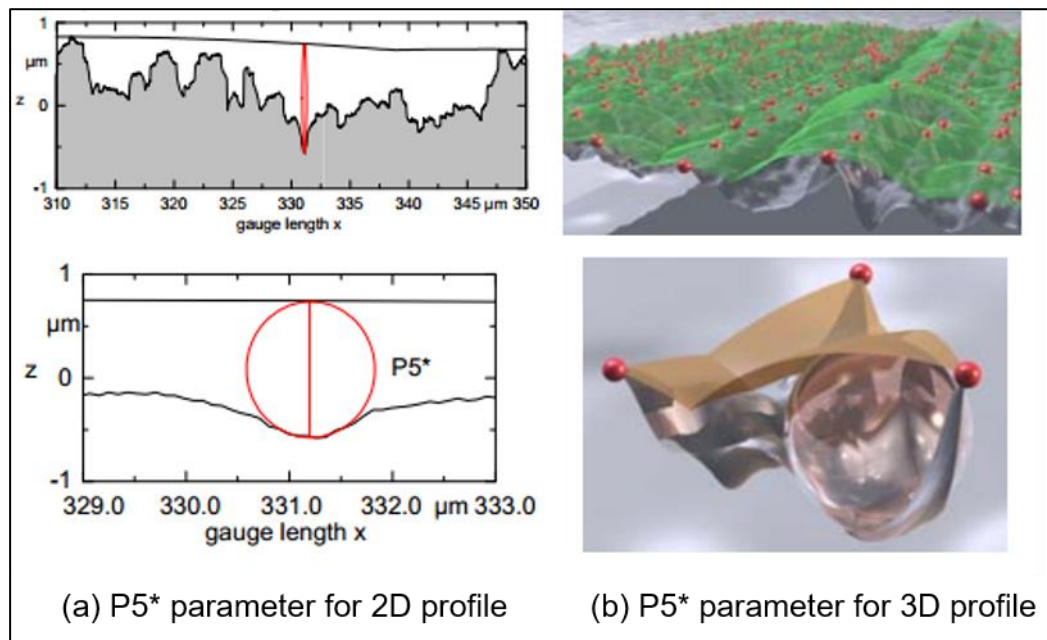
Figure 2.16: P5* parameter suggested by Luke for (a) 2D profile (b) 3D profile
[59]

2.3.1 Specific surface characterization parameters for EDM

The EDM process allows for the control of crater shape and size, and thereby affecting the parameter other than Ra like Rsm and $R\Delta q$ only (fig. 2.17), as shown by Klink et al. in [7].
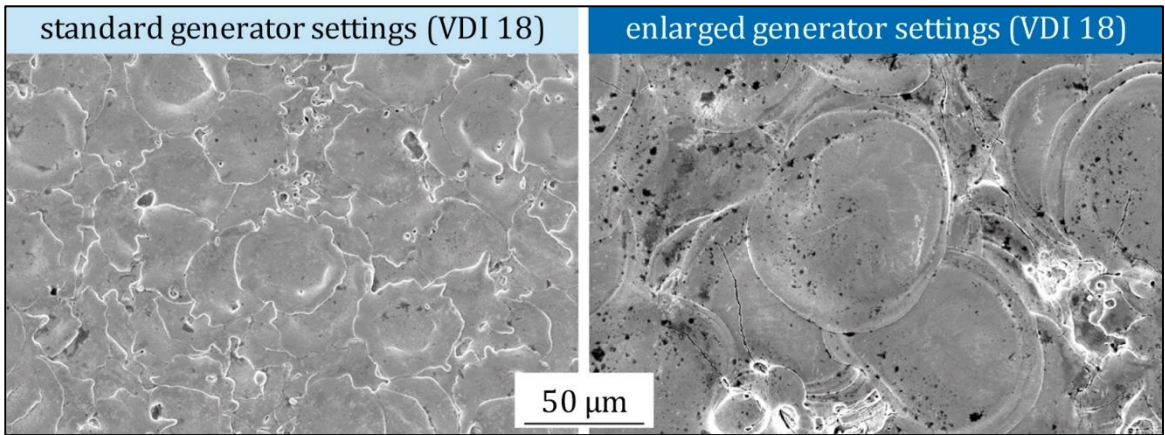
Figure 2.17: Different crater diameter within same roughness regime [7]

It has been observed that by increasing the pulse current (i_e), crater depth increases monotonously due to higher intensity of pulse energy and higher temperature of arc column, whereas with an increase in pulse discharge duration (t_e), crater depth increases and then decreases, owing to lower intensity of pulse energy on the workpiece due to expansion of the plasma channel [60]. EDM process is also affected by a change in dielectric fluid. In general, a higher material removal rate and lower roughness are obtained by using water as dielectric fluid compared to hydrocarbon oil [61].

Apart from normal ISO parameters, there are some surface characterization parameters proposed by some authors, considering the random, stochastic nature of the EDM process. Topographical indices of a "characteristic crater" of electrical discharge machined surfaces such as crater depth, crater diameter can be determined by using a simple Data Dependent System (DDS) methodology [62] as shown in Figure 2.18. Various derived

parameters like aspect ratio, volume, radius of curvature of the crater can be obtained after knowing the dimensions of the characteristic crater.

(a) Surface profile generation   (b) Section of characteristic crater
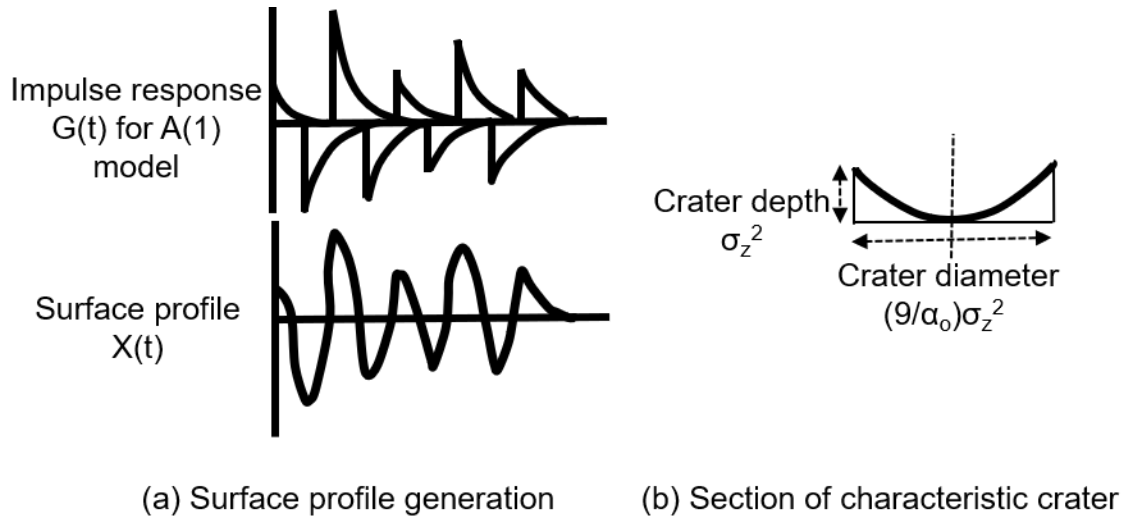
Figure 2.18: Data dependent system modeling for EDM surfaces [62]

The electrical discharged machined surface profile can be assumed as formed of superimposition of series of shock/impulses of variable intensity and spacing occurring at a finite interval t (t=1 for fig. 2.18 (a)). The impulses, also known as white noise Z(t), and its convolution with impulse response or Green function G(t) gives the corresponding surface profile X(t). α_o is called the autoregressive parameter. G(t) corresponds to the shape of the crater, and Z(t) corresponds to the scale of the crater. The first order A (1) stochastic differential equation model to describe surface profile generated by EDM is given by:

$$\frac{dX(t)}{dt} + \alpha_o X(t) = Z(t), \qquad\qquad 2.6$$

whose solution is given by,

$$X(t) = \int_0^\infty G(u)Z(t-u)du = \int_0^\infty e^{-\alpha_o u}\,Z(t-u)du \qquad 2.7$$

The review explains the need for looking closely at surface characterizing parameters of rough surfaces for boiling, that are specific to the manufacturing process.

2.4   Summary/research objectives and research plan

The objective of this research was to fabricate textured surfaces with electrical discharge machining (EDM) of Aluminum 6061 and investigate the enhancement in pool boiling heat transfer, in terms of EDM machining process parameters (pulse current (i_e), discharge duration (t_e)) as well as surface characterization parameters (ISO and Data dependent system parameters). Owing to the difficulty in correlating boiling data in terms of Ra as found in literature, alternative roughness parameters will be assessed against boiling data. It will be complemented by a qualitative analysis of bubble dynamics with high-speed imaging, to understand the differences in boiling performance associated with the changes in surface topography. The process limiting factors will be identified and optimized to enhance heat transfer. The most critical machining parameters that affect surface topography are pulse current (i_e) and pulse discharge duration (t_e). Although other EDM machining parameters like voltage (U), off-time (t_{off}), erosion time (t_e) are available; but their effect on surface topography is negligible. Boiling heat transfer curves will hence be characterized in terms of pulse current and pulse discharge duration.

Furthermore, re-entrant cavities will be developed on EDM textured surface by plastically deforming the peaks of the surface profile using a hydraulic press, and its thermal performance will be quantified. These mushroom-head type cavities act as more stable vapor traps. In addition, the boiling performance of EDM surface with the highest heat transfer coefficient will be compared with other enhanced surface geometries available in the boiling literature.

3 Experimental setup and methodology

3.1 Experimental setup

The experimental setup for investigating pool boiling consists of a boiling vessel as shown in Fig. 3.1. The vessel comprises a 20 cm diameter stainless steel pipe chamber, in which the bulk liquid is contained by means of a stainless-steel skirt fixed at the bottom. At the center of this skirt, the test block of 25.4 mm diameter and 71 mm length is affixed by mounting screws. The test block was insulated from the surrounding by a polystyrene-walled stainless-steel cylinder to prevent radial heat losses and direct heat flux only in the axial direction. Three 250-Watt WATLOW cylindrical heat cartridges of 6.35 mm diameter and 38.1 mm length were installed into test block at the bottom to provide heat flux at the boiling surface. These are referred to as Main heaters and can provide a maximum heat flux of 1.48 kW/m². Three type E thermocouples are installed on test block at 5 mm apart from the top surface as well from each other at 120 ° angle axially to each other to obtain temperature distribution in the test block, as shown in Figure 3.3. Two heaters of 3000 kW power are installed around the stainless-steel chamber to bring the fluid to saturation temperature. They are referred to as bulk fluid heaters. The temperature of the bulk fluid is monitored via 2 type E thermocouples which are immersed into the bulk fluid. The support disc at the bottom was used to prevent mixing of air around the test block and air in the room. It was supplemented by an air heater that kept the temperature of the air above the support disc closer to the test block temperature. A condensing coil is used to prevent fluid

loss during the experiment, for which a needle valve regulated the water flow rate, and a

heater is installed to heat the inlet condensing water to prevent subcooling.
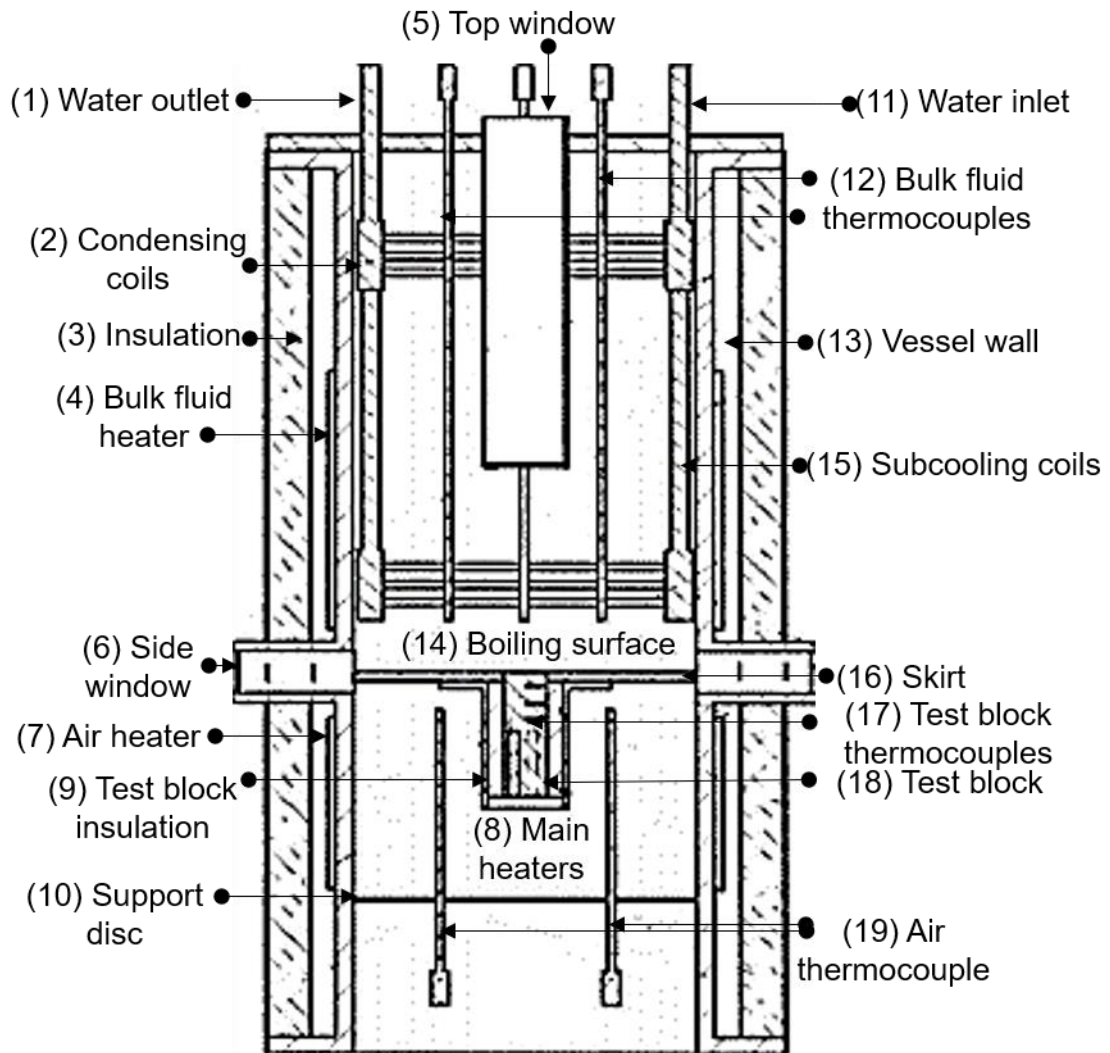
Figure 3.1: Pool boiling vessel

A thermocouple is installed to monitor inlet condensing temperature as well. Two

opposing glass side windows are used to visualize the boiling phenomenon on the test block

surface. A top window also allows for visualization of boiling phenomenon from above.

An aluminum cover lined with insulation is provided to protect the user from contacting the heaters and reduce heat loss.

3.1.1 Heater control
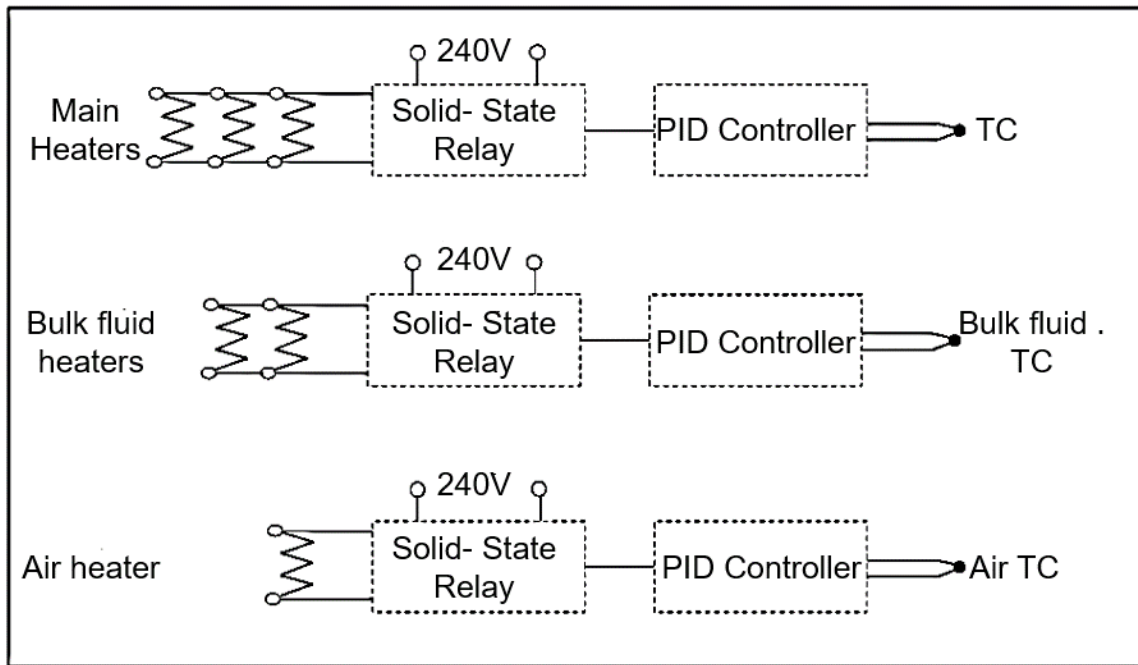
Figure 3.2: Heater controller circuit

Figure 3.2 shows the simplified diagram of the heater controller circuit. The bulk fluid heater, air heater, and main heaters power supply can be controlled by series of on/off solid-state relays via PID controllers. In the course of experiments for this study, the main heater was controlled manually by varying the input power as a percentage instead of using the PID controller. Therefore, all the experiments are based on heat flux-controlled boiling. The heaters were run up to 80% in the first stage and up to 60% of full capacity in the next

stages to prevent damage to heater and test block. The bulk fluid heater and air heater were controlled via a PID controller to maintain conditions for experiments using the feedback from thermocouple installed near the heaters.

3.1.2 Data acquisition

Thermocouples are connected to a Keithley data acquisition system Model 2700 which transfer thermocouple's readings to ExceLinx software and are thus become accessible to the user.
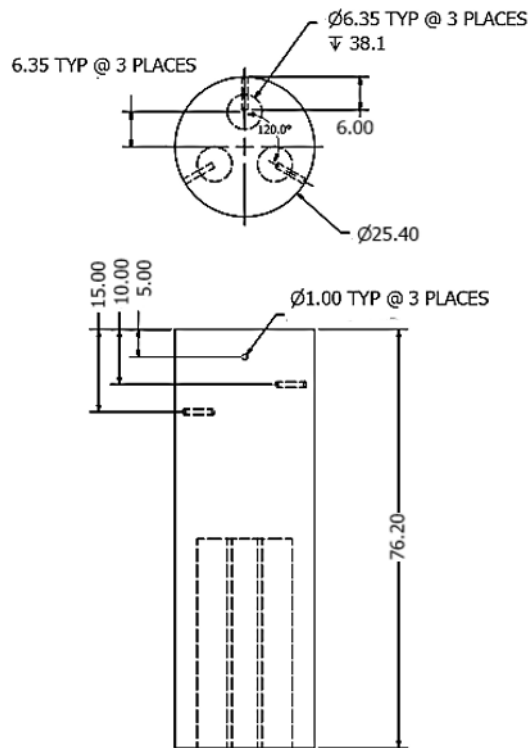
Figure 3.3: Test block

The temperature for the each of following thermocouples is measured at a frequency of 0.2 Hz. Figure 3.3 shows the diagram of the test block. In reference to Figures 3.1 and 3.3, thermocouples are embedded at the following positions:

- Three thermocouples in the test block

- Two Bulk fluid locations

- The air around the test block

- Water heater

- Air heater

- Inlet condensing water

3.1.3   Thermocouple calibration

All the thermocouples used in the experiment were calibrated against a high-precision resistive temperature detector probe (Omega DP251 precision RTD thermometer with PRP-3 probe) which is calibrated to 0.01 °C in the temperature range of -50 °C to 250 °C. This was carried out by submerging thermocouple probes in an insulated, heated oil bath (assuming uniform temperature field) and calibrating the thermocouples against RTD by increasing temperature of oil bath in sequence. A regression analysis between readings of thermocouple probes and RTD was used to determine the accuracy and precision, and document the equation for calibrated temperature in terms of the measured temperature.

3.1.4 Boiling setup extension for high-speed imaging

A major challenge in visualizing the boiling phenomenon was the obstruction caused by bubble incipience along test block periphery from the gap between test block and steel skirt. Therefore, for some of the experiments, where bubble visualization was necessary, a setup extension was used. The setup extension (Figure 3.4) consisted of a test plate placed on aluminum heating block and mounted on the Skirt (16) of the boiling vessel (Figure 3.1).
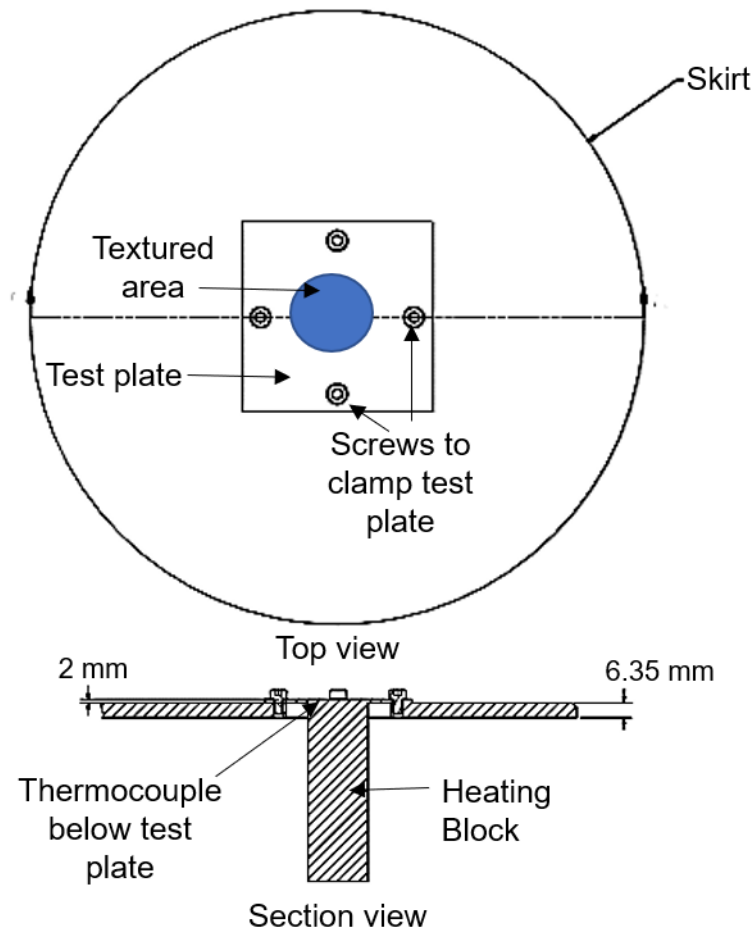
Figure 3.4: Setup for boiling visualization

A thermal paste with high thermal conductivity (k = 26.7 W/mK) was used to minimise the thermal resistance between test plate and heating block. A thermocouple was installed at the base of the test plate to measure the surface temperature via steady state heat conduction equation along the plate thickness. The wall heat flux was calculated from the thermal gradient in the heating block. This extended setup is similar to the boiling setup used by Cooke et al. [22]. Heat loss due to the extended surface of test plate was quantified to validate the test fixture. A maximum heat loss of 4 W was encountered during the experimental runs. Kim et al. [63] have used similar extended surface method for boiling visualisation, and were able to obtain repeatable results. A Photron FASTCAM 1024PCI high-speed imagining camera was employed to visualize boiling through one of the side windows. A 250 W halogen lamp illuminated the second window. High-speed images were captured at 3000 fps at a resolution of 512 x 512 pixel with 39 pixels per mm. The middle 25.4 mm area of the test plate was textured. Appendix A-1 shows the simulated temperature field for steady state heat transfer, assuming an intermediate heat transfer coefficient of (a) 30 kW/m^{2}K and (b) 200 kW/m^{2}K over the whole surface plate for 4.2% and 30% of total 750 W heater supply respectively. Furthermore, (c) shows the linear temperature distribution inside the test block for heater conditions of (b). This setup was considered adequate for boiling visualization from the EDM textured surface.

3.2 Determination of the applied heat flux (q") and the surface temperature (T_s)

Heat flux through the heated surface and surface temperature is determined from the temperature profile obtained from the thermocouples installed along the length of the block. Assuming the temperature profile is linear and no heat loss in the radial direction, the heat flux and surface temperature can be obtained from Equation 3.1:

$$T_s = \frac{\sum T_i \sum x_i^2 - \sum T_i x_i \sum x_i}{n \sum x_i^2 - (\sum x_i)^2} \qquad 3.1$$

The heat flux is determined by using the steady-state heat conduction equation for one dimension in the form of Equations 3.2 and 3.3:

$$q" = k.\frac{dT}{dx} \qquad 3.2$$

$$q" = k.\frac{\sum x_i T_i + \sum x_i \sum T_i}{N \sum (x_i^2) - (\sum x_i)^2} \qquad 3.3$$

Where k is the thermal conductivity of aluminum 6061 test block and T_i is the reading of thermocouple at distance x_i from the boiling surface.

3.3   Uncertainty analysis

An uncertainty analysis was carried out to find out the errors associated with determining the accuracy and precision of the boiling curve parameters using Eq. 3.4. These errors arise from the errors associated with inherent uncertainty and position of thermocouples in the experimental setup.

$$Y_R = \sqrt{\left(\frac{\partial R}{\partial X_1}Y_1\right)^2 + \left(\frac{\partial R}{\partial X_2}Y_2\right)^2 + \cdots + \left(\frac{\partial R}{\partial X_n}Y_n\right)^2} \qquad 3.4$$

where Y_R is total uncertainty in the parameter R which depends on variables X_1, X_2 ... X_n and Y_1, Y_2 ... Y_n is corresponding uncertainties in each of these independent variables.

3.3.1   Uncertainty in calculating the surface temperature (T_s)

The uncertainty associated with each thermocouple in the test block was $\pm$ 0.4 °C, uncertainty in the position of Thermocouple position is $\pm$ 0.1 mm. Using the equation, the maximum uncertainty in surface temperature was $\pm$ 1.14 °C for test block (Figure 3.3). Considering an average surface temperature of 115 °C, the uncertainty in surface temperature was 0.9%. For the boiling setup extension shown in Figure 3.4, a maximum uncertainty of $\pm$ 0.5 °C was obtained in calculating the surface temperature.

3.3.2   Uncertainty in calculating the heat flux ($q"_s$)

Using the equation of heat flux and considering uncertainty in temperature gradient in the test block and change in thermal conductivity of aluminum due to increasing temperature

yields a maximum uncertainty of $\pm$ 21.8 kW/m^2. Considering an intermediate heat flux of 800 kW/m^2 gives an uncertainty of 2.7%.

3.3.3 Uncertainty in calculating the bulk fluid temperature (T_{sat})

The equation gives the bulk fluid temperature is given as:

$$T_{sat} = (\frac{T_1 + T_2}{2})$$
3.5

Using the equation for bulk fluid temperature in the expression for uncertainty with an individual error of $\pm$0.4 °C in each thermocouple yields an uncertainty of $\pm$ 0.21 °C in calculating bulk fluid temperature, which is 0.21% at an average saturation temperature of 100 °C.

3.3.4 Uncertainty in calculating the surface superheat (T_s - T_{sat})

Based on uncertainty in surface temperature and bulk fluid temperature, the uncertainty in calculating surface superheat is $\pm$1.15 °C, which is equal to 8.6% assuming an intermediate superheat of 15 °C.

3.3.5 Uncertainty in calculating the heat transfer coefficient (h)

The heat transfer coefficient was computed using the Newton cooling equation:

$$h = \frac{q''}{T_s - T_{sat}}$$
3.6

A maximum uncertainty of 4.01 kW/m^{2}K at an intermediate heat flux of 800 kW/m^2 and superheat of 15 °C is obtained using uncertainty analysis.

3.4 Parameters investigated and experimental conditions

3.4.1 EDM texturing

Figure 3.5: Electrical Discharge machining setup

Figure 3.5 shows the EDM machine tool at McMaster University and the machining setup. It is an Agietron Impact 2 Sink EDM machine. The drive system, controlled by high-performance brushless AC servomotors, contains four degrees of freedom; three linear motions and one rotational motion with a resolution of 0.1 μm and 0.1 μ° respectively. The traversing range of the working tank is 350 mm, 250 mm, and 350 mm for X-, Y-, and Z-axis respectively, with the highest linear speed of 1500 mm/min. An Intelligent Power Generator (IPG) is capable of providing DC pulses of range 100 V - 200 V open circuit voltage and a peak current of 1.2 - 72A. Copper tool electrodes were used in all the

experiments. The EDM textured surfaces were prepared by changing the pulse current (i_e)

and pulse discharge duration (t_e) on the EDM machine. The open gap voltage is set affixed

at 100 V and pulse off-time ($t_{off} = t_e$) is chosen for stable machining. The pulse discharge

duration can be varied from 0.4 µs to 10000 µs and beyond. The current was chosen to be

$i_e = 39$ A for 25.4 mm circular cross-section area for experiments to study the influence of

pulse discharge duration; because the current density of 10 A/cm² gives the highest MRR

and allow for stable machining and prevent arcing due to concentrated discharge under

given conditions of flushing. The discharge duration was varied from 65 µs to 6500 µs;

allowing for a wide range of surface topographies. Similarly, for constant t_e experiments, a

pulse current of 21 A to 72 A was chosen at a constant discharge duration = 274 µs.

Aluminum 6061 was chosen as the workpiece material, with all the surfaces machined to a

depth of 0.15 mm unless noted otherwise.

After machining, the surface was cleaned with a commercial electrical contact

cleaner, and let dry for 20 minutes, after which surface characterization parameters were

obtained by analyzing the surface on a profilometer. Various surface characteristic

parameters were obtained from the surface profile that includes height and spacing

parameters, and secondary derived parameters.

3.4.2   Roughness range of EDM textured surface and polished surface

Using a polishing technique, a smooth polished surface with $Ra = 0.07$ µm surface was

obtained. The workpiece was polished for 15 minutes at 150 rpm on a METPOL-2V

grinding machine with the polisher particle size of 1µm. This surface was chosen as a reference for assessing boiling behavior of all the other EDM textured surfaces. The *Ra* for various EDM textured surfaces varied ranged from 14.1 µm to 93.48 µm, for given machining parameters (i_e = 21 - 72 A, t_e = 65 - 6500 µs) with de-ionized water and hydrocarbon oil as dielectric fluids.

3.5 Surface characterization

A Mitutoyo profilometer and Keyence confocal microscope (Fig 3.7) were chosen to obtain roughness parameters and visualize surface asperities at up to 100 X magnification.
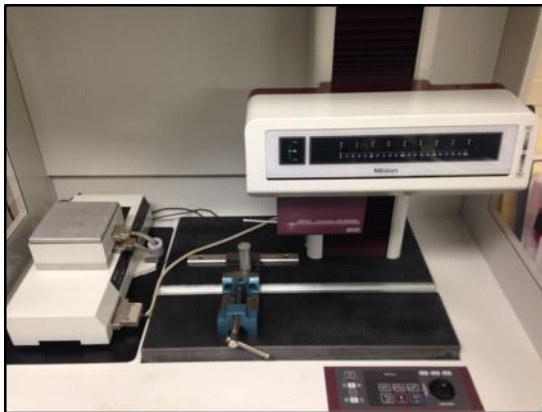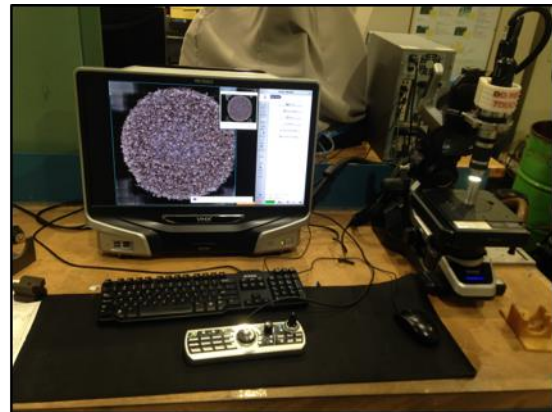
(a) Profilometer   (b) Confocal microscope

Figure 3.6: Metrological instrument used for surface characterization

3.5.1 ISO parameters

A profilometer with a tip radius of 5 µm was used to obtain the surface profile. The profilometer data was filtered based on cut-off wavelength suggested by ISO - 4287:1997

standard. The measurement trace of 20 mm was traced on 3 axial positions on surface and roughness parameters error was within 5% for all measurements. Various roughness parameters were calculated using the formulae as given below.
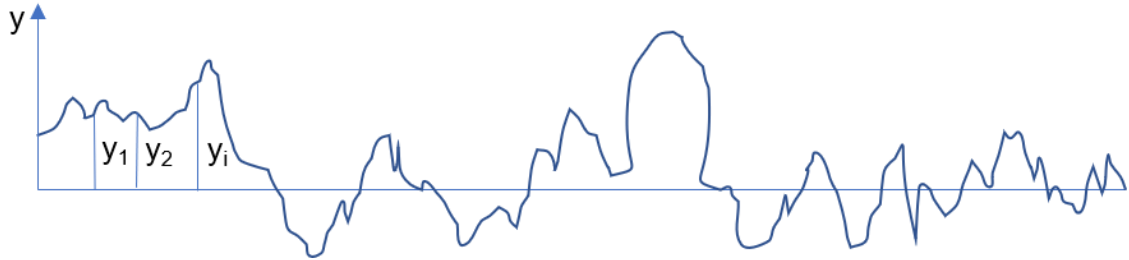
Figure 3.7: Surface profile

Ra: It is the arithmetic mean deviation of the absolute values of the distances (y_i) from the mean line to the profile.

$$Ra = \frac{1}{n}\sum_{i=1}^{n}|y_i| \qquad\qquad 3.7$$

Rp: It is the maximum value of the distances (y_i) from the mean line to the profile peak.

$$Rp = \max(y_i) \qquad\qquad 3.8$$

Rv: It is the absolute value of the deepest depth of the profile from the mean line.

$$Rv = \min(y_i) \qquad\qquad 3.9$$

Rz: It is the sum of the maximum peak height (*Rp*) and the deepest valley depth (*Rv*)

$$Rz = Rp + Rv \qquad\qquad 3.10$$

Rq: It is the root-mean-square sum of distances (y_i) from the mean line to the profile.

$$Rq = \sqrt{\frac{1}{n}\sum_{i=1}^{n} y_i^2} \qquad\qquad 3.11$$

Rsm: It is equal to mean spacing of profile irregularities (mean wavelength of the peak-valley cycles). The peak-valley cycle is determined by using the dead zone and count level zone which is defined as follows: The two lines drawn parallel to mean line at an equal distance from mean line at 10% of the maximum height of profile are known as count levels, and the range between the two count levels is called as the dead zone. The points when profile surpasses this dead zone is called peak and valley, and mean wavelength of this peak-valley cycle is called Rsm.

$$Rsm = \frac{1}{m}\sum_{i=1}^{m} |S_i| \qquad\qquad 3.12$$

Rs: It is equal to mean spacing of local peaks of the profile. Local peaks are defined as peaks on profile that are separated by maximum height/10 or more and evaluation length/10 or more.

$$Rs = \frac{1}{m}\sum_{i=1}^{m} |S_l| \qquad\qquad 3.13$$

56

Rmr: It is the ratio of the bearing length to the evaluation length. It is represented in percentage. The bearing length is the sum of section lengths obtained by cutting the profile with a line (slice level) drawn parallel to the mean line at a given level (10% for this case). An areal material ratio represents the area with a specific height c or higher.

Rsk: Skewness is defined as a value representing the degree of bias of the roughness shape

$$Rsk = \frac{1}{n.Rq^3} \sum_{i=1}^{1} y_i^3 \qquad \text{3.14}$$

Rku: Kurtosis is a measure of the sharpness of distribution of the roughness profile.

$$Rku = \frac{1}{n.Rq^4} \sum_{i=1}^{1} y_i^4 \qquad \text{3.15}$$

3.5.2   Data-dependent system parameters

Other hybrid parameters like characteristic crater depth and crater diameter were calculated using the formulas available from DDS methodology [62]. $4.5/\alpha_o$ is chosen as the effective correlation of characteristic crater because the value of Green's function approaches zero at this point ($e^{-4.5} = 0.01108$), or it represents the bottom of the crater. The data obtained from profilometer (5 µm stylus tip radius) is discretized with sampling interval ($\Delta = 1$ µm), which is less than half the radius of stylus tip and is considered adequate to give all the significant features of the profile. It was kept the same for all the specimens. The digitizing of profile was performed based on guidelines given in [64]. The number of measurements

(n) was chosen so that α_0 does not approach limiting values of 0 or infinity and was kept same for all specimens. As surface profile data is in the form of discretized data, the corresponding continuous parameters (α_o) for A (1) model can be obtained from discretized data as follows: If y_1, y_2, $y_{3\ldots\ldots}$ y_n are n measurements at sampling interval Δ, then

$$\alpha_0 = -\frac{\ln(\varphi_1)}{\Delta} \tag{3.16}$$

$$\varphi_1 = \frac{\sum_{t=2}^{n}(y_t - \bar{y})(y_{t-1} - \bar{y})}{\sum_{t=2}^{n}(y_{t-1} - \bar{y})^2}, \tag{3.17}$$

$$\bar{y} = \frac{1}{n}\sum_{t=1}^{n} y_t \tag{3.18}$$

$$\sigma_z = \sigma_a^2 \frac{2\alpha_o}{1 - \varphi_1^2} \tag{3.19}$$

Where $\sigma_a{}^2$ is the variance of a_t of the Uniformly Samples A (1) Model:

$$y_t - \varphi y_{t-1} = a_t \tag{3.20}$$

$$\sigma_a^2 = \frac{1}{N-1}\sum_{t=2}^{N}[(y_t - \bar{y}) - \varphi_1(y_{t-1} - y_t)]^2 \tag{3.21}$$

Effective correlation Length, Se = 4.5/α_o; Aspect ratio (AR) = 9/α_o 3.22

Crater Depth (CD) = $\sigma_z{}^2$, Crater Diameter (CDi) = 9/α_o.$\sigma_z{}^2$ 3.23

Radius of curvature $R_c = \frac{\sigma_z^2}{2}[1 + \frac{20.25}{\alpha_o^2}]$ 3.24

$$V_s = \frac{\pi}{6}(\sigma_z^2)^3[\frac{3}{4}(dia\ to\ depth\ ratio)^2 + 1] \tag{3.25}$$

$$V_e = 0.512(\sigma_z^2)^3(dia\ to\ depth\ ratio)^2 \tag{3.26}$$

58

3.6 Test procedure

The heat flux in the test block was increased using a controller in the first stage of experiments till heat flux of 1200 kW/m² for the initial trend of boiling curves with EDM machining parameters and were operated till heat flux of 900 kW/m² for subsequent analysis. These operating conditions were chosen to prevent any damage to the heater and keep the temperature in the test block below its melting temperature at any point (k_{Al} = 151 - 202 W/mK, melting point = 585°C). Experiments were performed at atmospheric pressure. The boiling vessel was washed with de-ionized water and dried before all experiments to remove all residual contamination. The thermocouples were installed into the test block and then assembled into the boiling vessel. 4 liters of deionized water was filled into the vessel from the top. The thermocouples were connected, and bulk fluid heaters and air heaters are turned on to set temperature of 110 °C and 105 °C respectively to bring bulk fluid close to saturation temperature. This slightly increased setting is to accommodate for heat loss. Once the temperature of the bulk fluid is close to 100 °C, the control of the heater was changed to manual mode at 50%, and bulk fluid is heated to remove incondensable gases. At the same time, the condensing water valve is opened, and the flow rate is maintained at 300 cm³/min with the needle valve. The heater of condensing coil is turned on to prevent subcooling and keep the temperature of condensing water at around 60 °C. After about 30 minutes, when all non-condensable gases are removed, the bulk fluid heater's control is changed back to the automatic setting with a set temperature of 100 °C. After this, the main heater for the test block are turned on to

0.5%, and reading is taken when the steady state is reached. It should be noted that the steady state condition is assumed when the temperature of all thermocouples is within 0.1 °C for 30 seconds. The power of the main heater is increased sequentially to 1%, 2%, 5%, 10%, 20%.....80% setting and steady state temperatures are recorded for analysis at each of these settings. After the pool boiling experiment is over, the heaters were turned off, and the liquid was allowed to cool using the sub-cooled coil before being drained out from the vessel.

3.7 Validation of water boiling curve

The boiling curve obtained for a smooth polished Aluminum surface (Ra = 0.07 µm) with de-ionized water, was validated against Rohsenow correlation with Csf = 0.012 for aluminum, and the obtained boiling curve was well within uncertainty ranges (Figure 3.8).
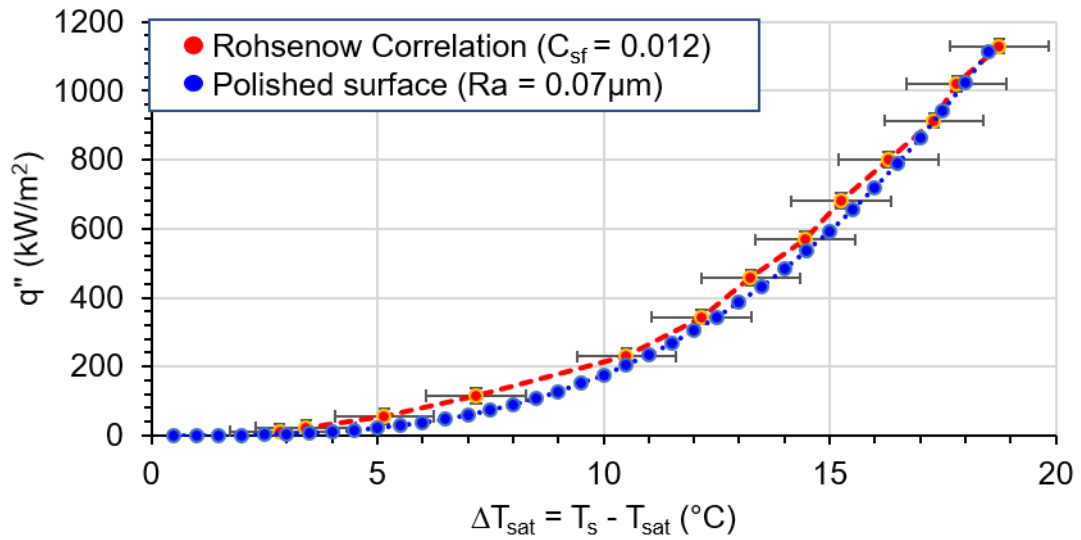
Figure 3.8: Validation of boiling setup

3.8 Experimental repeatability

Experiments were repeated for the polished surface as well the EDM textured surface with best boiling heat transfer performance. A good repeatability was obtained for all boiling curves as shown in Figure.3.10 for the polished surface. This point toward good accuracy and precision for surface preparation and boiling equipment.
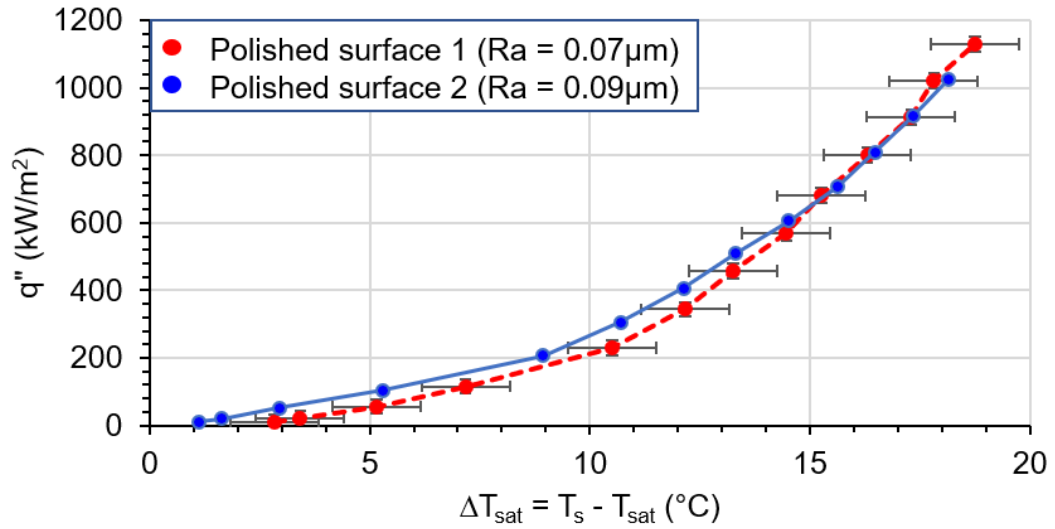
Figure 3.9: Repeatability for polished surfaces

Similarly, repeatability of boiling was tested for EDM textured surface with same machining parameters, and same roughness ($Ra = 42$ µm) and a good repeatability was obtained as shown in Figure 3.11.
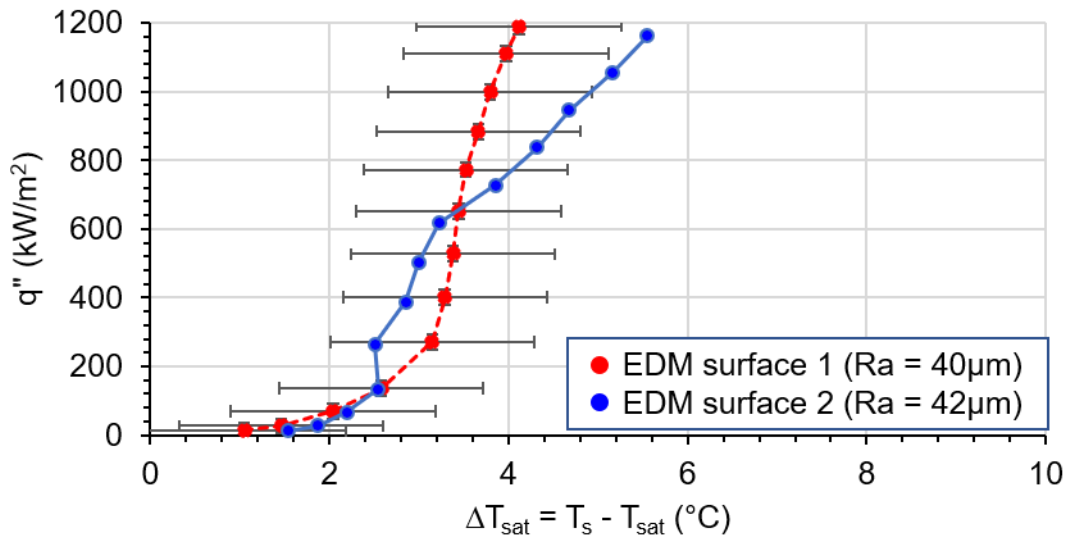
Figure 3.10: Repeatability for EDM textured surface

3.9   Static contact angle measurements

The static contact angle values were obtained for EDM textured surfaces, and polished surface using the DataPhysics Optical Contact Angle goniometer (OCA) 35 and were presented alongside machining and roughness parameters. The macroscopic contact angle was used as an indicator of physical and chemical interaction between liquid and solid. Sessile drop method was adopted in these measurements. A drop size of 6 µl was dispensed over the surface, and ellipse fitting method was chosen to compute the contact angle by SCA 20 software. Ellipse fitting method was chosen because of higher accuracy due to the precise location of three-phase intersection line of drop [65].

4 Results and discussion

The results of experiments carried out in this study are presented and discussed in this chapter. In most of the prior studies, boiling is studied in terms of surface roughness. features and not in terms of parameters associated with manufacturing techniques. However, in this study experiments were performed in terms of machining parameters first. The motivation for this was the idea that surfaces with same average roughness Ra can be made by different combination of EDM parameters [7]. Therefore, EDM parameters like pulse current (i_e) and discharge duration (t_e) are more fundamental in characterising surface than just the average roughness Ra. Also, it is clear from the literature review about the weakness in associating boiling heat transfer with Ra. Therefore, it was essential to study boiling initially in terms of machining parameter and later in surface characterisation parameters. Experiments were conducted in 3 stages. Stage 1 focused on the influence of EDM parameters on the enhancement of boiling heat transfer. EDM process limiting factor was identified, assessed and optimized in stage 2. Stage 3 focused on surface characterization in the context of pool boiling. Each stage is discussed separately.

4.1 Baseline experiment on plane polished horizontal surface

To investigate the effect of EDM surface texture on boiling performance, a baseline boiling test was performed with a plane polished surface ($Ra = 0.07$ µm), based on which relative enhancement from textured surfaces are assessed (Figure 4.1). Figure 4.1 (a) shows the

64

plane polished surface prepared for this purpose. A static contact angle measurement of 88.81° for this surface was obtained with sessile drop method (Figure 4.1(b)).
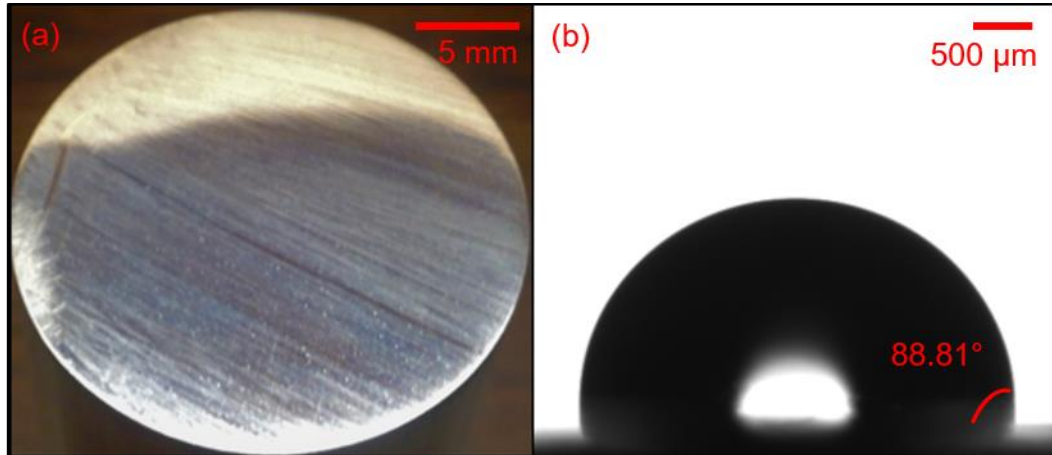
Figure 4.1: (a) Polished surface (Ra = 0.07 µm) (b)Water drop on the polished surface

Figure 4.2 shows the boiling curve obtained for this surface. The point of incipience of nucleate boiling is determined by computing the slope and curvature of the boiling curve at all steady-state points. The point where a sudden jump in the slope of the boiling curve occurs and the maximum curvature is obtained was chosen as the point of ONB (onset of nucleate boiling). An incipience superheat of 10.1 °C was obtained for the polished surface. Two distinctive zones of convection and nucleate boiling are clearly visible in the curves, separated by an ONB point. Some unwanted nucleation sites from the gap between test block and vessel's skirt along test block periphery were observed from the side window. Several authors have observed such unwanted nucleation sites and tried to avoid them by depositing epoxy and RTV sealant [23] and using extended surfaces [63]. In this study, the gap was minimized by having a transition fit for text block during assembly into the boiling

vessel and filling the gap with RTV sealant. Nevertheless, as all three thermocouples in test block are embedded 6 mm deep in the radial direction into the test block, the boiling curve represents the heat transfer coefficient near the center of the test block. Moreover, during this experimental study, only the relative effect of boiling behavior of various surfaces was investigated. Therefore, the net effect of the unwanted nucleation sites on heat transfer coefficients for all boiling curves was largely the same. Also, the phenomenon of incipience overshoot can influence the heat transfer coefficient in the convection regime, as discussed in the literature review [66].
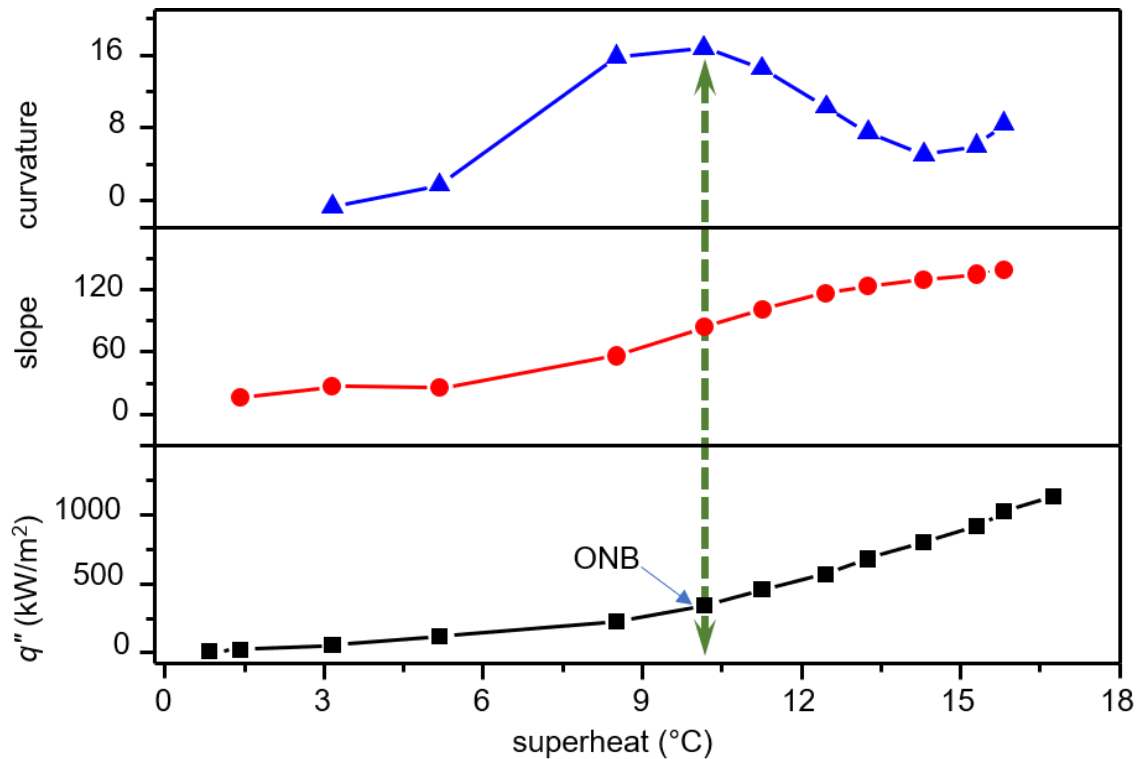
Figure 4.2: Identification of boiling incipience point for a polished surface

4.2 Stage 1: Effect of EDM parameters on boiling heat transfer

In stage 1, experiments were performed to obtain boiling curves as a function of pulse current (i_e) and discharge duration (t_e). The surfaces were machined by using a hydrocarbon dielectric fluid in the EDM machine. A description of machining parameters, the average roughness of the surface profile (Ra), the characteristic crater dimensions obtained using DDS methodology and static contact angle are provided in Table 4-1.

Table 4-1: Machining and roughness parameters of surfaces used in Stage 1

EDM machining parameters		Ra (µm)	Crater depth (µm)	Crater diameter (µm)	Contact angle (°)
pulse current (A)	discharge duration (µs)				
21	274	18.3 ± 1	15.09 ± 0.9	328 ± 6.2	129.7
39	274	25.3 ± 2.6	30.0 ± 1.6	799.8 ± 19	122.4
72	274	33.8 ± 1.7	85.34 ± 4.1	1350.2 ± 28	121.25
39	65	14.1 ± 1.1	8.1 ± 0.6	197.8 ± 2.8	117.5
39	1800	41.7 ± 0.5	62.87 ± 2.3	1895 ± 32.1	116.5
39	2400	39.3 ± 2.1	42 ± 3.1	2200 ± 34.3	116.9
39	4200	15.5 ± 1.8	13.9 ± 0.9	221 ± 4.5	121.2
39	6500	17.5 ± 0.6	11.8 ± 0.6	366 ± 6.1	117.2

Figure 4.3 shows the effect of pulse current (i_e) on boiling curve at a constant discharge duration, $t_e = 274$ µs. It was observed that the boiling performance increases monotonically with an increase in current. ONB was observed at lower temperatures with

an increase in current. Figure 4.4 shows the heat transfer coefficient as a function of wall heat flux for the same machining conditions as in Figure 4.3. At a very low heat flux (<50 kW/m^2), the heat transfer coefficient of the polished surface is higher than EDM textured surface. This might be due to obstruction of the buoyancy-driven flow of liquid by the surface features, and the size of features being larger than the developing thermal boundary layer, which leads to lower heat transfer from the wall [41].
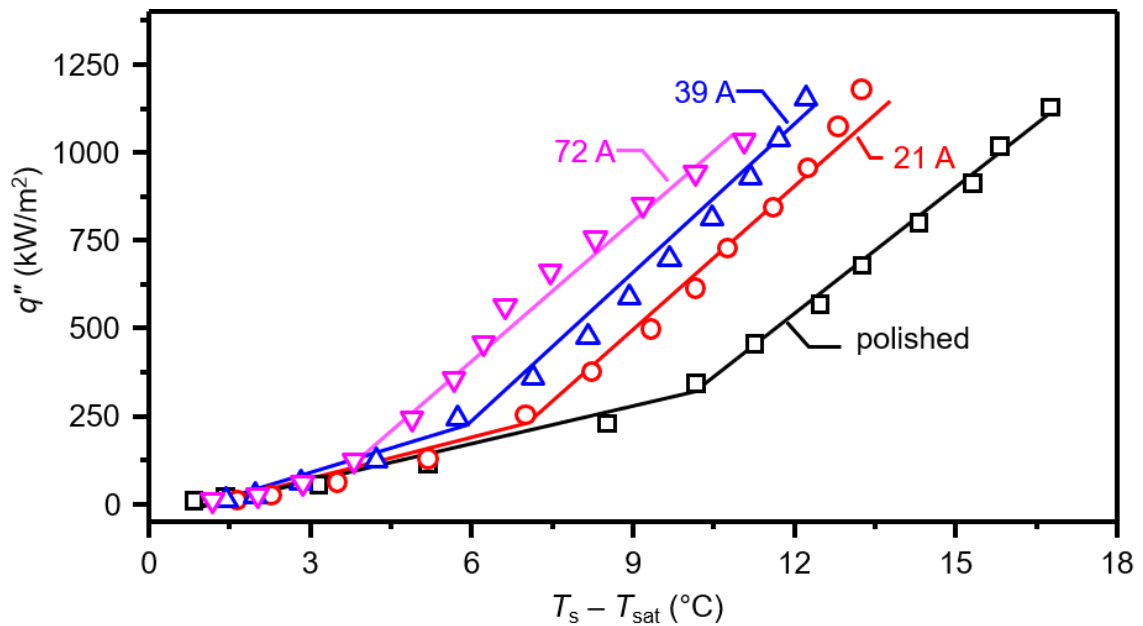
Figure 4.3: Influence of pulse current (i_e) at constant discharge duration ($t_e = 274$ μs)
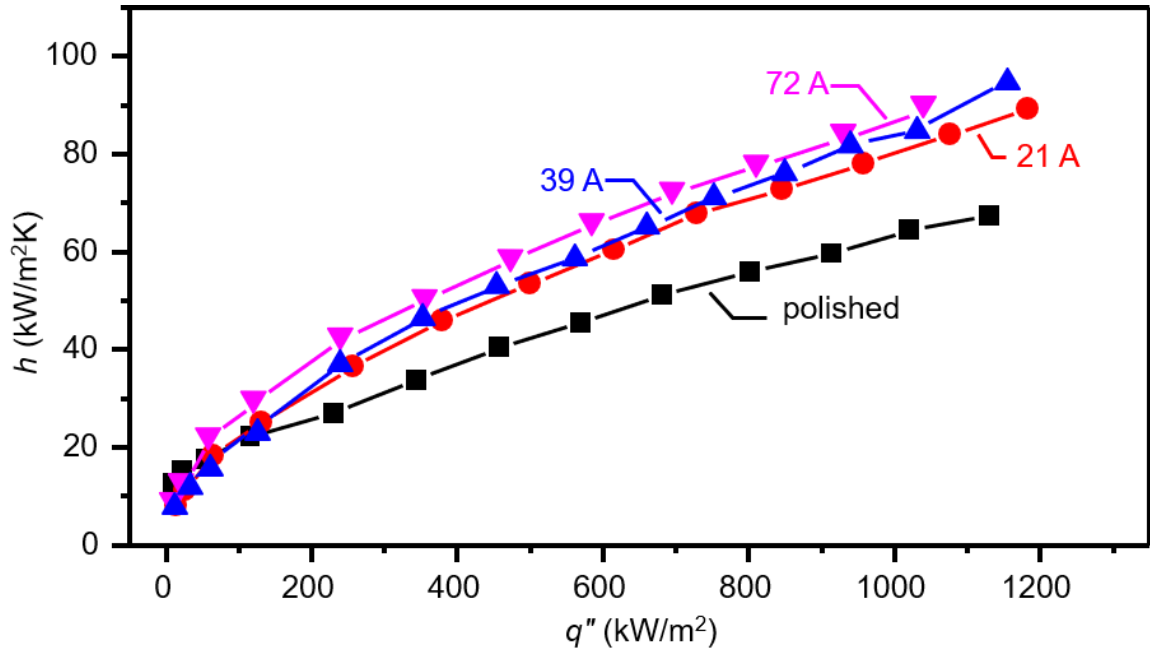
Figure 4.4: Heat transfer curves by changing the current (i_e) at constant $t_e = 274 \ \mu s$

However, at a heat flux above 50 kW/m², when a stable flow field is developed, and the thermal boundary layer is established, heat diffusion becomes the dominating mode of heat transport, and the heat transfer coefficient increases with an increase in surface area due to larger craters owing to the higher pulse current. After the incipience of nucleate boiling, the surfaces made by higher pulse current correspond to higher heat transfer coefficient, due to the larger diameter of more active nucleation sites, which needs lower superheat to activate and nucleate bubbles. A modest 50% times improvement was obtained by choosing the highest pulse current of 72 A for a discharge duration $t_e = 274 \ \mu s$, compared to the polished surface.

69

Figure 4.4 and 4.5 shows the effect of discharge duration (t_e) on the boiling curve at a constant pulse current i_e = 39 A. The discharge duration was varied from t_e = 65 µs to t_e = 6500 µs. Although better boiling performance was achieved for i_e = 72 A, the current setting was kept at i_e = 39 A to maintain a current density of 10 A/cm^2 for stable machining. It was observed that the highest HTC was obtained for t_{on} = 2400µs with an enhancement of 500% compared to the polished surface.
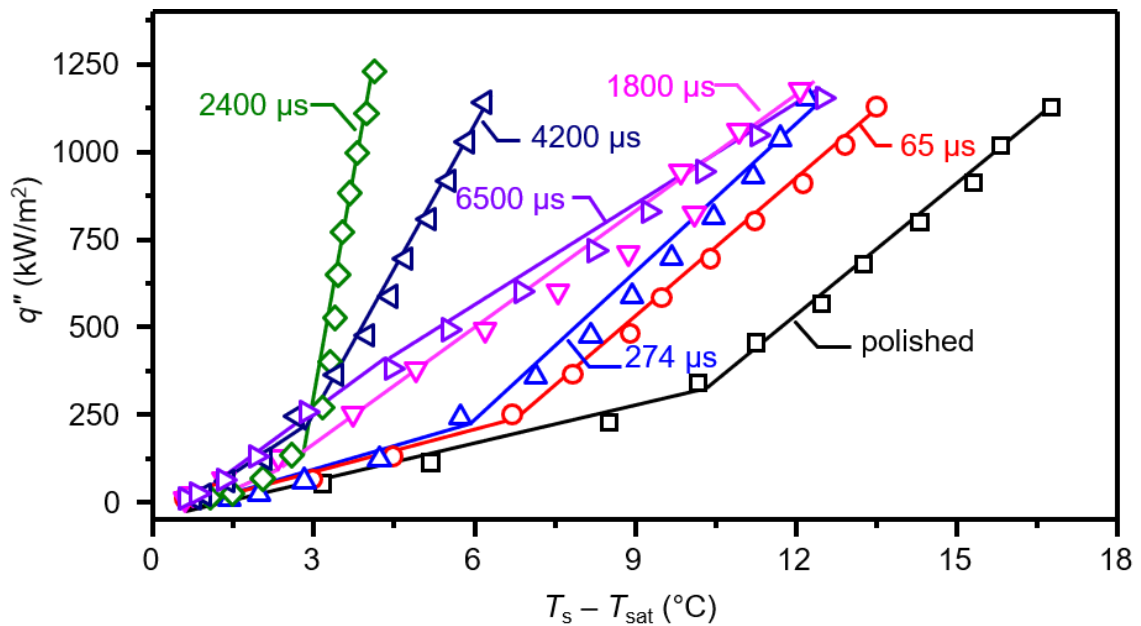
Figure 4.5: Influence of discharge duration (µs) at constant current (i_e = 39 A)

A lower onset of nucleate boiling was found with an increase in pulse duration, with a ΔT_{nuc} as low as 2.8 °C for surface machined with a pulse duration of 6500 µs. In the convective regime, the heat transfer coefficient increases with an increase in pulse duration. This is in accordance with some observations in literature where the Nusselt Number

increases with increase in the spacing of surface features [41, 44, 45], which aligns with the fact that larger pulse duration leads to bigger craters.
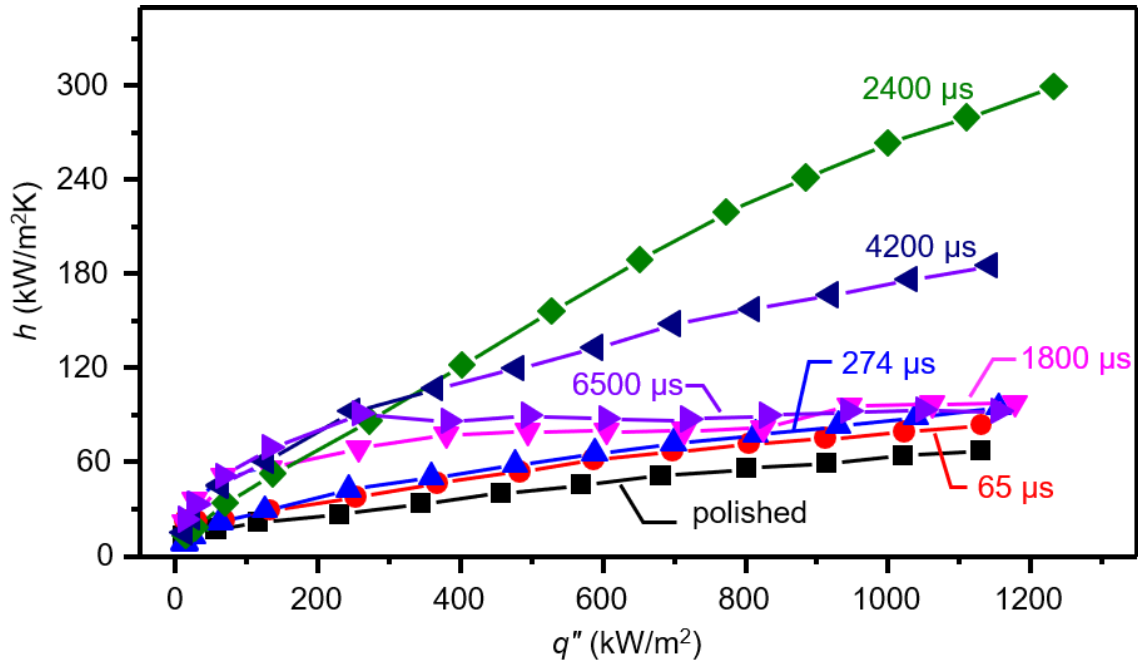
Figure 4.6: Heat transfer curves by changing discharge duration (µs) at $i_e = 39\,A$

In the nucleate boiling regime, the heat transfer kept increasing until a pulse duration of 2400 µs and started decreasing thereafter. A visual inspection of the machined surface showed a layer developing on the surface at discharge durations of 2400 µs and higher. A maximum heat transfer coefficient of 300 kW/m²K was obtained for $t_e = 2400$ µs. It was hypothesized at this point that the superficial layer is responsible for the declining heat transfer coefficient after $t_e = 2400$ µs, given that the layer is consistently formed on the surface from $t_e = 2400$ µs onwards. As seen in Table 4-1, no significant

71

change in static contact angle after surface preparation is observed with the formation of this layer. However, the average surface roughness started decreasing with this layer

4.3 Stage 2: Investigation of factors limiting boiling performance

In this stage, the causes and effects of the surface layer formed at high discharge duration ($t_e > 2400$ µs) on the surface, and its influence on wettability and boiling behavior were studied. The deterioration in boiling performance observed in Figure 4.5 and Figure 4.6 due to layer formation can be attributed to a change in chemical composition, which can affect wetting behavior, or due to a difference in resultant surface topography, which suppresses bubble nucleation. It is also possible that this layer acts as thermal resistance whose effect needs to be taken into account while calculating heat flux and surface temperature as discussed in Chapter 3 (Equation 3.2). It was also noticed in Figure 4.6 that convection heat transfer coefficients increased continually with an increase in t_e, even after the formation of the superficial layer.

In the subsequent part, an analysis of the conditions that lead to the formation of the layer was investigated. The influence of machining time (by varying machining depth) was also carried out. Also, a different dielectric fluid other than hydrocarbon oil (de-ionized water) was chosen to see whether the dielectric fluid composition was responsible for the formation of this superficial layer. Alongside, contact angle measurements were taken to see if wettability of the surface had any influence on this peculiar behavior of boiling heat transfer deterioration after a certain t_e.

72

Figure 4.7 (a,b) shows two distinctive surface textures formed as a result of the layer for the surface with machining parameters (39 A, 4200 µs) with hydrocarbon oil as the dielectric fluid. An overall lower surface roughness with a smaller peak-to-valley height was observed for the profile where the layer was deposited as shown in Figure 4.7 (c).
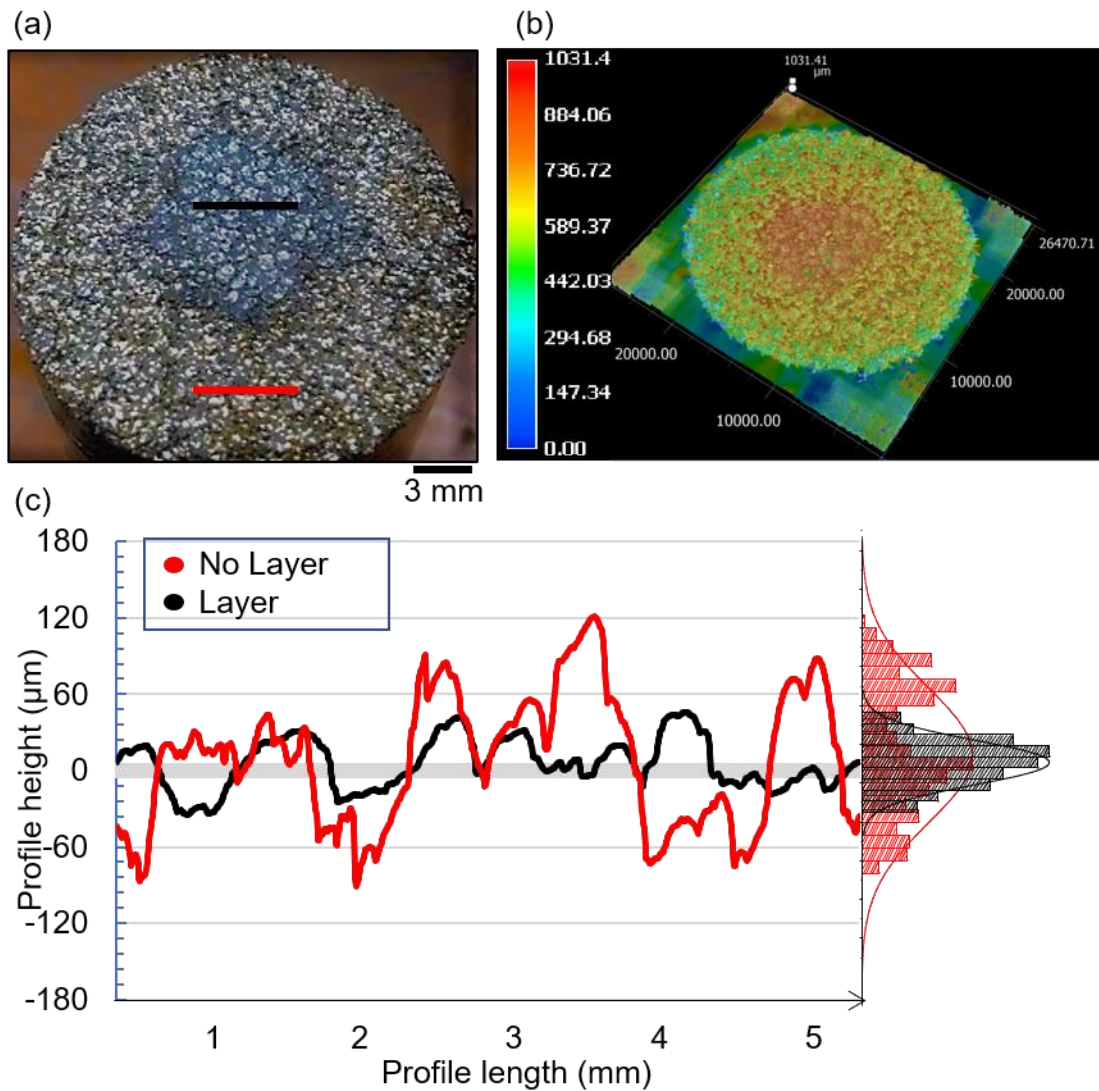
Figure 4.7: Formation of the superficial layer at high discharge duration (39 A, 4200 µs)

4.3.1   Influence of dielectric fluid

Experiments were conducted by changing the dielectric fluid from hydrocarbon oil to de-ionized water, to investigate the source of this layer by choosing the same EDM machining parameters as those used with using hydrocarbon dielectric fluid, i.e. (i_e = 21 - 72 A, t_e = 274 - 6500 µs). Table 4.2 shows the values of average roughness, characteristic crater depth and diameter, and static contact angle measurements for these surfaces before boiling experiments.

Table 4-2: Machining and roughness parameters with water as the dielectric fluid

EDM machining parameters		*Ra* (µm)	Crater depth (µm)	Crater diameter (µm)	Contact angle (°)
pulse current (A)	discharge duration (µs)				
21	274	22.8 ±0.7	11.9 ± 0.6	384 ± 6.2	22.9
39	274	25.6 ± 2.5	26.0 ± 1.8	588.9 ± 16	26.1
72	274	29.5 ±2.0	23.2 ± 2.1	758.5 ± 19	21.3
39	2400	59.1 ± 4.9	80.1 ± 6	3111 ± 34.3	12.1
39	6500	69.2 ± 4.7	71.7 ± 3.9	5322.5 ± 88	6.2

Surprisingly, there was no layer formation when using water and boiling heat transfer showed a monotonically increasing trend with increasing pulse current (i_e) and discharge duration (t_e) for same machining parameters as were used for using hydrocarbon oil as dielectric, as shown in Figure 4.9, compared with boiling performance by using hydrocarbon oil (Figure 4.3 and Figure 4.5). For constant discharge duration, heat transfer

increases with increase in pulse current in both convection and boiling regime. Similarly, for constant pulse current, heat transfer coefficient increases with an increase in discharge duration. This suggests that the layer was responsible for deterioration of boiling heat transfer while using hydrocarbon oil as dielectric fluid in EDM.
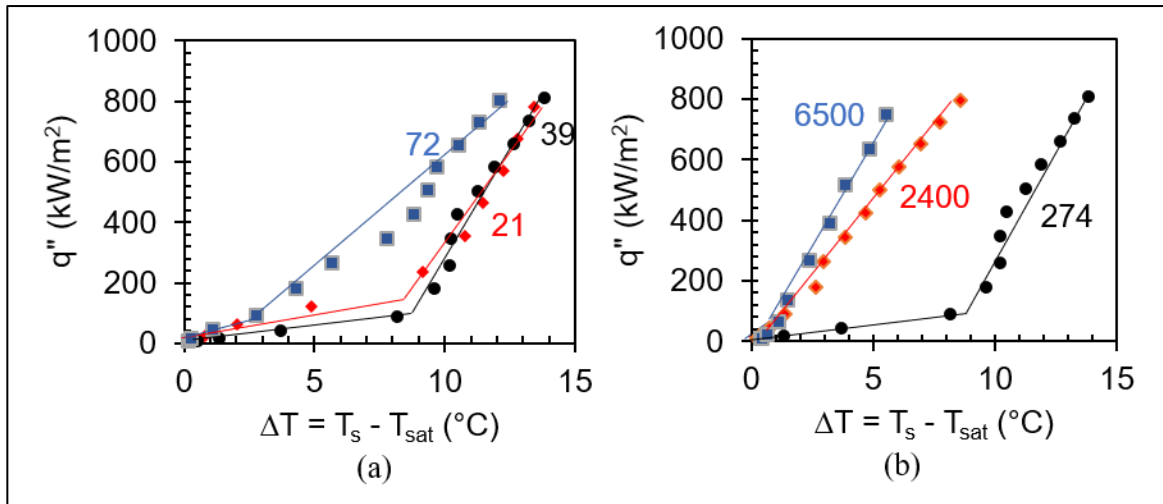
Figure 4.8: Boiling curves by using deionised water as dielectric fluid (a) variation of pulse current (A) at constant discharge duration (274 µs) (b) Variation of discharge duration (µs) at constant pulse current (39 A)

Similar layer of Titanium Carbide (TiC) formation has been reported in EDM of Ti and Ti6Al4V alloys with positive tool electrode polarity at all pulse durations [67]. No such layer was found for γTiAl alloy or Al alloys because of the higher amount of Aluminum content in these alloys. Aluminum has higher conductivity than Titanium, which prevents the formation of carbide layer in the first place due to the dissipation of concentrated heat at the gap. Once the TiC layer forms, it acts as a thermal barrier and lowers MRR. However, such layer was not found for negative polarity tools because pulse energy density difference

with changing polarity offsets the formation of TiC layer. It may be possible that similar layer of Aluminum Carbide is formed in this case but at pulse discharge duration (t_e) 1-2 order of magnitude higher than that for Ti6Al4V, that acts as a thermal barrier for further machining. It is clear from surfaces machined using water as the dielectric fluid that this superficial layer was formed from the chemical content of the hydrocarbon dielectric fluid and not from the tool electrode or the workpiece itself. It can be hypothesized at this point, that the temperature is very high for larger pulse duration, that breaks down hydrocarbon oil chemically, which react chemically with alloying elements of Aluminum and formed this superficial layer. Once this layer forms, it acts as a thermal barrier due to its lower thermal conductivity and high melting point. The temperature available from pulse energy density is not adequate to melt this layer, and therefore there is a net reduction in material removal rate. This proposition was tested in subsequent section by investigating the influence of change in machining time on material removal rate and propagation of this layer over the surface. Some chemical analyses like Energy Dispersive X-ray (EDS), X-Ray Diffraction (XRD) or Wavelength Dispersive X-ray Spectroscopy (WDS) analysis is required to have a better understanding about conditions that lead to the formation of this superficial layer and assess the composition of this layer.

4.3.2   Influence of machining time

In this section, the propagation of this superficial layer on the textured surface as a function of machining time for the machining parameters given in (Table 4-3) with hydrocarbon oil

as dielectric fluid was studied. These set of experiments were carried out to study the influence of this layer on material removal rate. Furthermore, pool boiling experiments were carried out to quantify the effect of this layer on boiling performance.

Table 4-3: EDM parameters to study the influence of machining time

EDM machining parameters		Machining time (s)	Contact angle (°)
pulse current (A)	discharge duration (µs)		
39	2400	30	116.9
39	2400	400	120.44
39	2400	900	117.7

As the surface was textured for a longer time using the same machining parameters (39 A, 2400 µs), the layer starts growing over the surface as shown in Fig. 4.9. A very small layer on the surface of the test block was found at a machining time of 30 seconds, but it grows all over the surface as machining time increases. The MRR drops significantly on the formation of the layer, and it took 900 seconds to machine to a depth of 1.5 mm compared to 30 seconds required to machine to a depth of 0.15 mm. The layer got deposited at a random location on the surface and expanded over the surface with an increase in machining time as shown in Figure 4.9.
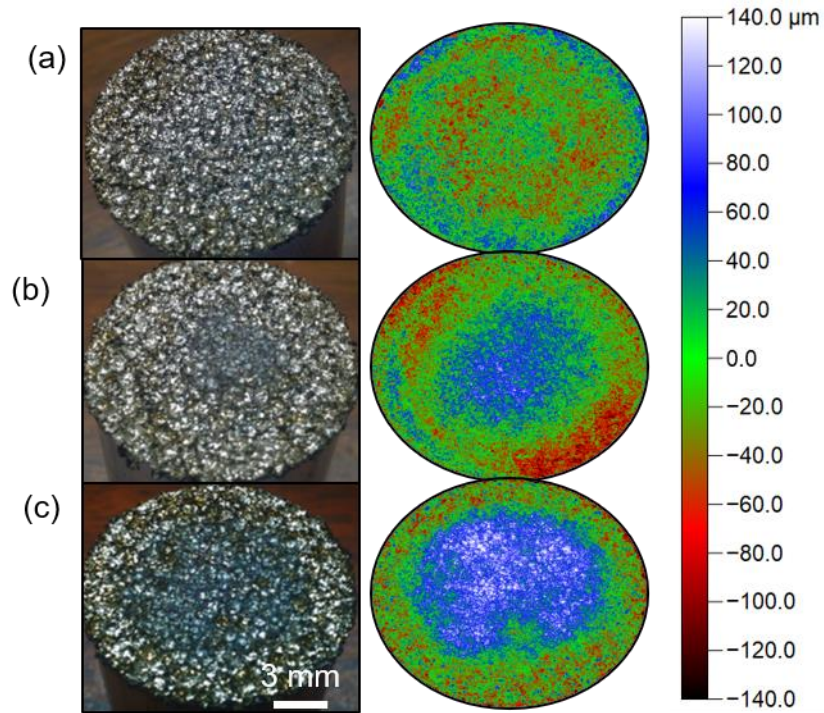
Figure 4.9: EDM textured surfaces using hydrocarbon oil, 39 A ,2400 µs (a) t = 30 s (b) t = 400 s (c) t = 900 s

Figure 4.10 shows the influence of machining time on the boiling curve. An increase in heat transfer was observed for the convective regime, with an earlier ONB point, but heat transfer coefficient deteriorates for the boiling regime with an increase in machining time. This is probably due to larger cavities on the of the superficial layer, which needs smaller superheat to activate and nucleate. An equal onset of nucleate boiling point (ΔT_{nuc} = 1.5 °C) was observed for surfaces with large surface area of the layer, compared to the onset of nucleate boiling point (ΔT_{nuc} = 2.8 °C) for the surface with a smaller proportion of this layer, which means onset of nucleation point is defined by size of cavities on the superficial layer.
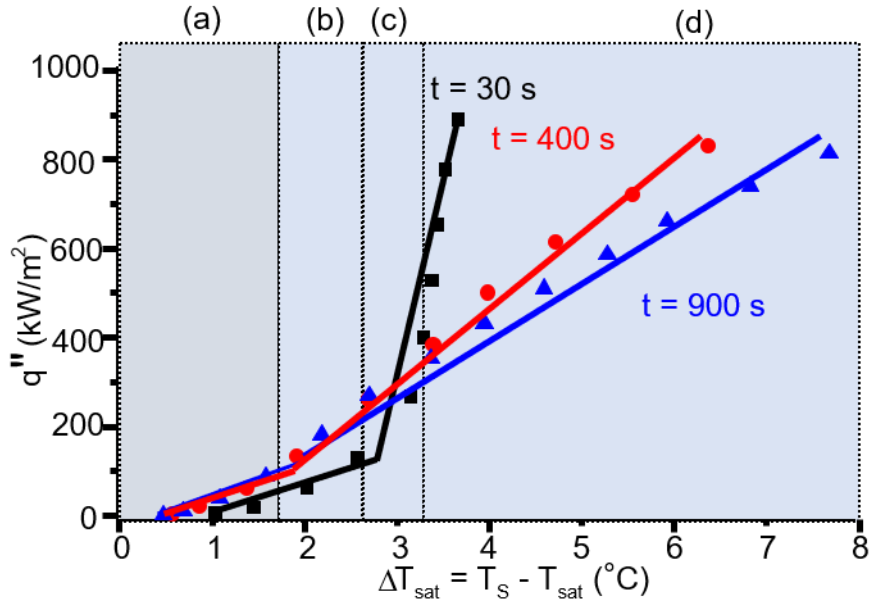
Figure: 4.10: Influence of machining depth on boiling curve with surface machined in hydrocarbon oil with $i_e = 39A$, $t_e = 2400\ \mu s$ for t = 30 s, 400 s, 900 s

It is seen from the comparison of images of bubbles nucleating from these surfaces, obtained by the high-speed camera that boiling started earlier for surfaces with higher area of deposited layer. Figure 4.11 explains the boiling behavior obtained with these surfaces. A second setup with extended fin feature (as discussed in Chapter 3) was used for these studies. It was observed that nucleation started late for the surface that had a minimum proportion of layer, but the boiling was most vigorous for this surface. At $\Delta T = 3.5\ °C$, this surface was in the fully developed nucleate boiling zone, with bubbles merging horizontally and growing in the form of slugs and columns. Also, a large number of small-sized departing bubbles were observed for surfaces with a significant proportion of the superficial layer deposited over the surface. In general, bubble departure dimeter for cavities with large

dimeter is smaller compared to cavities with smaller diameter cavities, due to surface tension forces dominance over inertial forces for larger cavities in defining bubble departure diameter [24, 37]. This points toward a greater number of bigger cavities on surface with higher proportion of the superficial layer. However, wider and shallower craters were observed with this layer as seen in Figure 4.7. This implies that "bigger" cavities means "wider" characteristic cavities in boiling heat transfer context.
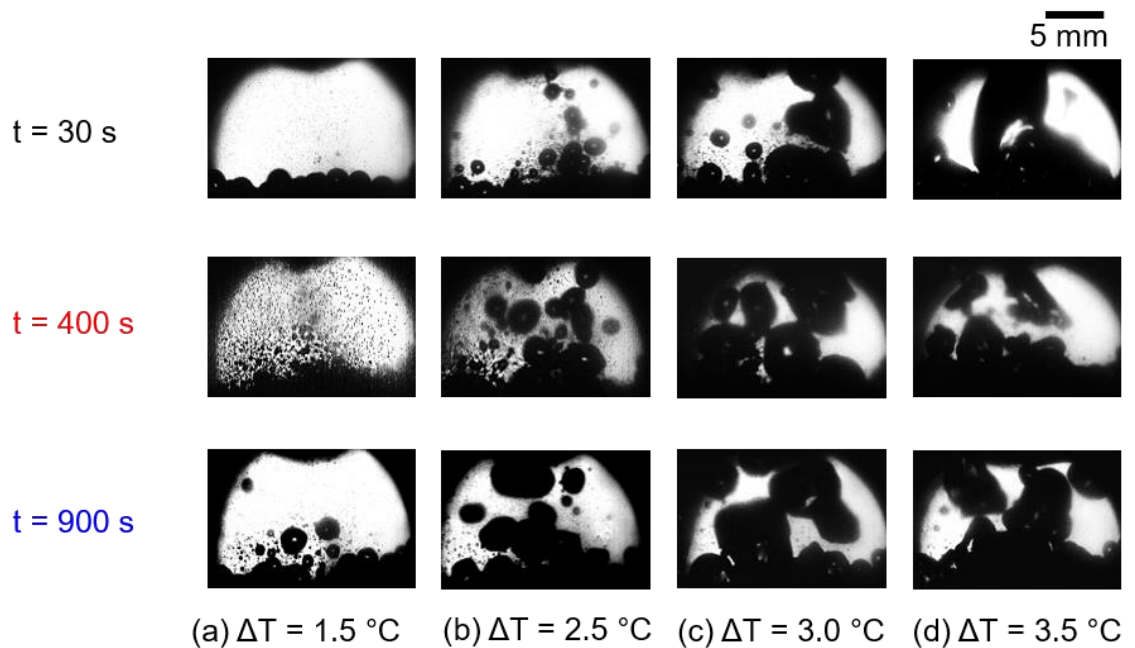
Figure 4.11: Bubble visualization for different machining time at different superheat

As the surface roughness decreases with deposition of the layer as shown in Figure 4.7, this points to enhancement in the convective regime because of lower obstruction to buoyancy-driven flows. In the nucleate boiling regime, the heat transfer coefficient is a function of bubble dynamic parameters like nucleation site density, bubble departure

80

diameter, bubble frequency, waiting period, growth period as shown in Equation 2.3, which can significantly change its magnitude. Although the nucleation site density of bigger cavities increased with deposition of the layer, that is evident by lowered ONB, more heat is carried away from the wall by larger bubbles initiating from smaller cavities on the surface with the smallest amount of deposited layer.

Another reason for the difference in boiling behavior due to deposited layer might be because this layer acts as a thermal barrier for heat conduction, which leads to different temperature drop along the length of the test block length due to its thickness, thus leading to a difference in the calculation of temperature on the surface. Without knowing the thermal conductivity of this layer, which is probably made by carburization during the EDM process, it is inconclusive to say how this layer is affecting the boiling behavior. Therefore, further investigations are necessary to quantify the effect of the thickness of the layer.

4.3.3 Influence of static contact angle

The static contact angle did not change significantly with the formation of the layer ($\theta =$ 121°) as shown in Table 4-3. EDM textured surfaces made by using hydrocarbon oil as the dielectric fluid has contact angles in the range of ($\theta = 115°$ - 125°) even with no carbide layer formation as shown in Table 4-1, compared to a contact angle $\theta = 88.81°$ for the polished surface. These surfaces are most probably in Cassie-Baxter state. However, the contact angle obtained for EDM textured surface made by using dielectric water showed

hydrophilic nature ($\theta = 12° - 26°$), as shown in Table 4-2. These surfaces are most probably in Wenzel state. However, all the surfaces can be assumed to be in the Wenzel state due to degassing before the boiling experiment [39]. The hydrophilicity for EDM surface textured by using deionized water might be due to the presence of Aluminum Oxide which is hydrophilic, and amplification of this hydrophilicity by roughness into the Wenzel state. This strange hydrophilic nature has been reported by Guo et al. [65].
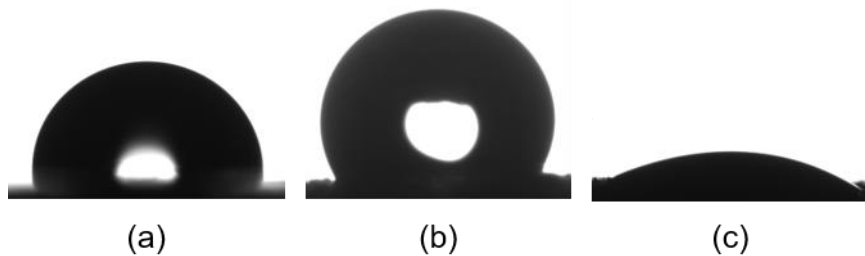
Figure 4.12: Contact angle for different surfaces (a) Polished (Ra=0.07 µm) (b) EDM textured using hydrocarbon oil, 39 A, 2400µs (c) EDM textured using water, 39A, 2400µs

The boiling characteristics of EDM surfaces prepared using deionized water as dielectric fluid showed a slight shift of the boiling curve to the right by $\Delta T = 1 - 2$ °C superheat for similar machining parameters compared to surfaces made by using hydrocarbon oil as a dielectric as shown in Figure 4.3, 4.7 and 4.9. This slight shift can be because of change in wetting behavior of EDM textured surface, which showcases hydrophilic nature when using water, and the hydrophobic nature when using hydrocarbon oil as a dielectric fluid for preparation. Some authors like Mpholo questioned the relevance of macroscopic contact angle for analysis of boiling from microcavities [39].

4.4 Stage 3: Analysis of surface roughness effects on nucleate boiling

In chapter 2, it was shown through literature review that the effect of surface texture on nucleate boiling is not completely understood. Most studies rely on correlating the effect of surface features on boiling performance in terms of average roughness Ra. However, this form of correlation based on Ra has met with limited success [23, 48], for small roughness range $(< 10 \, \mu m)$. Many studies have found weakness in correlating boiling data with Ra [28, 46, 47]. Similar weakness was observed in this study. Figure. 4. 13 shows the average roughness Ra for all the surfaces machined using hydrocarbon oil and deionized water as a dielectric fluid by changing EDM parameters. The best boiling performance was obtained when machining at 39 A and 2400 μs by using hydrocarbon oil dielectric. It is also observed in Figure 4.13 that the best boiling performance does not correspond with the highest surface roughness. Therefore, a detailed analysis of surface characterizing parameters became essential to understand the underlying effect of roughness on nucleate boiling. A study was carried out to correlate boiling heat transfer with the roughness parameters reviewed in Chapter 3.
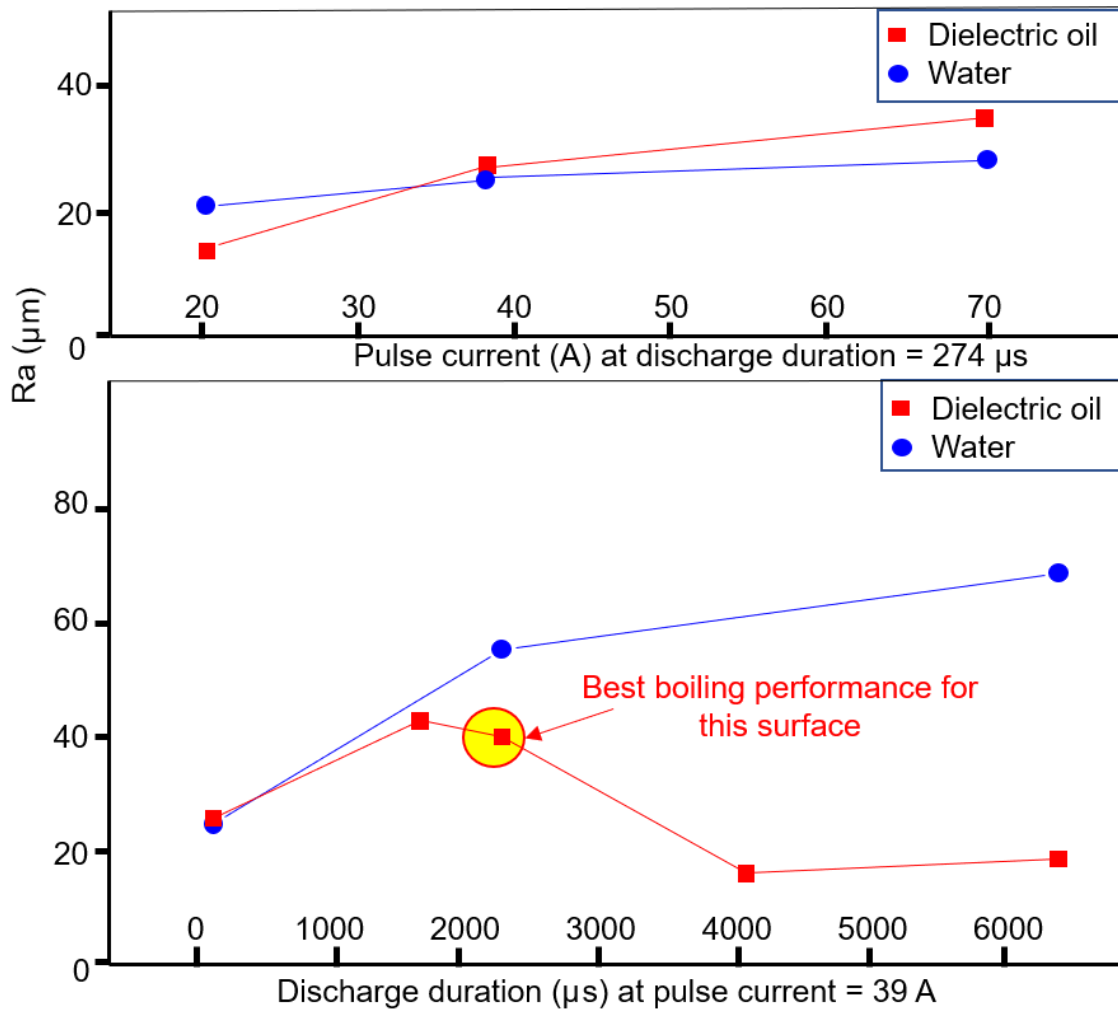
Figure 4.13: Average surface roughness (Ra) for all EDM surfaces

The strength of correlations was compared in terms of mean absolute error (MAE), maximum error and coefficient of determination (R^2). Most of the studies in the past used MAE to quantify the predictability of the correlations as well [23, 48, 54, 55]. However, they used different methods to calculate the MAE. Therefore, two types of mean absolute errors were calculated to compare the results of this study with studies from the past. MAE [23] and MAE2 [56] were defined as follows:

$$MAE = \frac{1}{n} \sum_{i=1}^{n} \frac{|h_{cor,i} - h_{exp,i}|}{|h_{exp,i}|}$$

$$MAE2 = \frac{\Sigma |h_{cor} - h_{exp}|}{\Sigma |h_{exp}|}$$

Where i is the experimental data point at a given heat flux. All the pool boiling data were arranged into two regimes (convective and nucleate boiling), and heat transfer coefficients were correlated to surface characterization parameters at a fixed heat flux value (q" = 62.5 kW/m^2 for the convective regime, and q" = 450 kW/m^2 for nucleate boiling regime). These heat fluxes were chosen so that the maximum number of points can be considered while correlating heat transfer data with surface characterization parameters, making sure that the surfaces are operating in the same heat transfer regime. As a new material species was developing on the surfaces at high pulse discharge durations, these surfaces were excluded from the analysis.

The heat transfer coefficient was correlated in the form h = aR^b for individual parameters (R), where a and b are coefficients obtained by best-fit power-law equations. This type of fit seems reasonable for studying boiling over EDM surface, which has isotropic nature and geometrically similar features (craters) on the surface. The power law best describes effects of convection, nucleation site density, bubble frequency, bubble departure diameter, and other influencing factors as an accumulated sum of heat transfer coefficient associated with different modes of heat transport [23] .

It was important to consider the dependence of roughness parameters on each other. Therefore, the strength of predictability of a correlation was assessed in terms of parameters like MAE, MAE2 and R^2. The values of MAE, MAE2, and R^2 were compared to evaluate the magnitude of uncertainty when correlating with one predictor relative to another. DDS parameters are advantageous in the aspect of interdependence as spacing and amplitude parameters are explicitly defined in terms of crater diameter and crater depth respectively. DDS parameters provide a more robust measure of the effect of spacing and amplitude of surface asperities in correlating boiling heat transfer. Both ISO and DDS parameters were correlated and compared for their predictive power.

4.4.1   Convection regime

In the convective regime, for q" = 62.5 kW/m², the heat transfer coefficients were correlated for parameters of ISO 4287-1997 and DDS parameters for all the EDM textured surfaces. Table 4.4 shows the correlations and the corresponding mean absolute errors (MAE, MAE2), maximum error and R^2 by correlating predicted data with experimental data. The Table is categorized into ISO 4287-1997 and DDS parameters.

The results show best fitting correlations with parameter *Rsm* (MAE = 35.7%). *Rsm* accounts for spacing between peaks assuming a dead zone (10%) based on the definition of ISO 4287-1997 standard. Similarly, for DDS parameters, the best fit was obtained with *AR* (aspect ratio of the characteristic crater) with MAE = 34.7%. These parameters provide better prediction compared to *Ra* (MAE = 38.5%).

86

Table 4-4: Summary of correlations with individual parameters (convection regime)

Parameter		Correlation	MAE (%)	MAE2 (%)	Max error (%)	R^2
ISO 4287-1997	Ra	$h = 3.92\,Ra^{0.58}$	38.5	29.7	163.2	0.51
	Rz	$h = 0.71\,Rz^{0.69}$	38.6	28.6	196.8	0.49
	Rp	$h = 1.01\,Rp^{0.71}$	40.2	28	238.2	0.43
	Rv	$h = 1.66\,Ra^{0.53}$	37.6	29.2	156.6	0.53
	Rq	$h = 3.34\,Rq^{0.5}$	38.6	29.8	169.3	0.5
	Rsm	$h = 0.08\,Rsm^{1.12}$	35.7	26.3	199	0.51
	Rs	$h = 0.09\,Rs^{0.89}$	39.9	32.2	139.9	0.47
	Rmr	$h = 3.92\,Rmr^{0.26}$	49.4	40	107.0	0.14
	Rsk	$h = 22.1\,Rsk^{-0.2}$	43.1	36.2	145.6	0.22
	Rku	$h = 743.8\,Rku^{-2.7}$	39.6	32.3	102.8	0.37
DDS	CD	$h = 9.694\,CD^{0.32}$	47.5	35.2	167.6	0.31
	CDi	$h = 4.8\,CDi^{0.26}$	40.9	31.5	159.8	0.45
	AR	$h = 3.49\,AR^{0.62}$	34.7	27.1	171.9	0.44
	Rc	$h = 7.47\,Rc^{0.2}$	34.8	27.2	166.7	0.47
	Vs	$h = 5.98\,Vs^{0.09}$	42.5	32.6	158.9	0.43
	Ve	$h = 5.8\,Ve^{0.09}$	42.5	32.6	159	0.43

A very high scatter in the sample was obtained in the convective regime, which might be attributed to the high percentage error due to uncertainty associated at lower heat flux as shown in Figure 4.14. The percentage error is very high (40 - 50%) at heat flux below 50 kW/m^2, which plateaus down to 2.8% at high heat flux (> 400 kW/m^2). This explains high values of MAE associated with the convective regime. Also, incipience overshoot might be responsible for a high percentage error associated at low heat flux [2].
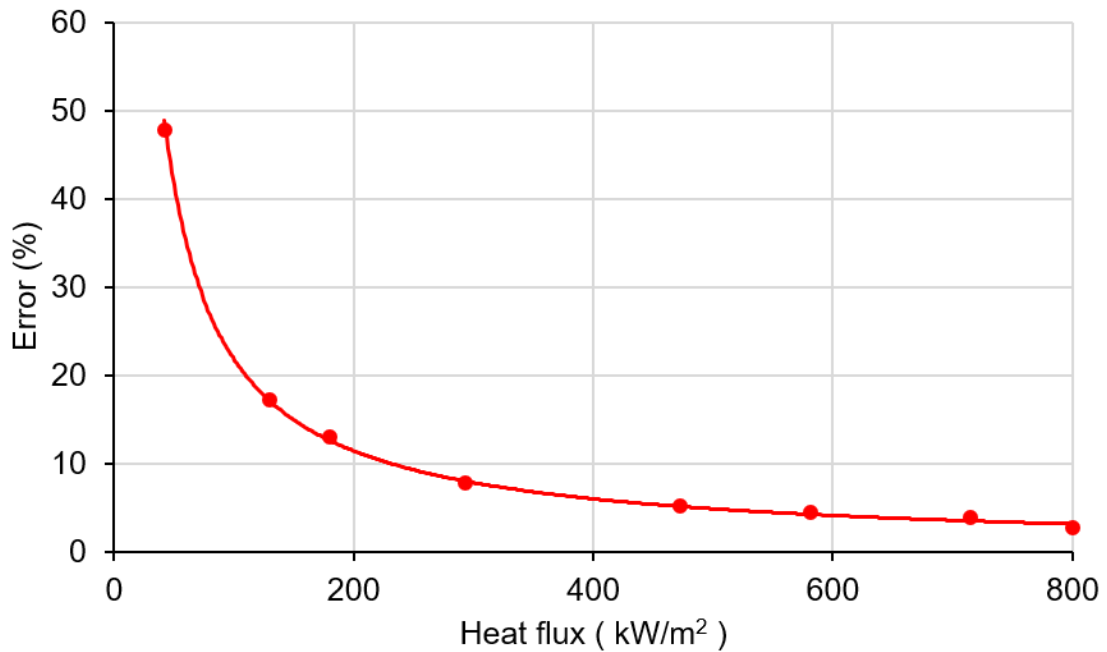
Figure 4.14: Variation of uncertainty with heat flux

4.4.1.1 *Discussion*

As *Rsm* and *AR* (aspect ratio of the characteristic crater) relates to the spacing between profile asperities, it can be asserted that the spacing plays a significant role in

enhancing heat transfer in the convective regime. Based on both ISO parameters and DDS parameters, the heat transfer coefficient increases with an increase of the distance between profile peaks. Similar observations were seen by Pretot et al. [42] who saw that the Nusselt Number increases with an increase in the period for a surface with sinusoidal profile. Kim et al. [46] and Mahmoud et al. [43] found a similar trend in their results for micro fins arrays, where heat transfer coefficient decreased with increase in fin height and increased with increase in spacing. This analysis is also in alignment with two previous observations in this study. First, convective heat transfer increased with an increase in discharge duration, as wider craters are formed (Figure 4.5). Secondly, the surfaces with the superficial layer (discussed in Section 4.2) formed at high discharge durations had better performance in the convective regime because of higher Rsm and aspect ratio for "characterstic crater" as seen in Figure 4.7.

4.4.2 Nucleate boiling regime

In the nucleate boiling regime, q" = 450 kW/m^2 was chosen as a reference to correlate heat transfer coefficients. Table 4.5 shows the summary of correlations and corresponding errors with individual ISO 4287-1997 and DDS parameters.

Table 4-5: Summary of correlations with individual parameters (boiling regime)

Parameter		Correlation	MAE (%)	MAE2 (%)	Max error (%)	R^2
ISO 4287-1997	*Ra*	$h = 2.1\,Ra^{0.95}$	17.6	13.6	45.3	0.91
	Rz	$h = 0.13\,Rz^{1.3}$	25.1	19.1	54.4	0.85
	Rp	$h = 0.2\,Rp^{1.18}$	32.6	25.6	85.2	0.72
	Rv	$h = 0.59\,Rv^{0.99}$	18.4	15	44.6	0.90
	Rq	$h = 1.61\,Rq^{0.96}$	17.8	13.5	45.6	0.92
	Rsm	$h = 0.03\,Rsm^{1.05}$	33.6	32.1	103	0.36
	Rs	$h = 0.005\,Rs^{1.04}$	16.6	17.2	38.0	0.89
	Rmr	$h = 30.6\,Rmr^{0.7}$	38	35.9	84.4	0.43
	Rsk	$h = 36.05\,Rsk^{-0.37}$	26.6	24	101.9	0.54
	Rku	$h = 1331\,Rku^{-2.5}$	38.4	34.2	144.5	0.3
DDS	*CD*	$h = 6.7\,CD^{0.61}$	24.1	22.3	108.4	0.68
	CDi	$h = 2.5\,CDi^{0.45}$	13.1	9.8	43.8	0.94
	AR	$h = 1.91\,AR^{1.00}$	23.1	19.4	79.2	0.82
	Rc	$h = 0.47\,Rc^{12.45}$	17.3	13.8	49.5	0.92
	Vs	$h = 3.32\,Vs^{0.17}$	14.9	12	48.5	0.91
	Ve	$h = 3.17\,Ve^{0.17}$	14.9	12	48.4	0.91

Smaller scatter with a minimum MAE of 13.1% was observed for nucleate boiling data, which means nucleate boiling was more predictable as compared to convection. This is due to lower percentage error of measurement at higher heat flux ($\sim$ 3% at heat flux > 400 kW/m^2) as shown in Figure 4.15. In terms of ISO parameters, the best correlation was obtained with *Rs* at MAE = 16.6%, compared to MAE = 17.6% for *Ra*. For DDS parameters, the best fit was obtained with CDi with MAE = 13.1%.

4.4.2.1 Discussion

The observed data clearly states that *Ra* is not the best parameter to characterize boiling. *Rs* is slightly better predicting parameter in terms of ISO 4287-1997 parameters based on MAE and maximum error. Here *Rs* corresponds to the spacing between local peaks. It means spacing between local profiles plays a significant role in nucleate boiling compared to global peaks that correspond to *Rsm* (MAE = 33.6%). It was observed that the heat transfer coefficient increased with an increase in crater diameter as well as crater depth (MAE = 24.1%).

These results explain contradictions found in the literature regarding the usage of *Ra* as a defining parameter for heat transfer characterization. As Jones et al. [23] did not provide information on machining parameters, the boiling data obtained by Jones correlated with *Ra* because *Ra* increases with crater diameter as well. The EDM machining parameters are more fundamental compared to surface characterization parameters in terms of correlating boiling data, as clear trends were obtained with pulse current (i_e) and discharge

duration (t_e) in stage 1 of this study. The results from this analysis also explain observations from some studies where the heat transfer coefficient becomes constant or started to decrease after a certain value of Ra [5, 46, 47, 28] as the spacing between profile asperities became constant although Ra kept changing. The conclusions are also in agreement with the observation that shallow pits or cavities are more effective in boiling heat transfer than deeper cavities [27]. It is worth noticing that heat transfer coefficient was most sensitive to radius of curvature of the characteristic crater, which was similar to parameter P5* defined by Luke et al. [59] to correlate nucleation site density.

In terms of mean absolute error (MAE2), which was used as a comparative index by McHale [56] for testing the strength of correlations with different predictors, the correlation obtained by using CDi was the best choice as well, with the lowest MAE2 of 9.8%. As studies of McHale and Jones were conducted in different roughness regime (0.2 µm < Ra < 10 µm), it is not completely fair to compare errors with their results. However, MAE2 for the correlation with the best predictability in this study (9.8%) is close to minimum MAE of (7.8%) obtained by correlating linearly with filtered area ratio (Ar) parameter in the studies of McHale et al. [56] for water. But the coefficient of determination for the best correlation ($R^2 = 0.94$) for this study is better than R^2 of 0.8 obtained by McHale et al. [56] for water. Similarly, results in this study were better predicted than Jones et al.[23] study with Cooper correlation that had MAE from 5.3% to 29.2% for heat flux range upto 400 kW/m^2. For surfaces with comparable roughness features (5 - 40 µm) for micropillars formed by MEMS techniques, Kim et al. [55] predicted heat transfer

coefficients within 30% maximum error (though, there were points outside the ± 30% band) with the correlation developed by using roughness ratio (r) of surface features with pin-fin analysis (Figure 4.15). The results for the best correlation in this study produced a maximum error of 35.63% for Equation 4.1, which are close to errors obtained by Kim et al. [55].
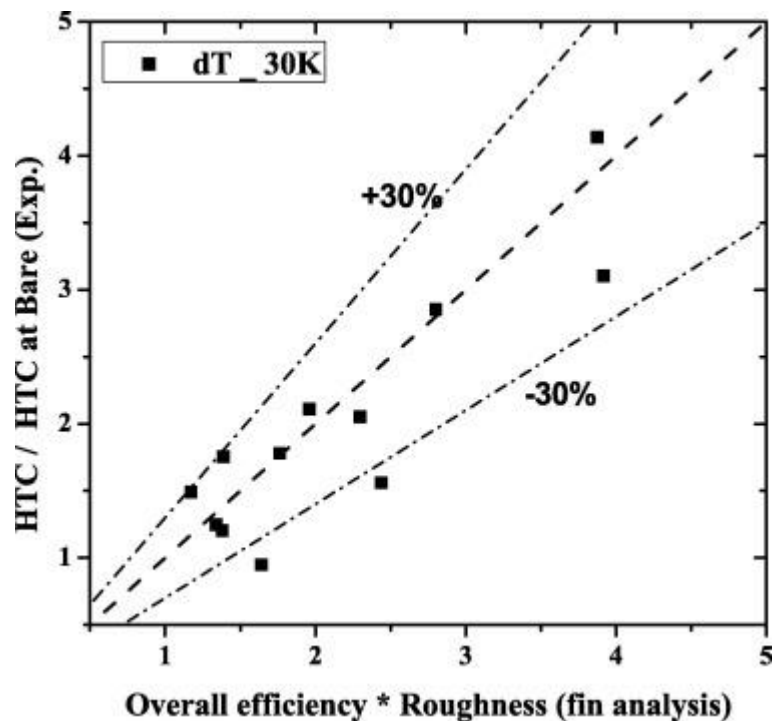
Figure 4.15: Experimental vs predicted HTC values by pin-fin analysis by Kim et al. [55]

These results are in accordance with nucleation theory, as cavities with a larger mouth diameter need smaller superheat to nucleate, and thus transfer larger heat from the wall at lower superheat. However, the increase in crater diameter can increase the heat transfer coefficient in other ways too. The volume of crater increases as a result of an

increase in crater diameter, which traps more vapor volume during initial wetting stage. It is still possible that the wider craters lead to separation of flow of liquid and vapor, which induces a highly efficient heat transfer via better convection. Performance of some of the high heat transfer surfaces is attributed to this reasoning [6, 13, 15]. More vigorous boiling was observed for surfaces with high heat transfer coefficients through the side window, which means a greater number of active nucleation sites. As waiting period of bubbles and other bubble dynamic parameters are not considered in this study, it is inconclusive whether transient heat conduction due to boundary layer phenomena play a dominant role over vaporization or convection by virtue of a change in crater shape and size [15]. This analysis is also in agreement with the previous analysis of boiling performance with EDM parameters in Stage 1, in which boiling performance from EDM textured surface was found to increase with an increase in pulse current as well as discharge duration. A detailed quantitative study of bubble dynamics will validate the effect of EDM texture on the heat transfer mechanism.

4.4.2.2 *Applicability and limitations of nucleate boiling correlation*

The boiling data derived for a single heat flux of 450 kW/m^2 provides only a preliminary insight about the comparison of boiling behavior by choosing different parameters instead of *Ra*. Therefore, a generalized correlation was also developed for all the boiling data, and limitations of using such correlation were also discussed.

It should be noted that the diameter and depth defined for characteristic crater may not be a true representative of craters on the surface as it is modeled based on autoregressive and stochastic parameters derived using AR (1) model. The DDS model is based on the effect of stochastic nature associated with the EDM process on surface profile. The true textured surface is not composed of individual cavities of the same size arranged systematically but is composed of overlapping craters of different sizes at different locations as shown in Figure 2.17. Modelling such surface into just one "characteristic crater" can be a representative of the EDM process, but assuming that the textured surface is formed of only the cavities of size and shape given by "characteristic crater" is incorrect, as the shape of real craters on the surface changes as successive discharges happen randomly over the surface and the machining time increases. Also, it should be noted that, when the CDi is defined, it constitutes the effect of distance between active nucleation sites as well as for the mouth cavity diameter of individual nucleation cavity. Therefore, the total number of physical surface cavities on the surface area might increase or decrease by a change in discharge duration, the heat transfer is influenced by only the number of active nucleation sites, and not just the physical cavities on the textured surface. From Table 4.5, it seems that CDi correlates best with boiling data, so a generalized correlation in terms of the CDi encompassing all the boiling data was developed of the form:

$$q'' = A.(CDi)^B.\Delta T^C \qquad\qquad 4.1$$

Where A, B, and C are coefficients determined using power law fit. Similar correlation in terms of *Ra* was developed for comparison. All the experimental data points in the boiling regime with 4 °C < ΔT$_{sat}$ < 15 °C were chosen in developing the correlation as shown in Figure 4.16. The surfaces used for correlation have roughness parameters in the range of 14 µm < *Ra* < 70 µm with the "characteristic crater" dimension 197 µm < CDi < 5325 µm. The results show a large error in prediction using the correlations at lower heat flux. This large scatter can be a result of error associated with prediction of onset of nucleate boiling point and large percentage error associated with experimental uncertainty (Figure 4.14).
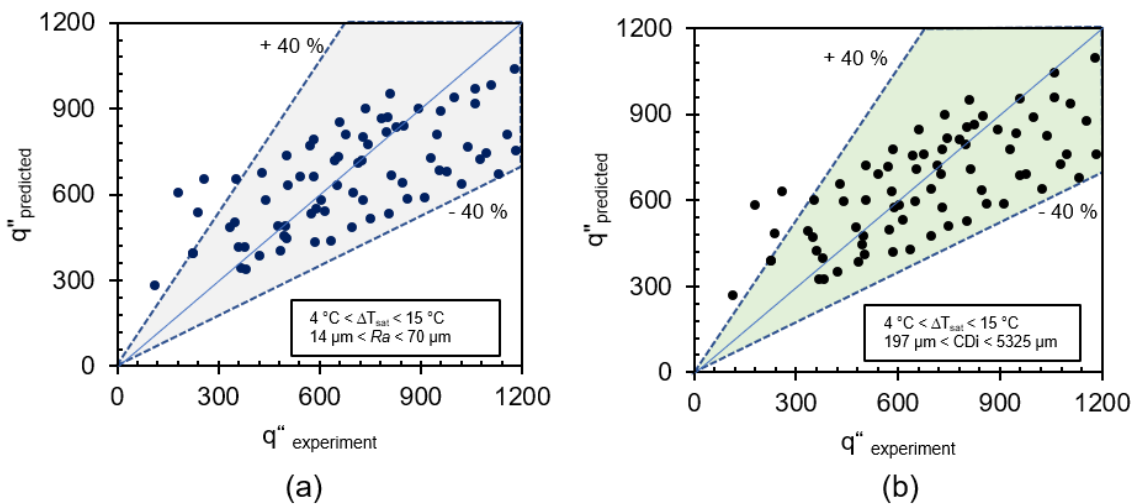
Figure 4.16: Nucleate boiling correlation developed for EDM textured surfaces for 4 °C < ΔT$_{sat}$ < 15 °C using (a) Ra (b) CDi

Convective correlations for 0 °C < ΔT$_{sat}$ < 4 °C were not developed as they yielded a high percentage error due to high uncertainty of determining heat transfer coefficient at low heat flux. It should be noted that the onset of nucleate boiling cannot be predicted with these

equations. Equation 4.2 and 4.3 shows the generalized nucleate boiling correlations using the CDi of "characteristic crater" with MAE of 27.9% compared to correlation with MAE of 29.2% obtained using Ra.

$$q" = 4.6\ (CDi)^{0.28}.\Delta T^{1.35} \qquad\qquad 4.2$$

$$q" = 6.57\ (Ra)^{0.53}.\Delta T^{1.24} \qquad\qquad 4.3$$

It was assumed that Ra was missing the information about spacing between nucleation sites and cavity mouth diameter of individual nucleation sites, which lead to higher MAE. However, a mere 1.3% decrease in MAE suggests that it is still possible that Ra includes some representative effect of spacing between active nucleation sites and mouth cavity diameter of active nucleation sites. The thickness of profile asperities determines the position of the mean line, from which Ra is measured. This means Ra does not explicitly takes into spacing and thickness of surface profile, but indirectly by the movement of the mean line (area above mean line = area below mean line) after filtering before calculation by the formula Eq. 3.7. Ra could be related with both the diameter and depth of "characteristic crater" as well. No situation was observed where correlation with Ra provided the best correlation. It can be concluded that, there are some heat transfer effects missed by using Ra, which correlation using the CDi accounted for. Otherwise, it can be asserted that boiling heat transfer increases with Ra if the same manufacturing technique (EDM) is employed. Bubble dynamics analysis is necessary in future to see how parameters like nucleation sites density, departure diameter, bubble frequency, waiting time, growth

time are influenced by a change in *Ra* compared to change in dimensions (CD, CDi, α_o) of the "characteristic crater".

4.5   Comparison of boiling performance with other research
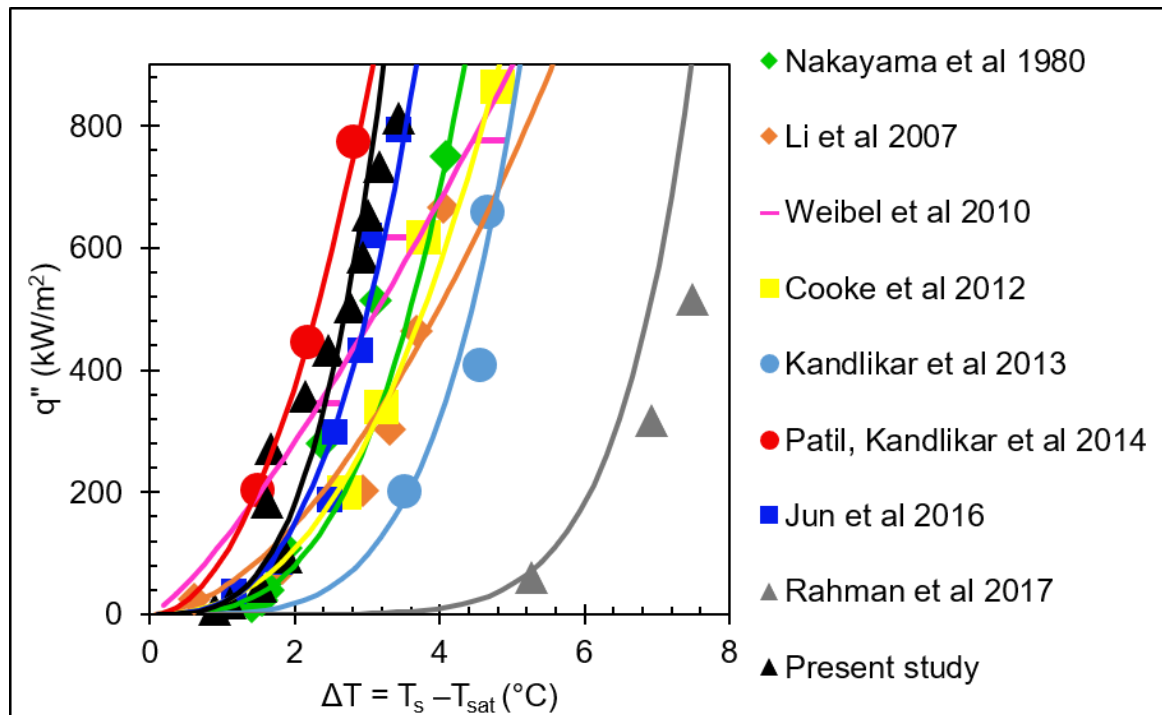
Figure 4.17: Comparison of boiling performance with other studies

Figure 4.17 shows the performance of the surface with the best boiling curve in this study (with EDM parameters i_e = 72A, t_e = 2400 µs, using hydrocarbon oil as dielectric), compared to boiling curves of other engineered surfaces with very high heat transfer coefficients [6, 12, 13, 14, 15, 16, 19, 22]. A close comparison can be drawn with the best-performing surface reported by Patil and Kandlikar [6] made by electrodeposition of super-hydrophilic microporous coating on microchannels made by CNC milling. However,

surfaces made by EDM texturing are advantageous compared to other manufacturing techniques as EDM is a one-step process with smaller texturing time (less than a minute for 10 x 10 mm^2 surface). Heat flux was varied till 900 kW/m^2 for the best performing surface in the present work, compared to heat flux operated up to 2500 kW/m^2 by other studies in the literature. An extrapolation technique cannot be employed without knowing the value of critical heat flux. A maximum heat transfer coefficient of 237 kW/m^{2}K at $\Delta T = 3.4$ K was obtained for the best performing surface.

4.6   Surfaces with the re-entrant cavities

4.6.1   Generation of re-entrant cavities

Several re-entrant cavities were created by plastically deforming the profile peaks of EDM textured surface using a Carolina 50 tonne heavy-duty hydraulic press, and the resultant surface looked like the one shown in Fig. 4.18. The surface with the highest heat transfer coefficient was chosen based on correlations developed in terms of roughness parameters. Only the hydraulic pressure was monitored to deform the tips of EDM surface to create a mushroom-like structure. A force of 5 ton on 3-inch diameter ram was assumed adequate (based on visual inspection of the surface deformation) to plastically deform the surface asperities and turn profile peaks into mushroom-like surface features, which can act as stable cavities for nucleation during boiling as shown in Figure 4.18 (b). It is still possible that more re-entrant cavities are formed at a certain optimized pressure. Only a preliminary experiment with one pressure value was chosen for this study.

a. Setup for making re-entrant cavities
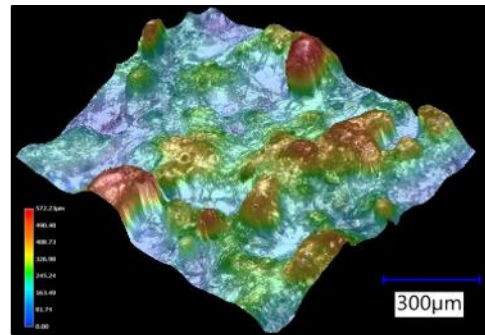
b(i). EDM textured surface (before machine press)
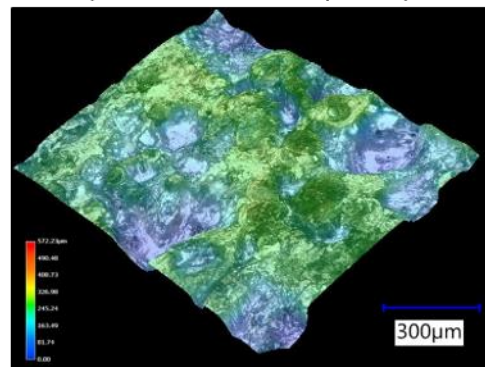
b(ii). EDM textured surface (after machine press)

Figure 4.18: Setup for making re-entrant cavities

4.6.2 Boiling performance

Based on the study of the influence of machining parameters, it was found that the highest boiling performance can be obtained for the surface with the highest pulse current and the highest pulse duration at which no superficial layer is formed. EDM parameters of $i_e = 72$ A, $t_e = 2400$ µs were used to create the surface that showed the highest boiling heat transfer performance.
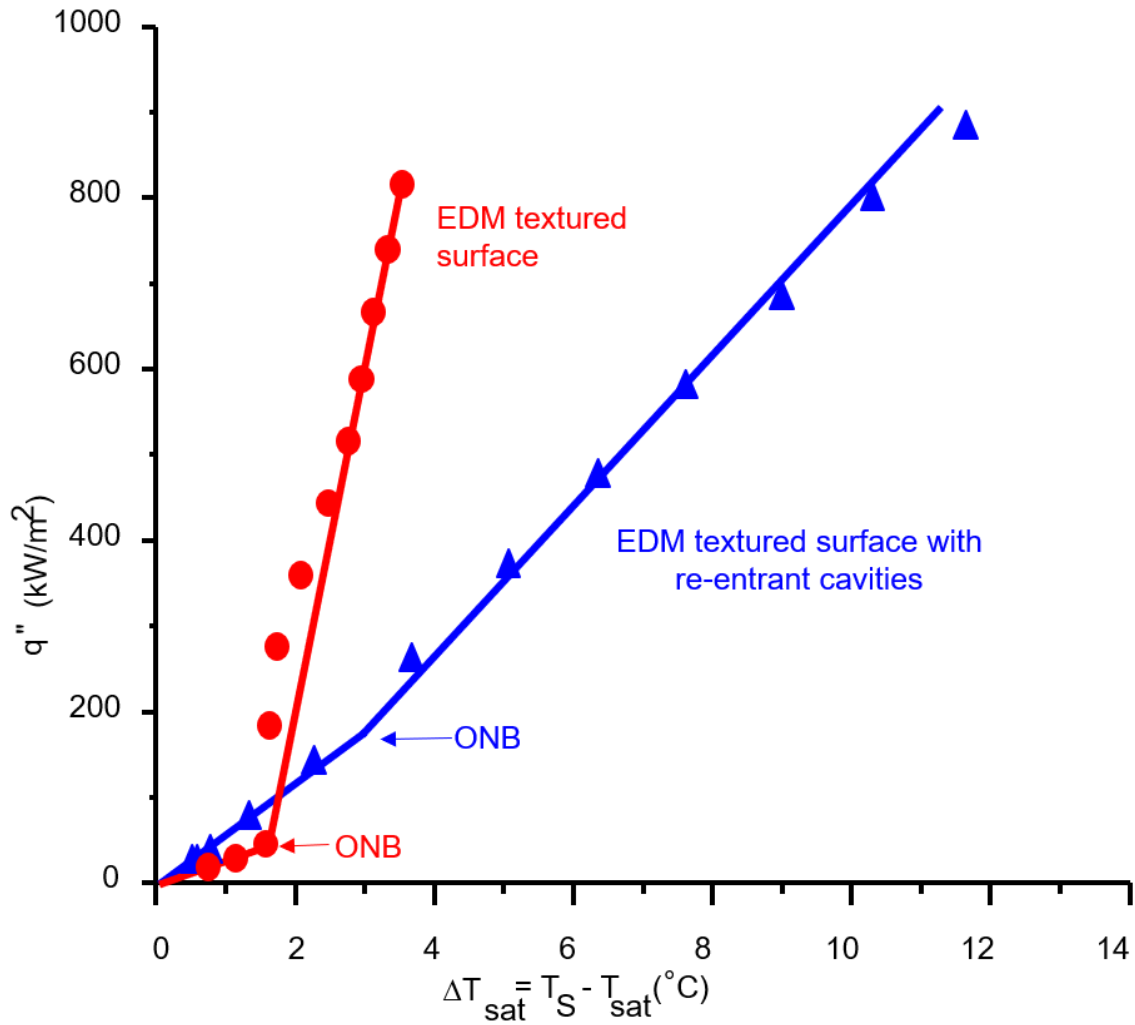
Figure 4.19: Boiling curve for the surface with re-entrant cavities

Figure 4.19 shows that a late incipience of boiling is observed but the overall boiling performance was not as good as what was obtained from the EDM textured surface alone. However, the heat transfer coefficients are higher in the convective regime. This may be attributed to more amount of vapor trapped during initial wetting, but a lesser number of active nucleation sites on the surface with re-entrant cavities.

5 Conclusions and future work

5.1 Conclusions/summary

1. An experimental study was carried out to study the role of textured surfaces produced by Electrical discharge machining (EDM) of Aluminum 6061 on boiling heat transfer enhancement.

2. Heat transfer enhancement of approximately ten times compared to the polished surface by surface modification with EDM by choosing machining parameter of $i_e = 72$ A, $t_e = 2400$ µs, and a highest heat transfer coefficient of 237 kW/m^{2}K at $\Delta T = 3.4$ K was obtained.

3. Potential limiting factors on machining capability of using EDM to create enhanced surfaces were identified, such as a superficial layer formed at higher pulse discharge durations by using hydrocarbon oil as a dielectric fluid. The root cause analysis was carried out to identify the source of this layer and its diffusion over the surface with machining time was studied.

4. The boiling curves were assessed in terms of EDM machining parameters (pulse current and pulse discharge duration) as well as surface characterization parameters (ISO and Data dependent system). Overall, *Rsm* and crater diameter (*CDi*) were found to be the most important parameter in characterizing EDM textured surfaces for convective and nucleate boiling regime on boiling curve respectively.

5. Limitations associated with using the nucleate boiling correlation developed during these studies were discussed.

6. A re-entrant type cavity manufacturing techniques were proposed by using the hydraulic press in combination to EDM by plastically deforming peak asperities, which provided enhancement in the convective regime.

5.2   Future work

1. This experimental study was carried out up to heat flux of 1200 kW/m^2 for the first phase and up to 900 kW/m^2 for subsequent analysis. A critical heat flux study needs to be carried out to assess the highest heat transfer achievable from surface prepared by EDM.

2. A detailed material characterization analysis of the superficial layer obtained at high pulse discharge duration (t_{on}) by using hydrocarbon oil as dielectric fluid can help overcome process limiting factors associated for preparing enhanced surfaces for boiling.

3. Better correlations and physical models for boiling can be developed by analysis of bubble dynamics parameters as a function of spacing and amplitude parameters based on ISO standards and Data Dependent System methodology.

4. The correlations developed in this study can be applied only in the conditions specified, and are bound by the limitations associated with the definition of the parameters. The limitations and assumptions used in this study can be addressed and explored in more detail

in further studies. More sophisticated boiling equipment can be employed to achieve lower experimental errors, which can lead to correlations that can be applied to wide ranges of operating conditions.

5. Effect of hydraulic ram pressure and other process parameters on surface features of potential re-entrant type nucleation sites can be studied. These cavities can act as stable nucleation sites for prolonged use. More analysis of the surface features as a result of this deformation is required to assess the role of these supposed re-entrant cavities in boiling performance. Only pressure was monitored while creating these re-entrant cavities. A detailed analysis of the effect of pressure on the plastic deformation needs to be carried out to quantify the enhancement or deterioration in pool boiling achieved with these mushroom-head features.

6 Appendix A-1
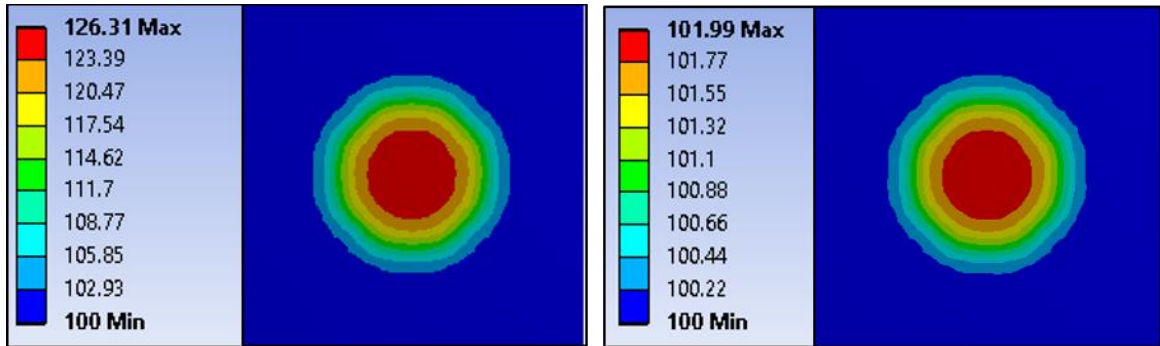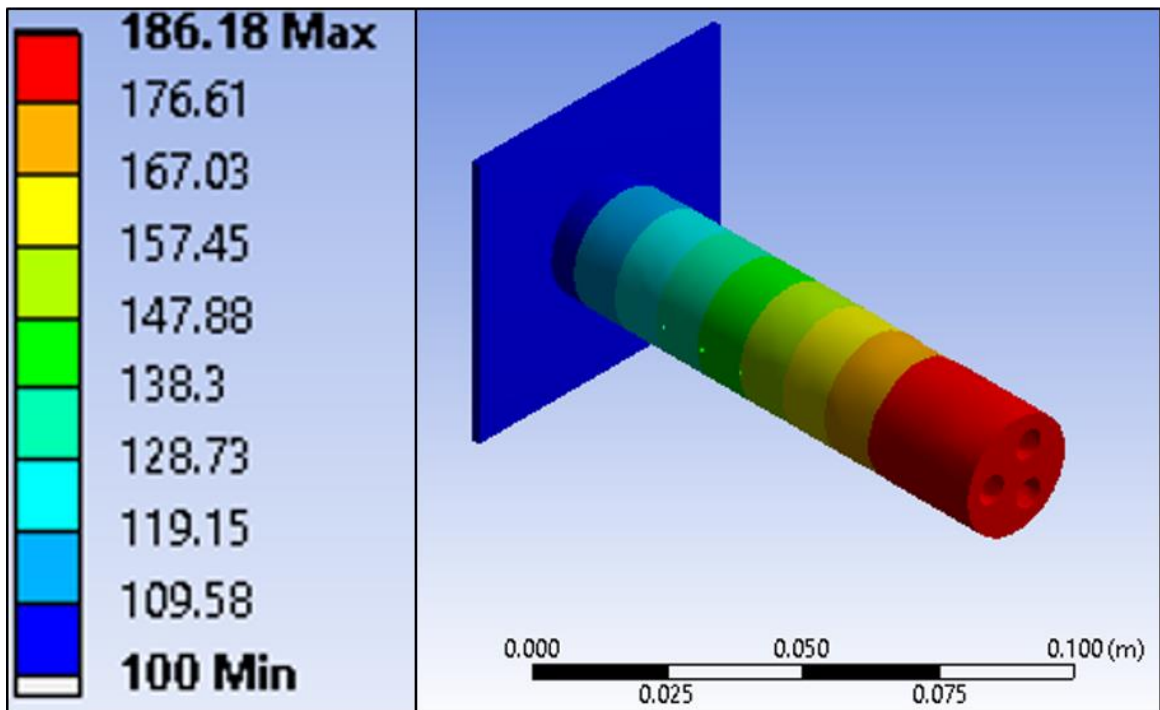
Figure 6.1: Boiling setup for visualizing bubble dynamics (a) Temperature profile for 30% heat flux (b) Temperature profile for 4.2% heat flux (c) Temperature profile along the length at 4.2% heat flux

105

7 References

[1]   F. P. Incropera and D. P. DeWitt, *Introduction to Heat Transfer*. 2002.

[2]   G. Liang and I. Mudawar, "Review of pool boiling enhancement by surface modification," *Int. J. Heat Mass Transf.*, vol. 128, pp. 892–933, 2019.

[3]   D. Attinger *et al.*, "Surface engineering for phase change heat transfer: A review," *MRS Energy Sustain.*, vol. 1, p. E4, 2014.

[4]   S. Nukiyama, "The maximum and minium values of the heat Q transmitted from metal to boiling water under atmospheric pressure." International Journal of Heat Mass Transfer volume 9, pp. 1419–1433, 1934.

[5]   P. J. Berenson, "Experiments on pool-boiling heat transfer," *Int. J. Heat Mass Transf.*, vol. 5, no. 10, pp. 985–999, 1962.

[6]   C. M. Patil and S. G. Kandlikar, "Pool boiling enhancement through microporous coatings selectively electrodeposited on fin tops of open microchannels," *Int. J. Heat Mass Transf.*, vol. 79, pp. 816–828, 2014.

[7]   A. Klink, M. Holsten, and L. Hensgen, "Crater morphology evaluation of contemporary advanced EDM generator technology," *CIRP Ann. - Manuf. Technol.*, vol. 66, no. 1, pp. 197–200, 2017.

[8]   M. Kunieda, B. Lauwers, K. P. Rajurkar, and B. M. Schumacher, "Advancing EDM through Fundamental Insight into the Process," *CIRP Ann.*, vol. 54, no. 2, pp. 64–87, 2005.

[9]   I. P. Kruth, I. Stevens, I. Froyen, and I. Lauwers, "Study of the White Layer of a Surface Machined by Die-Sinking Electro-Discharge Machining," *CIRP Ann. -*

Manuf. Technol., vol. 44, no. 1, pp. 169–172, 1995.

[10] O. Blatnik, J. Valentincic, and M. Junkar, "Percentage of harmful discharges for surface current density monitoring in electrical discharge machining process," *Proc. Inst. Mech. Eng. Part B J. Eng. Manuf.*, vol. 221, no. 12, pp. 1677–1684, 2007.

[11] R. L. Webb, "Heat transfer surface having a high boiling heat transfer coefficient,United States Patent 3696861," no. 15, pp. 0–3, 1956.

[12] N. W and T. Daikoku, "Dpamic Model of Enhanced Boiling Heat Transfer on Porous Surfaces Part I : Experimental Investigation," *J. Heat Transfer*, vol. 102, no. August 1980, pp. 445–450, 1980.

[13] S. G. Kandlikar, "Controlling bubble motion over heated surface through evaporation momentum force to enhance pool boiling heat transfer," *Appl. Phys. Lett.*, vol. 102, no. 5, 2013.

[14] S. Jun, J. Kim, D. Son, H. Y. Kim, and S. M. You, "Enhancement of Pool Boiling Heat Transfer in Water Using Sintered Copper Microporous Coatings," *Nucl. Eng. Technol.*, vol. 48, no. 4, pp. 932–940, 2016.

[15] M. M. Rahman and M. McCarthy, "Effect of Length Scales on the Boiling Enhancement of Structured Copper Surfaces," *J. Heat Transfer*, vol. 139, no. 11, p. 111508, 2017.

[16] C. Li and G. P. Peterson, "Parametric Study of Pool Boiling on Horizontal Highly Conductive Microporous Coated Surfaces," *J. Heat Transfer*, vol. 129, no. 11, p. 1465, 2007.

[17] R. Chen, M. Lu, V. Srinivasan, Z. Wang, H. Hee, and A. Majumdar, "Supporting Information for Nanowires for Enhanced Boiling Heat Transfer," 2009.

[18] S. Mori and K. Okuyama, "Enhancement of the critical heat flux in saturated pool boiling using honeycomb porous media," *Int. J. Multiph. Flow*, vol. 35, no. 10, pp. 946–951, 2009.

[19] J. A. Weibel, S. V. Garimella, and M. T. North, "Characterization of evaporation and boiling from sintered powder wicks fed by capillary action," *Int. J. Heat Mass Transf.*, vol. 53, no. 19–20, pp. 4204–4215, 2010.

[20] Y. Yang, X. Ji, and J. Xu, "Pool boiling heat transfer on copper foam covers with water as working fluid," *Int. J. Therm. Sci.*, vol. 49, no. 7, pp. 1227–1237, 2010.

[21] Z. Yao, Y.-W. Lu, and S. G. Kandlikar, "Direct growth of copper nanowires on a substrate for boiling applications," *Micro Nano Lett.*, vol. 6, no. 7, p. 563, 2011.

[22] D. Cooke and S. G. Kandlikar, "Effect of open microchannel geometry on pool boiling enhancement," *Int. J. Heat Mass Transf.*, vol. 55, no. 4, pp. 1004–1013, 2012.

[23] B. J. Jones, J. P. McHale, and S. V. Garimella, "The Influence of Surface Roughness on Nucleate Pool Boiling Heat Transfer," *J. Heat Transfer*, vol. 131, no. 12, p. 121009, 2009.

[24] J. P. McHale and S. V. Garimella, "Bubble nucleation characteristics in pool boiling of a wetting liquid on smooth and rough surfaces," *Int. J. Multiph. Flow*, vol. 36, no. 4, pp. 249–260, 2010.

[25] K. J. L. Geisler, A. Bar-cohen, G. L. M. Hall, and C. Park, "Ht2005-72666," pp. 1–11, 2018.

[26] V. V. Nirgude and S. K. Sahu, "Enhancement of nucleate boiling heat transfer using structured surfaces," *Chem. Eng. Process. Process Intensif.*, vol. 122, no. October,

pp. 222–234, 2017.

[27]   A. D. Messina and E. L. Park, "Effects of precise arrays of pits on nucleate boiling," *Int. J. Heat Mass Transf.*, vol. 24, no. 1, pp. 141–145, 1981.

[28]   J. M. Saiz Jabardo, "An Overview of Surface Roughness Effects on Nucleate Boiling Heat Transfer," *Open Transp. Phenom. J.*, vol. 2, no. 1, pp. 24–34, 2010.

[29]   T. Fujii and H. Imura, "Natural-convection heat transfer from a plate with arbitrary inclination," *Int. J. Heat Mass Transf.*, vol. 15, no. 4, pp. 755–767, 1972.

[30]   P. Griffith and J. D. Wallis, "The role of surface conditions in nucleate boiling," *Chem. Eng. Prog., Symp. Ser.*, vol. 56, no. 30, pp. 49–63, 1960.

[31]   S. G. Bankoff, "Entrapment of gas in the spreading of a liquid over a rough surface," *AIChE J.*, vol. 4, no. 1, pp. 24–26, 1958.

[32]   C. H. Wang and V. K. Dhir, "On the Gas Entrapment and Nucleation Site Density During Pool Boiling of Saturated Water," *J. Heat Transf.*, vol. 115, no. 3, pp. 670–679, 1993.

[33]   V. Carey, *Liquid-vapor phase-change phenomena*. 1992.

[34]   R. L. Webb, "Nucleate boiling on porous coated surfaces," *Heat Transf. Eng.*, vol. 4, no. 3–4, pp. 71–82, 1983.

[35]   Y. Y. Hsu, "On the size range of active nucleation cavities on a heating surface," *J. Heat Transfer*, pp. 207–213, 1962.

[36]   C. Gerardi, J. Buongiorno, L. wen Hu, and T. McKrell, "Study of bubble growth in water pool boiling through synchronized, infrared thermometry and high-speed video," *Int. J. Heat Mass Transf.*, vol. 53, no. 19–20, pp. 4185–4192, 2010.

[37] R. L. Hwang and K. S. Judd, "A comprehensive model for nucleate pool boiling heat transfer including microlayer evaporation," *J. Heat Transfer*, vol. 98, no. 4, pp. 623–629, 1976.

[38] A. Halton and I. Hall, "Photographic study of boiling on prepared surface." Proceedings of the Third International Heat Transfer Conference, pp. 24–37, 1966.

[39] T. P. Allred, J. A. Weibel, and S. V. Garimella, "Enabling Highly Effective Boiling from Superhydrophobic Surfaces," *Phys. Rev. Lett.*, vol. 120, no. 17, p. 174501, 2018.

[40] K. Kripa, G. R. Brown, K. K. Varanasi, T. Deng, M. Hsu, and N. Bhate, "Hierarchical Superhydrophobic Surfaces Resist Water Droplet Impact, Technical Proceedings of the 2009 NSTI Nanotechnology Conference," 2015.

[41] N. Heya, M. Takeuchi, and T. Fujii, "Influence of Surface Roughness on Free-Convection Heat Transfer From a Horizontal Cylinder.," *Chem. Eng. J.*, vol. 23, no. 2, pp. 185–192, 1981.

[42] S. Prétot, B. Zeghmati, and P. Caminat, "Influence of surface roughness on natural convection above a horizontal plate," *Adv. Eng. Softw.*, vol. 31, no. 10, pp. 793–801, 2000.

[43] S. Mahmoud, R. Al-Dadah, D. K. Aspinwall, S. L. Soo, and H. Hemida, "Effect of micro fin geometry on natural convection heat transfer of horizontal microstructures," *Appl. Therm. Eng.*, vol. 31, no. 5, pp. 627–633, 2011.

[44] R. Jofre and R. Barron, "ASME Paper No. 67-WA/HT-38 1967," *ASME*, 1968.

[45] R. Prasolov, "On the effects of surface roughness on natural convection heat transfer from horizontal cylinders to air. (in Russian). .," *Inzhenerno Fiz. Zhurnal*, vol. 4, pp.

3–7, 1961.

[46] J. S. Kim, B. K. Park, and J. S. Lee, "Natural convection heat transfer around microfin arrays," *Exp. Heat Transf.*, vol. 21, no. 1, pp. 55–72, 2008.

[47] S. K. Roy Chowdhury and R. H. S. Winterton, "Surface effects in pool boiling," *Int. J. Heat Mass Transf.*, vol. 28, no. 10, pp. 1881–1889, 1985.

[48] R. I. Vachon, G. E. Tanger, D. L. Davis, and G. H. Nix, "Pool Boiling on Polished and Chemically Etched Stainless-Steel Surfaces," *J. Heat Transfer*, pp. 231–238, 2013.

[49] J. Kim, S. Jun, R. Laksnarain, and S. M. You, "Effect of surface roughness on pool boiling heat transfer at a heated surface having moderate wettability," *Int. J. Heat Mass Transf.*, vol. 101, pp. 992–1002, 2016.

[50] I. L. Pioro, W. Rohsenow, and S. S. Doerffer, "Nucleate pool-boiling heat transfer. II: Assessment of prediction methods," *Int. J. Heat Mass Transf.*, vol. 47, no. 23, pp. 5045–5057, 2004.

[51] M. G. Cooper, "Heat Flow Rates in Saturated Nucleate Pool Boiling-A Wide-Ranging Examination Using Reduced Properties," *Adv. Heat Transf.*, vol. 16, no. C, pp. 157–239, 1984.

[52] W. Leiner, "Heat transfer by nucleate pool boiling-general correlation based on thermodynamic similarity," *Int. J. Heat Mass Transf.*, vol. 37, no. 5, pp. 763–769, 1994.

[53] D. Gorenflo, "State of the art in pool boiling heat transfer of new refrigerants," *Int. J. Refrig.*, vol. 24, no. 1, pp. 6–14, 2001.

[54] H. Fedders, "Messung des Wärmeüberganges beim Blasensieden von Wasser an metallischen Rohren," *Kernforschungsanlage Jülich Rep. No. Jül740-RB.*, 1971.

[55] S. H. Kim and G. C. Lee, "Boiling heat transfer and critical heat flux evaluation of the pool boiling on micro structured surface," *Int. J. Heat Mass Transf.*, vol. 91, pp. 1140–1147, 2015.

[56] J. P. McHale and S. V. Garimella, "Nucleate boiling from smooth and rough surfaces - Part 2: Analysis of surface roughness effects on nucleate boiling," *Exp. Therm. Fluid Sci.*, vol. 44, pp. 439–455, 2013.

[57] M. Mpholo, T. Mathaba, and H. H. Bau, "A 2D analysis of surface roughness for prediction of boiling incipience," *Int. J. Heat Mass Transf.*, vol. 53, no. 7–8, pp. 1313–1318, 2010.

[58] "ISO 4287:1997,Geometrical Product Specifications (GPS) -- Surface texture: Profile method -- Terms, definitions and surface texture parameters."

[59] A. Luke, "Preparation, measurement and analysis of the microstructure of evaporator surfaces," *Int. J. Therm. Sci.*, vol. 45, no. 3, pp. 237–256, 2006.

[60] S. N. Joshi and S. S. Pande, "Thermo-physical modeling of die-sinking EDM process," *J. Manuf. Process.*, vol. 12, no. 1, pp. 45–56, 2010.

[61] C. R. Sanghani and G. D. Acharya, "Effect of Various Dielectric Fluids on Performance of EDM: A Review," *Tmet*, no. January, pp. 55–71, 2016.

[62] S. M. Pandit and K. P. Rajurkar, "Crater Geometry and Volume from Electro-discharge Machined Surface by Data Dependent Systems," *J. Eng. Ind.*, vol. 102, pp. 289–295, 1980.

[63] H. Kim, H. S. Ahn, and M. H. Kim, "On the Mechanism of pool boiling critical heat flux enhancement in nanofluids," *ASME*, vol. 132, pp. 061501-1–11, 2010.

[64] D. G. Chetwynd, "The digitization of surface profiles," *Wear*, vol. 57, no. 1, pp. 137–145, 1979.

[65] C. Guo, "Sink electrical discharge machining of superhydrophobic surfaces," McMaster University, 2018.

[66] S. M. You, T. W. Simon, A. Bar-Cohen, and W. Tong, "Experimental investigation of nucleate boiling incipience with a highly-wetting dielectric fluid (R-113)," *Int. J. Heat Mass Transf.*, vol. 33, no. 1, pp. 105–117, 1990.

[67] M. Holsten, P. Koshy, A. Klink, and A. Schwedt, "Anomalous influence of polarity in sink EDM of titanium alloys," *CIRP Ann.*, vol. 67, no. 1, pp. 221–224, 2018.